Science and Technology Facilities Council

Central Laser Facility

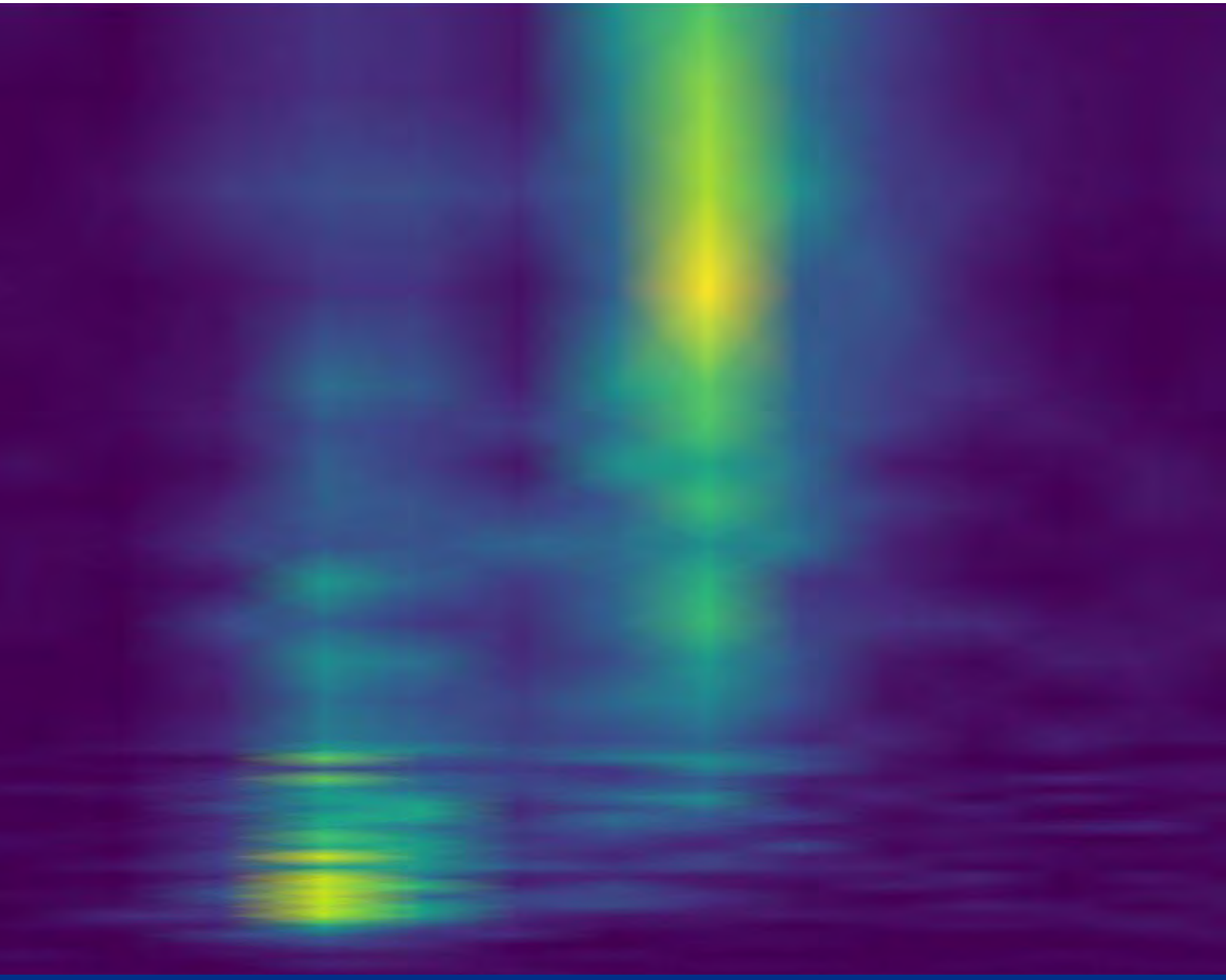

Central Laser Facility Annual Report

2022–2023

Central Laser Facility
Science & Technology Facilities Council
Rutherford Appleton Laboratory
Harwell Campus
Didcot, Oxfordshire OX11 0QX
T: +44 (0)1235 445647
E: clfannrep@stfc.ac.uk
W: www.clf.stfc.ac.uk

The production team for this Annual Report was as follows:

Editor: Raoul Trines

Production: Tracey Burge and Raoul Trines

Section Editors: Hamad Ahmed, Nicolas Bourgeois, David Carroll, Dave Clarke, Rob Clarke, Marco Galimberti, James Green, Greg Greetham, Robert Lees, Pedro Oliveira, Rajeev Pattathil, Jonathan Phillips, Alex Robinson, Igor Sazanovich, Christopher Spindloe, Emma Springate, Dan Symes, Steph Tomlinson, Martin Tolley, Christopher Tynan

This report is available on the CLF website at www.clf.stfc.ac.uk

Design, layout and production: STFC's Digital Creative Services: Poppy Holford and Dominic Read

Thanks to all of the above for their contribution towards producing this report and, of course, to all of the authors for their submissions.

Front cover image: Time-resolved photoelectron spectrum of TMA Courtesy of R.S. Minns, University of Southampton.

Contents

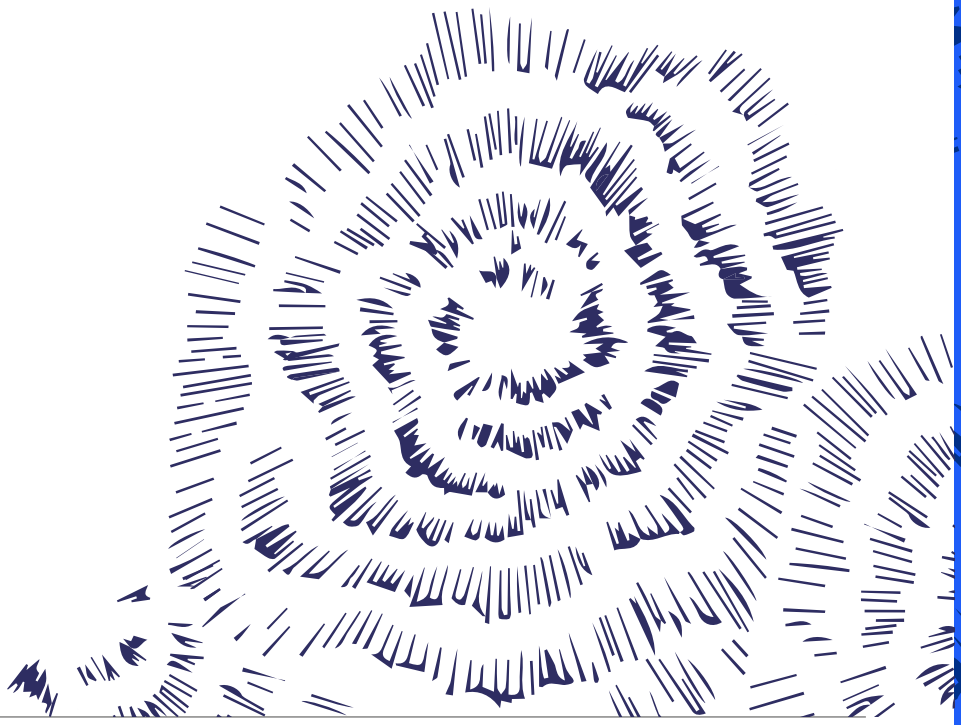

Foreword

John Collier Director, Central Laser Facility, STFC Rutherford Appleton Laboratory, Harwell Campus, Didcot, UK | Email address: john.collier@stfc.ac.uk | Website: www.clf.stfc.ac.uk

***"No photon left behind!"* was the rather poetic way that the Chair of the Central Laser Facility's Facility Board summarised our performance and forward strategy after the last meeting. This external Board oversees what we do, and the Chair was reflecting on the breadth, depth, and volume of the work that we are doing. Her opinion backed that of the earlier CLF Review – a tour de force of everything CLF, past, present, and future – which gave a rousing endorsement of what we are, what we are doing, and what we want to do. Certainly, when the scale of our endeavour is presented in a single forum, it is clearly impressive and something of which we can be really proud.**

Our science programme has continued unabated, delivering some world-class, high-profile results and publications. However, we are not resting on our laurels and have developed an ambitious strategy for the next decade that sets out, in black and white, where we want the CLF to go and what we want to achieve.

The Extreme Photonics Applications Centre (EPAC) forges ahead. At the same time, we have plans to upgrade our Vulcan, Ultra and Artemis facilities, which we hope to begin in the coming year, enabling new and improved user applications and helping to secure the international leadership of the UK in several areas of science into the next decade. Beyond large facility investments, we have applied for funding for several new initiatives. We are planning a ground-breaking facility, based around a new form of Raman spectroscopy with application in cultural heritage, drawing in the Arts and Humanities Research Council as a sponsor for the first time. In a more familiar area, we have submitted a proposal for a joint CLF and Technology project to develop a new laser design for laser fusion, with the government Department of Net Zero and Energy Security as the sponsor. If these bids are successful, the CLF will have three government departments funding our work, which is a tremendously powerful statement.

In the environmental sciences, we are reaching out to the Environment Agency and are planning new European Union opportunities now that the UK has joined Horizon Europe, the EU's key funding programme for research and innovation. We have launched a new international programme with our colleagues in India in bio-imaging and AI applied to cancer research, expanding the scope of the highly successful EPIC project. CALTA is building the DiPOLE100-S laser system, the latest addition

to its DiPOLE series, for installation in the ELI Beamlines Facility in Prague.
This system runs at 100 Hz, another world first! One of its predecessors, the DiPOLE100-X system, has been commissioned on an instrument at the European XFEL in Hamburg, and the very first experiment is scheduled to take place very shortly. As the repetition rate of high-power lasers rises, the demand for large numbers of targets is also rising. Scitech Precision, our target fabrication spinout, is able to deliver the highest quality targets fulfilling the most complex of experimental demands, and not surprisingly has had its best year ever.

There are so many things I could write about this year and our accomplishments, but *"No photon left behind!"* sums it up perfectly!

This annual report offers you an insight into some of the scientific and technical research that has been carried out by users of the CLF and its staff over the financial year 2022/23. The research spans a broad range of science areas, and supports wide-reaching efforts to solve major scientific, economic, and societal challenges. I do hope that you enjoy reading this selection of abstracts, and feel inspired by the achievements of all those involved. I think we can be really proud of what we are doing, the impact it is having, and the difference we are making.

Professor John Collier FLSW
Director, Central Laser Facility

Overview of the Central Laser Facility (CLF)

Cristina Hernandez-Gomez

Central Laser Facility, STFC Rutherford Appleton Laboratory, Harwell Campus, Didcot, UK

Email address: cristina.hernandez-gomez@stfc.ac.uk | **Website:** www.clf.stfc.ac.uk

Introduction

The CLF is a world leading centre for research using lasers in a wide range of scientific disciplines. This section provides an overview of the capabilities offered to our international academic and industrial community.

Vulcan

Vulcan is a versatile high power laser system that is composed of Nd:glass amplifier chains capable of delivering up to 2.6 kJ of laser energy in long pulses (nanosecond duration) and up to 1 PW peak power in a short pulse (500 fs duration) at 1053 nm. It can currently deliver up to eight beam lines. Two of these beam lines can operate in either short pulse mode or long pulse mode, while the remaining six normally operate in a long pulse mode. The short-pulse can be directed to two different target areas, enabling sophisticated interaction and probing experiments, with all eight beamlines available to one target area (TAW).

The installation of the new short-pulse OPCPA beamline (VOPPEL) continued through this year. This beamline aims to demonstrate a PW-level pulse (30 J in 30 fs) OPCPA system to the Vulcan Petawatt Area (TAP). The compressor chamber was installed into the experimental area, but the final folding chamber arrangement was not able to be installed.

Gemini

Gemini is a dual-beam petawatt-class Ti:Sapphire laser system that provides unique capabilities for relativistic laser-matter interactions and secondary source production. Gemini is one of the leading centres for laser-driven plasma accelerators and applications.

In the reporting year, ATA2 was closed for user operations to set it up for EPAC prototyping and testing. Part of this work involved separating ATA1 (the old Artemis area) from ATA2 in terms of laser interlocks, and moving the short pulse probe into ATA1 in order to have a separate laser system in there for EPAC component testing.

Gemini had a significant system access period to replace the pump lasers for its third Amplifier. Following this installation, Gemini has continued to operate, delivering four experiments in TA3.

Target Fabrication

The Target Fabrication Group made the majority of the solid targets shot on the CLF's high-power lasers, and also supported target design for the academic access on the Orion Facility at AWE. Commercial access to target fabrication capabilities was available to external laboratories and companies via the spinout company Scitech Precision Ltd. The group also supported the Lasers for Science Facility (LSF) with microfabrication capabilities to enable their experimental campaigns, and provided support for the wider STFC community with micro-fabrication.

A range of microtarget types were produced to enable the exploration of several experimental regimes. Fabrication techniques included thin film coating, precision micro-assembly, laser micromachining, and chemistry processes, all verified by sophisticated characterisation. This year saw the completion of the MEMS targetry facility as a high repetition rate component manufacturing capability. The enhancement of the advanced capabilities in this area, as well as further development in single point diamond machining, enabled

the Group to support high profile experiments in the US for the first time. The Group's processes and component tracking system provided a high level of traceability and the group contributed to a number of publications, either directly as a co-author or by providing critical characterisation data for targets that were supplied.

The high repetition-rate tape drive project matured into a commercial product, which was provided to a number of international facilities commercially and also collaboratively through the European IMPULSE project. This provided the group with crucial data on EMP and x-ray shielding for eventual fielding on EPAC. Development of the liquid target system for EPAC was a high priority, with designs for nozzles and catching systems being explored, and a collaboration with Queen's University Belfast and SLAC National Accelerator Laboratory started to develop systems for testing in the CLF.

Advanced 3D printing has been added to the capabilities in Target Fabrication, with a system that has 5 µm resolution being installed in the laboratory. The Group is able to produce target components on a short lead-time with high accuracy and with the ability to make modifications to designs within a few days. Targets with additive manufacturing (AM) components have already been fielded on all of the CLF facilities.

Theory and Modelling

The Plasma Physics Group supports scheduled experiments throughout the design, analysis and interpretation phases, as well as users who need theoretical support in matters relating to CLF science. PPG supports principal investigators using radiation hydrodynamics, particle-in-cell, hybrid and Vlasov-Fokker-Planck codes, as well as by providing access to large-scale computing (SCARF).

Strong support of users throughout this period has continued, including the provision of the PRISM suite. Alongside the core mission of the PPG, the group continues to engage with the academic community to contribute to Laser fusion research.

Artemis (Research Complex at Harwell)

This was the second year of operations for Artemis in the Research Complex, following the lab move and completion of the upgrade project.

The new XUV beamline for the 100 kHz laser system was fully aligned and commissioned, and is now delivering user experiments. The new beamline enables smaller XUV spot sizes, plus better energy and angular resolution due to reduced space charge. The Artemis team commissioned a novel analyser, which enables the measurement of two dimensions of electron momentum space, for time-resolved photoemission. The team also added new experiments using high harmonic generation from solid materials as a spectroscopic technique to the portfolio. The first paper from an experiment in the new labs was accepted by Physical Review Letters.

Following the award of the £17.2M HiLUX project, the Artemis team has worked to prepare for project kick-off by preparing tenders for the new laser system, which will have both high average power for harmonic generation and tuneable UV-IR pulses, and the new momentum microscope, and they are starting recruitment.

Ultra (Research Complex at Harwell)

The structural dynamics facilities at Ultra explore molecular structure during changes, such as chemical reactions, or in complex environments. Ultra's unique combination of multiple laser amplifiers provides light across UV to IR, spectrally narrow and broad, measuring dynamics across femtoseconds to seconds, to address a diverse portfolio of scientific problems. The scientific themes span the dynamics of drug binding and protein folding, to structural changes in battery charging and catalytic cycles. The available techniques provide highly sensitive time-resolved vibrational and electronic absorption spectroscopies or Kerr-gated Raman spectroscopy to observe weak signals obscured by strong emission from samples.

Octopus (Research Complex at Harwell)

In the imaging area, the Octopus cluster offers a range of microscopy stations linked to a central core of pulsed and CW lasers, offering "tailor-made" illumination for imaging. Optical resolution techniques offered include total internal reflection (TIRF) and multi-wavelength single-molecule imaging, confocal microscopy (including multiphoton), fluorescence energy transfer (FRET), fluorescence lifetime imaging (FLIM), and Light Sheet Microscopy. Super-resolution techniques are also available: 2D and 3D Stochastic Optical Reconstruction Microscopy (STORM), Photo-activated Localization Microscopy (PALM), Structured Illumination Microscopy (SIM), gated 3D Stimulated Emission Depletion Microscopy (STED), 3D MINFLUX, and super-resolution cryo-microscopy. Laser tweezers are available for combined manipulation/trapping and imaging with other Octopus stations, and can also be used to study Raman spectra and pico-Newton forces between particles in solution for bioscience and environmental research. Two cryo focused ion beam scanning electron microscope (FIB-SEM) systems are also available. One is dedicated to 3D volume electron imaging, and the other, currently being commissioned, is dedicated to the preparation of lamellas and lift-out to prepare samples for cryo electron tomography. This latter system forms part of a correlative light and electron microscopy (CLEM) workflow currently under development.

Chemistry, biology, and spectroscopy laboratories support the laser facilities, and the CLF offers access to a multidisciplinary team providing advice to users on all aspects of imaging and spectroscopy, including specialised biological sample preparation, data acquisition, and advanced data analysis techniques. Access is also available to shared facilities in the Research Complex, including cell culture, scanning and transmission electron microscopy, NMR, and x-ray diffraction.

Engineering Services

Engineering is fundamental to all the operations and developments in the CLF. The engineering division operates across all of the CLF's facilities. Mechanical, electrical and software support is provided to deliver the experimental programmes, and the research and development activities. Support can range from making small-scale modifications to existing equipment to improve its performance, through to carrying out larger scale projects, such as the design and development of commercial projects. In addition, there are active engineering collaborations with regional and international partners such as, HiLASE (Prague, Czech Republic), the European XFEL (Hamburg, Germany) and TIFR (Hyderabad, India).

The CLF Engineering and Technology Centre (ETC) is now fully operational. The ETC brings all the engineering lab spaces together into a central hub. All engineering manufacturing and assembly areas are now in the same building, which makes collaborative working much easier. This year, the Electrical team completed its move to the first floor of the ETC. This brings the workshop technicians into the same area as the interlocks and control team's prototyping and development area, providing a working space that allows the sharing of skills. ETC is also an excellent area for the training of apprentices and development of staff.

The Centre for Advanced Laser Technology and Applications (CALTA)

CALTA aims to deliver societal, scientific and economic impact from developments in the CLF. CALTA continues to support the EPAC Project, which will use three DiPOLE-style amplifiers in its petwatt-class laser chain. The next generation of 100Hz DIPOLE lasers is also being developed as part of a Widespread teaming project. Construction of this new 100 Hz DiPOLE system is almost complete, and it is expected to break new ground in the coming year. Commissioning

of the D-100X laser system at the European XFEL continues, with the first two stages of the laser amplifier chain now commissioned and operating as expected. Completion of this system will be ready for user experiments later in 2023. The in-house DiPOLE 10 J laser was used to demonstrate a new laser shock peening (LSP) technique that does not require a water confinement layer. This will broaden the application space of LSP and unlocking the potential for higher repetition rate use, particularly in combination with CALTA's DiPOLE laser systems, for which the beam behaviour can be controlled closely and adapted for optimal results.

The Extreme Photonics Applications Centre (EPAC)

EPAC, a new facility at the CLF, will enable the development of a transformational generation of laser-driven radiation sources and accelerators, and will maximise their scientific and economic exploitation through engagement of multiple end-user communities.

EPAC will initially deliver a petawatt laser operating at 10 Hz to dedicated experimental areas housed in a stand-alone building. In order to achieve this high peak power and repetition rate, DiPOLE technology will be used to pump a high energy Titanium Sapphire amplifier operating at 10 Hz.

The first experimental area (EA1) will be especially designed for laser wakefield acceleration (LWFA), where multi-GeV electron beams and synchrotron-like x-ray beams can be generated. The second experimental area (EA2) will be a very versatile area for fundamental science and applications with flexible focusing geometries. A third experimental area is still to be specified.

The building was handed over last year and the installation of equipment into EPAC has started, with the focus on the second floor where the laser rooms will be the first areas brought online. STFC has provided additional funding to enable the design and fit-out of the two top floors of the east wing of EPAC.

The floors have been designed to house a mixture of open plan office space, collaborative zones and meetings rooms for staff and future users of EPAC.

Access to Facilities

The CLF operates "free at the point of access" and is available to any UK academic or industrial group engaged in open scientific research, subject to external peer review. European collaboration is fully open for the high power lasers, whilst European and International collaborations are also encouraged across the CLF suite for significant fractions of the time. Dedicated access to CLF facilities is awarded to European researchers via the Laserlab-Europe initiative (www.laserlab-europe.net) funded by the European Commission.

Hiring of the facilities and access to CLF expertise is also available on a commercial basis for proprietary or urgent industrial research and development.

Industrial access and partnerships

The Industry Partnership and Innovation (IPI) Group has been responsible for the delivery of the industrial access and establishing new collaborations with industry. The IPI group ensures that the interactions delivered are strategically aligned to the CLF and of the highest economic and societal impact to the UK. This year, industry contract-access projects has continued across all CLF facilities.

The CLF remains a strong department for innovation. Internationally, the CLF has driven forward its innovation policy and the growth of industry liaison offices, through shared learning and knowledge exchange across EU laser facilities as a project partner organisation on the European Horizon 2020 IMPULSE project.

Please visit www.clf.stfc.ac.uk for more details on all aspects of the CLF.

Industry Engagement and Innovation

Sneha Banerjee and Pavel Matousek

Central Laser Facility, STFC Rutherford Appleton Laboratory, Harwell Campus, Didcot, UK

Email address: sneha.banerjee@stfc.ac.uk | Website: www.clf.stfc.ac.uk

Introduction

In the dynamic landscape of scientific innovation, the Central Laser Facility (CLF) has established itself as the hub for collaboration and scientific advancement. This article provides an overview of the CLF's engagements with industrial partners and highlights its innovative initiatives spanning the period from April 2022 to March 2023.

Empowering Industry Engagement

The past few years have seen an increase in industry engagement, with around 20 weeks of facility access extended to industry users across both the high-power laser (HPL) and the laser for science (LSF) divisions during this reporting period. The Industry Partnership and Innovation (IPI) group at the CLF have actively consulted with stakeholders from diverse sectors, including life science, net zero initiatives, and healthcare.

A noteworthy Proof of Concept (PoC) study by Johnson Matthey (JM) yielded promising results. This was carried out utilising Octopus's Fluorescence Lifetime Imaging Microscopy (FLIM) to characterise particulate filters and washcoat layers and understand deposition on the filters. Similarly, Finden, a RAL based company, revisited the CLF for commercial beamtime following successful POC work on the Raman microscope, demonstrating the tangible impact of collaborative research ventures.

Sustained partnerships with academia and industry have resulted in significant advancements. For example, Professor Jim Thomas's research endeavours, alongside his spin-out company MetalloBio, focused on understanding the mechanism of action of the various antimicrobial complexes to aid further development using the facility's suite of imaging equipment. The researcher was also awarded the 2023 CLF Societal Impact Award at the facility user meeting. Further experiments are planned with MetalloBio in the next financial year.

A collaborative effort has emerged between the CLF and researchers from the University of Kent and Fujifilm-Diosynth Biotechnologies, to explore alternative approaches for extracting functional proteins from E. coli, offering promising avenues for enhancing protein mass production processes. Utilising advanced Structural Illumination Microscopy from Octopus, the team delves into E. coli membrane structures, aiming for super-resolution insights to enhance protein extraction mechanisms. The goal is to develop scalable techniques applicable to numerous fields like drug delivery, vaccination, and protein storage.

The CLF has also facilitated Proof of Concept (POC) consultations with the STFC Food Network, General Fusion, ConnectomX, UKHSA, Phytoceuticals Ltd, NATA, and SomaServe. These collaborations exemplify the CLF's dedication to fostering long-term relationships and driving meaningful research outcomes.

Fostering Industry Partnership

The CLF continues to prioritize cultivating partnerships with both academic and industrial stakeholders. Under the Innovation Partnership Scheme, collaborations with the University of York, UCB Pharma and the CLF Ultra facility have been instrumental in exploring novel applications of two-dimensional IR spectroscopy as a liquid-biopsy diagnostic technique. These collaborations highlight the transformative potential of interdisciplinary research in driving innovation in healthcare diagnostics. Professor Neil Hunt and his team at the University of York have subsequently been awarded the 2023 CLF Economic Impact Award.

Continuing to build a relationship, consultations were held with LightOx for their next A4i proposal, utilising ULTRA's time resolved IR and transient absorption spectroscopy set-up, to look at the dynamical properties of light-activated probes.

Additionally, the CLF's ongoing partnership with JM, explores advanced techniques on novel materials signifying a commitment to exploring cutting-edge technologies and fostering innovation in industries. The appointment of a new joint research fellow further emphasises the CLF's dedication to advancing research through collaborative efforts.

Driving Innovation and Impact

The CLF's IPI group remains at the forefront of identifying novel concepts and technology transfer opportunities to deliver industrial and societal impact.

Notably STFC and the CLF collaborated with partners including the University of Oxford, Agilent, and Serum Institute of India, funded by WHO, in utilising a specialised laser spectroscopy technique developed at CLF (Spatially Offset Raman Spectroscopy - SORS) for verifying falsified COVID-19 vaccines in supply chains. These efforts emphasize commitment to addressing global challenges through innovative solutions and collaborative partnerships.

In a momentous occasion in July 2022, the CLF celebrated the completion of the Extreme Photonics Applications Centre (EPAC) building with a diverse array of collaborators present, marking a significant step forward. The completion of EPAC's construction phase in May 2022 paved the way for the installation phase to begin, with full operations anticipated for 2026. EPAC, a shared endeavour between the UKRI, the MoD, academia, and industry, represents a pioneering initiative aimed at harnessing interdisciplinary expertise to develop and apply novel laser-based accelerators and particle sources with unique properties. EPAC is expected to drive scientific breakthroughs and catalyse innovative solutions for complex challenges, and holds the promise of advancing UK science and technology in new areas, bolstering healthcare and fostering a cleaner, more productive economy.

The Central Laser Facility's continued work to develop collaborative partnerships and drive innovation plays a pivotal role in advancing scientific knowledge and addressing global challenges. As projects move forward, these collaborations will continue to shape the landscape of scientific research and technological innovation, propelling us towards a brighter, more sustainable future.

Collaborations such as the Extreme Photonics Innovation Centre (EPIC) between the CLF and the Tata Institute of Fundamental Research, India, highlight the facility's global impact in fostering technological advancements and skill development.

Communications and Outreach Activities within the CLF

Helen Towrie

Central Laser Facility, STFC Rutherford Appleton Laboratory, Harwell Campus, Didcot, UK

Email address: helen.towrie@stfc.ac.uk | **Website:** www.clf.stfc.ac.uk

Twitter: @CLF_STFC | **LinkedIn:** Central Laser Facility

The CLF's Communication Strategies

The role of the CLF's Impact and Engagement team is to promote CLF science and technology to some of our key audiences to share what we are capable of, to engage with our community and to recruit new people. Different audiences require different types of interaction, and we continually work to develop and harness the tools needed to communicate with each effectively.

We are responsible for internal and external engagement functions, including: the CLF website and social media for our general science audience, staff and user community; talks, tours and activities for our general and 'next gen' audiences; and a fortnightly newsletter for CLF staff.

Social Media

Twitter

Since October 2022, we have seen some significant changes to Twitter that have caused some users to leave for other platforms, and for UKRI and STFC to consider whether we should also move to another platform. With the advice of UKRI and STFC, combined with our own analysis, we have determined it is currently most beneficial to remain on Twitter for now. However, we have also started a LinkedIn profile for the CLF. This is so we can expand our horizons to help capture lost Twitter users, and to keep an active, established backup in case Twitter is no longer viable.

Social media is incredibly important for interacting with some of our key audiences. Monthly analyses of the CLF Twitter account show that, despite the recent changes to the platform, we have grown in followers and that these followers are largely users and the scientific community. This means that, when we share a tweet, we know that what we are sharing will impact the right people.

2020/21	850	(263 more than the year before)
2021/22	1,067	(217 more than the year before)
2022/23	1,315	(308 more than the year before)

Connecting with users

Our primary goal on social media is to increase or maintain our engagement rates on the tweets we share. Our impact is captured in a monthly meeting where we discuss what went well and what did not, and we then adjust our posts accordingly.

Some of our most impactful tweets from the financial year are shown below:

As can be seen, more casually written tweets seem to do well, and we have found that our audience tends to engage with pictures of our staff. This may well be because our audience, mostly made up of staff and users, may recognise the people in the photo. Additionally, general data suggests that most audiences prefer people-focused photos.

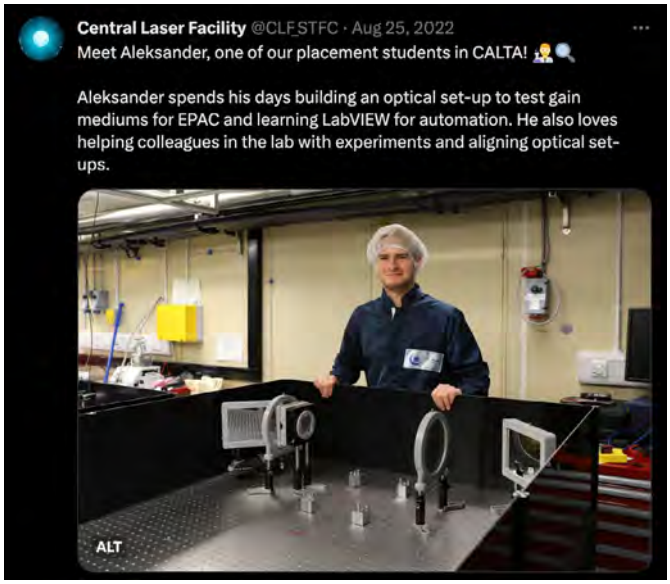

LinkedIn

Created with the purpose of engaging and connecting with users and potential new recruits in November 2022, our LinkedIn had 298 followers as of 1st April 2023. The majority of our followers are working in research, education, operations, and engineering. Analysis shows that job adverts get better in engagement on LinkedIn than on Twitter.

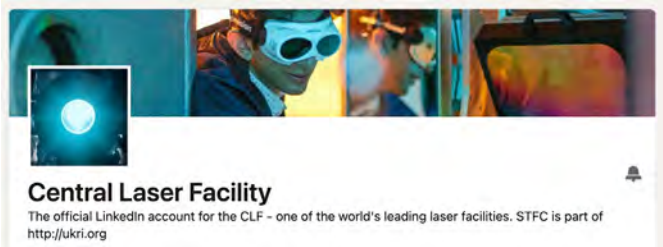

Keeping connected

We continue to keep in close contact with the STFC Twitter and Instagram team, through whom we can reach a more general public audience, as opposed to the general scientific audience that the CLF Twitter aims to attract. To aid these discussions and others, a CLF representative attends a monthly Social Media meeting, where all the departments can communicate new ideas, campaigns, and best practices.

The CLF Website

The CLF website continues to get a lot of visits. Many people find us by organic search - they search for something relative and the CLF pops up!

In the six months from October 2022 to April 2023, we had:

16,000 new users

3,500 returning users

65,000 page views

The top three most visited pages were:

- CLF Homepage
- CLF Facilities
- CLF News

Engaging the Public

As part of our goal to engage with the next gen audience, we often host visits to our facilities. These visits, organised through RAL Public Engagement, have allowed us to engage with a key demographic: 8 – 14-year-olds. This is the age at which children are starting to think about their future careers, and is also around the age when many young girls unfortunately decide that science and engineering is not for them.

Overall, from FY 2022 – 2023 we hosted 120 visits for our facility for nearly 1,500 guests.

Broken down, this looks like:

19 Next Gen	**1** General Public	**29** Scientific	**26** Industry
28 Stakeholders	**13** VIPs	**14** Others	

Total number of people engaged with: **1,490**

Looking more closely at Next Gen Public Engagement efforts

- Total people engaged via public engagement programme between April 2022 and March 2023: 1312, of which:

999 public
family audiences, so estimate ~30% were age 8 – 14, a key target

162 secondary school
teachers and students

5 work experience placements

150 primary school
teachers and students

12 CLF staff volunteered at least once
note that some staff volunteered at non-CLF events

A New CLF Public Engagement Activity is Piloted

After some brainstorming and trying out different activities with the Public Engagement team, we started a new CLF activity where school visitors make a paper Chinese lantern complete with a light inside, powered by a simple circuit. The idea behind this activity was that different coloured lanterns have different but significant meanings in Chinese culture, much like how we use different colour lasers to do different things in the CLF.

We introduce this activity by explaining how many of the "colours" around us are invisible to the naked eye, but can be very useful when used with scientific lasers. We then teach the children how to build the circuit and lantern, encouraging experimentation with the number of lights and diode colours, and creativity with the style of lanterns.

This lantern workshop has now been delivered three times to a total of 150 children, and we have improved upon it each time, establishing it as a unique CLF workshop. We will be conducting it again during Daresbury Open Week.

Welcoming New Staff

The CLF and other STFC departments have created a rota for hosting virtual tours for new starters. These tours take place throughout the year and are designed to show staff what is going on all around them in the place they work. It also helps CLF staff themselves, because often we find that people from one part of the CLF do not realise what is happening in another.

Below is some feedback from a New Starters' tour we hosted alongside the Scientific Computing Department:

- 66.67% of attendees marked the tours 5/5, with the remainder marking them at 4/5
- 83.33% of attendees said the tours were at the right level for them
- 83.33% of attendees said the tours were just the right length

When asked what the audience learnt, comments received included:

> *"Cool stuff about stretching, squeezing and flattening laser beams."*
>
> *"I liked learning about how the lasers could recreate the supernova."*
>
> *"An overview of computing and laser capability and their application at UKRI. A case study presentation about laser application for simulation of supernovae, amazing lesson."*
>
> *"Thank you very much and it was a great experience for me."*

Such positive feedback makes it feel worthwhile presenting staff tours and talks, and we are thankful for the support we have received to pull everything together.

Attracting a Wider Audience

Communication this year has begun to look a little more like how we operated pre-pandemic, although it is clear that we may never entirely return to how things were before. For example, many audiences are now far more comfortable with online engagement, and this means that we can reach people without the constraints of distance and capacity.

We have completed an array of projects to help make the CLF more appealing to a wide range of audiences. We have so far highlighted a multitude of projects in this summary, however, a few more are highlighted below.

CLF Impact Awards

On UNESCO's International Day of Light (16th May 2023), we will be officially announcing the winners of the CLF's first ever Impact Awards.

These awards, for Societal and Economic Impact, were available on an application basis to any staff and user who has used our facility for published research.

The entries have been judged by the CLF Communication and IPI (Industry Partnerships and Innovation) groups. They followed the Research England definition of impact for the REF, where impact is referred to as *"… an effect on, change or benefit to the economy, society, culture, public policy or services, health, the environment, or quality of life, beyond academia"* in the UK and internationally.

The winners will receive beautiful, laser-target sized trophies hand built by our target fabrication team, a certificate, and a written case study and promotion on social media.

The Magic of Laser Levitation at Talking Science

Back in May 2022, Dr Andy Ward hosted a Talking Science! This is an initiative with RAL Public Engagement that orchestrates talks from STFC scientists and technicians that are open to the public. Andy gave a talk once at lunchtime and once in the evening on his work with laser trapping – even though it sounds like science fiction, we really can levitate objects mid-air using lasers – very small objects of course!

Getting the news out there

A particular highlight this year was allowing ITV into our labs to film a news segment on the Laser Fusion breakthrough back in Autumn 2022. The segment was filmed inside the Vulcan laser facility and we, alongside Vulcan scientists, helped the TV host talk accurately yet accessibly about the laser on national television.

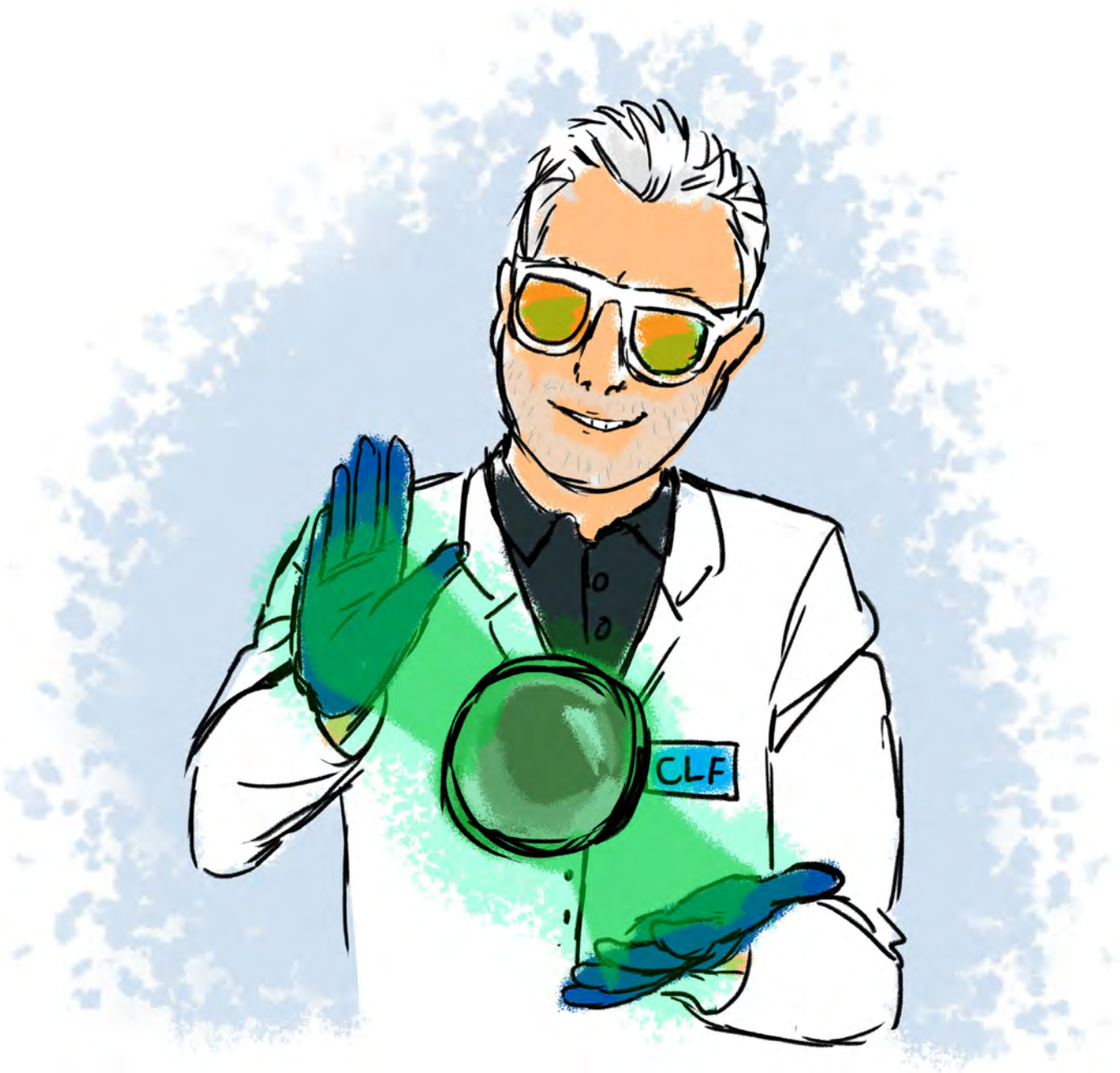

Unusual avenues of engagement

As a slightly less mainstream way to help engage the scientific community, where possible we have offered our illustration services to staff and users who have the opportunity to submit a journal front cover image for research completed at the CLF. We work with the researchers to create an image that is unique and professional, and reflects their work accurately. These images give our researchers a higher chance of being awarded the front cover spot, and this, along with the journal's image credit to the CLF, increases our chances of exposure to the journal's audience.

As a positive aside, this project has given our team the opportunity to work with researchers on a more personal level, resulting stronger relationships and an art piece that celebrates their incredible work.

EPAC Open Day

On 25th May 2022, we helped host EPAC Open Day for around 200 attendees from the CLF and surrounding buildings.

We were responsible for creating posters and signage for this event to help guests navigate the building and learn about the different parts of EPAC. On the day of the event, as well as Live-Tweeting, we also organised an Instagram Takeover via STFC's account to reach a wider audience.

Daresbury Open Week 2023

Looking forward, we will soon be attending Daresbury Open Week in July 2023. This Open Week, consisting of two days for school visits and one public day, will involve lots of preparation work from CLF comms, including to inspecting and risk assessing several CLF demos, training staff on activities and demos, creating freebees and posters, and liaising with RAL public engagement to make sure everything is shipped and ready for Daresbury.

Pages 21 – 80 contain a selection of abstracts that offer an insight into some of the scientific and technical research that has been carried out by users of the CLF and its staff this year. Due to issues with space, we cannot include the details of institutes with the author names on these abstracts, but there is a full Author Index starting on **page 112** that includes these details. Where possible, the online version of this report on the CLF website will also provide links to published papers, which contain these details.

High Energy Density and High Intensity Physics

Cellular irradiations with laser-driven carbon ions at ultra-high dose rates

Carbon is an ion species of significant radiobiological interest, particularly in view of its use in cancer radiotherapy, where its large Relative Biological Efficiency is often exploited to overcome radio resistance. A growing interest in highly pulsed carbon delivery has arisen in the context of the development of the FLASH radiotherapy approach, with recent studies carried out at dose rates of 40 Gy s^{-1}. Laser acceleration methods, producing ultrashort ion bursts, can now enable the delivery of Gy-level doses of carbon ions at ultra-high dose rates (UHDRs), exceeding 10^9 Gy s^{-1}. While studies at such extreme dose rate have been carried out so far using low LET particles such as electrons and protons, the radiobiology of high-LET, UHDR ions has not yet been explored. Here, we report the first application of laser-accelerated carbon ions generated by focussing 10^{20} Wcm^{-2} intense lasers on 10–25 nm carbon targets, to irradiate radioresistant patient-derived Glioblastoma stem like cells (GSCs).

Authors: S.J. McMahon, K.M. Prise, A. McIlvenny, A. McMurray, K. Polin, M. Borghesi, G. Milluzzo, H. Ahmed, C. Maiorino, L. Romagnani, D. Doria, S.W. Botchway, P.P. Rajeev

Contact authors: P. Chaudhary (p.chaudhary@qub.ac.uk)
M. Borghesi (m.borghesi@qub.ac.uk)
K.M. Prise (k.prise@qub.ac.uk)

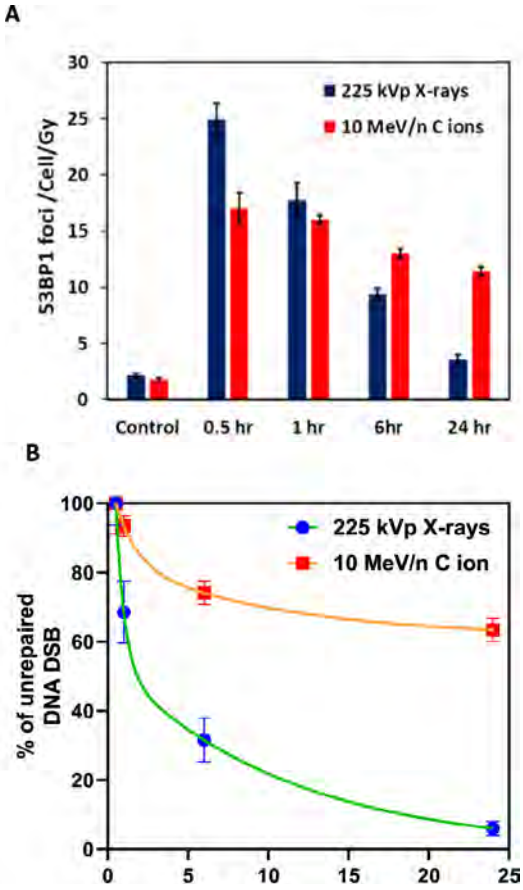

A). DNA DSB damage induced by 1 Gy of 225 kVp X-rays or 10 MeV n^{-1} laser-driven carbon ions and repair kinetics studied through 53BP1 foci formation assay. 53BP1 foci are expressed as mean no. of foci per cell per Gy. (B) DNA DSB repair expressed as percentage of unrepaired DNA DSB obtained by normalizing the amount of unrepaired DNA DSB at different time points, to the amount of unrepaired DNA DSB observed at 30 min (Error bars represent Standard deviation). The percentage repair kinetics over time is fitted with a two-phase decay analysis function (orange line carbon ions and green line x-rays) available in Graph pad Prizm software version 9.

Gas Target Characterization at OPAL

Plasma fluorescence measurements were performed for two different multi-centimetre laser wakefield targets. These measurements demonstrate the usefulness of this technique for target characterization. The gas cell target was shown to be uniform, while the gas jet target was shown to have a density dip of ~20%.

Authors: L. Feder, J. Chappell, J. Cowley, E. Archer, S. Kalos, D. McMahon, W. Wang, R. Walczak, S.M. Hooker

Contact author: L. Feder (linus.feder@physics.ox.ac.uk)

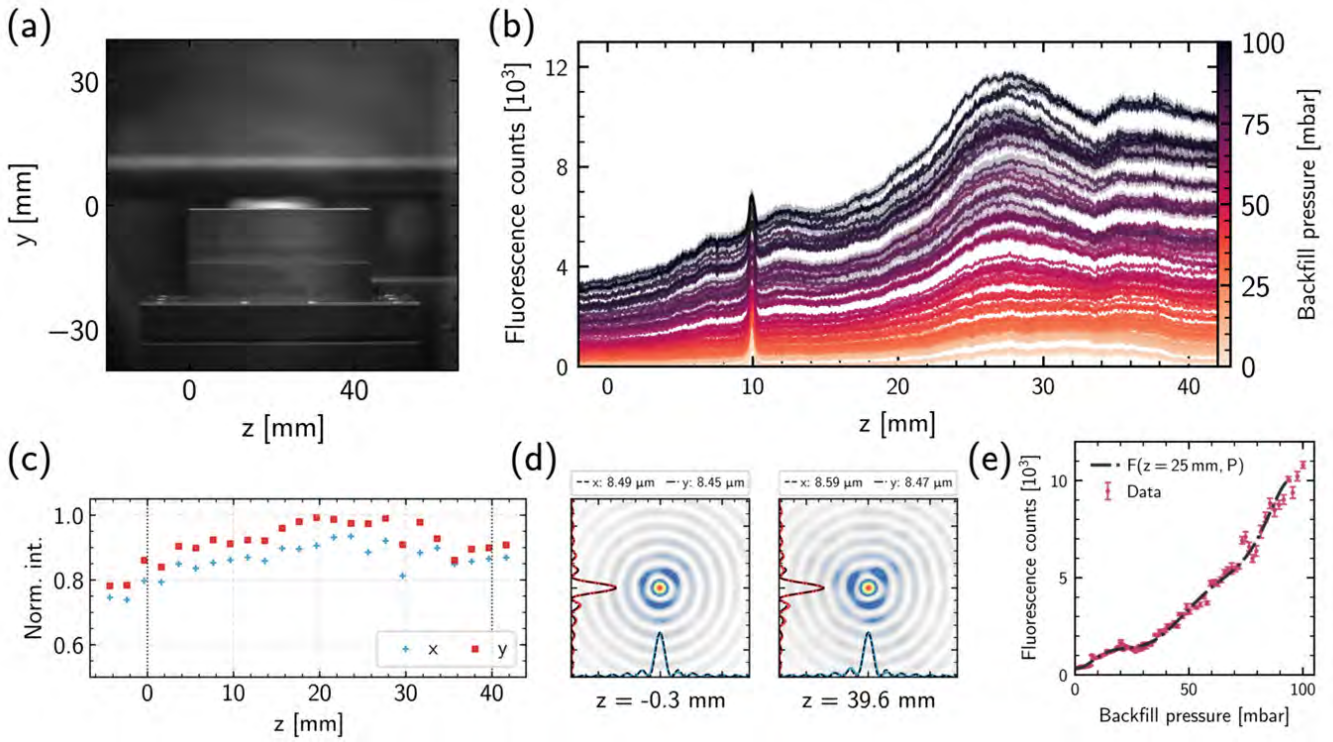

Figure 1: (a) Image of the 40 mm-long slit jet in place at OPAL; (b) example calibration curves demonstrating the measured average longitudinal fluorescence as a function of the backfill pressure; (c) measurements of the normalised peak intensity of the axicon focus at the position of the slit-jet; (d) measured axicon focal spots at either end of the slit-jet, with fits to the transverse intensity profiles; (e) example backfill calibration curve for z = 25 mm.

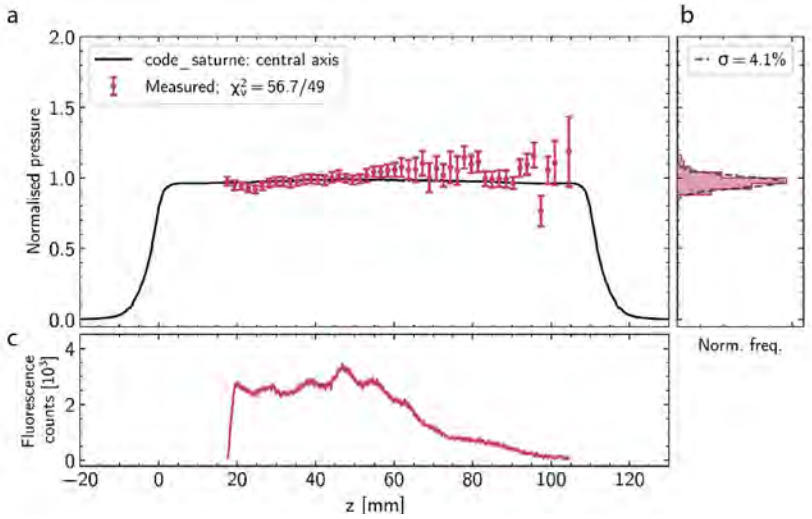

Figure 2: (a) Measurement of the pressure of the gas cell vs longitudinal position, along with the predicted profile from fluid simulations; (b) histogram of the measurements; (c) raw fluorescence signal from the cell.

Gas Target Design and Characterisation for EPAC EA1

Experimental Area 1 (EA1) in the Extreme Photonics Applications Centre (EPAC) will predominantly support experiments that utilise a long focal length parabola to focus the laser onto a gas target to generate high energy electrons and x-rays. The gas density profile can be tailored to favour the accelerator properties required for a particular application. The EPAC facility will provide users with a number of facility designed, characterised and maintained options for gas targetry depending on their requirements. The first design is a rectangular gas jet nozzle. Fluid simulations have been performed to design a prototype, which has been manufactured. Preliminary characterisation has been done on the manufactured nozzle by measurement of the nozzle throat size, and of the density profile through interferometry.

Authors: O.J. Finlay, N. Bourgeois, A. Stallwood, D.R. Symes, X.J. Gu, B. John, D.R. Emerson, L. Feder

Contact author: O. Finlay (oliver.finlay@stfc.ac.uk)

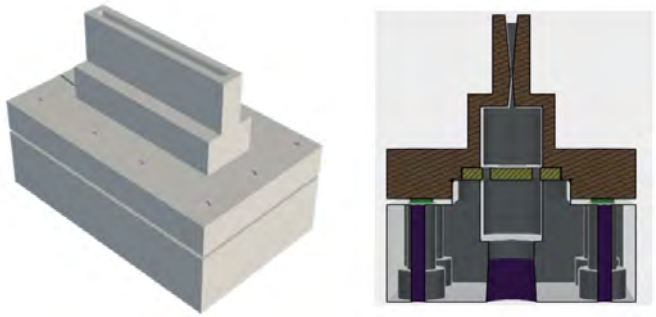

Figure 1: CAD drawing of the designed slot nozzle.

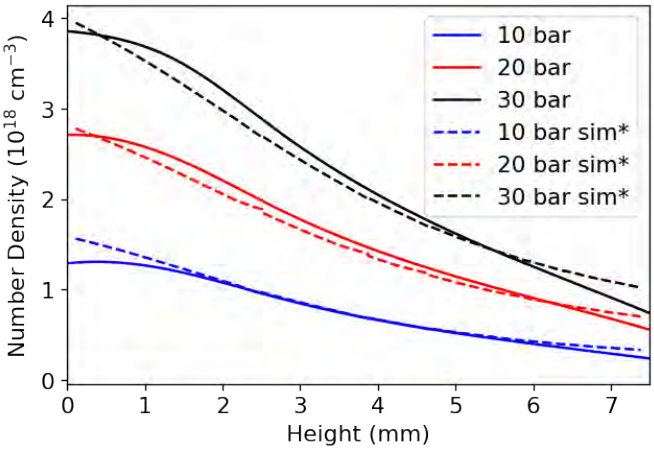

Figure 2: Neutral gas density measurement with probe traversing long direction of 40 mm EPAC slot nozzle. Simulation scaled to match inefficiency in gas line experimentally.

Automated control and optimization of laser-driven ion acceleration

The interaction of relativistically intense lasers with opaque targets represents a highly non-linear, multi-dimensional parameter space. This limits the utility of sequential 1D scanning of experimental parameters for the optimization of secondary radiation, although to-date this has been the accepted methodology due to low data acquisition rates. High repetition-rate (HRR) lasers augmented by machine learning present a valuable opportunity for efficient source optimization. Here, an automated, HRR-compatible system produced high-fidelity parameter scans, revealing the influence of laser intensity on target pre-heating and proton generation. A closed-loop Bayesian optimization of maximum proton energy, through control of the laser wavefront and target position, produced proton beams with equivalent maximum energy to manually optimized laser pulses but using only 60% of the laser energy. This demonstration of automated optimization of laser-driven proton beams is a crucial step towards deeper physical insight and the construction of future radiation sources.

Authors: B. Loughran, M.J.V. Streeter, M. Borghesi, C. Hyland, P. Parsons, O. McCusker, C.A.J. Palmer, H. Ahmed, S. Astbury, N. Bourgeois, S.J.D. Dann, T. Dzelzainis, J.S. Green, C. Spindloe, D.R. Symes, M. Balcazar, S. Dilorio, A.G.R. Thomas, C.B. Curry, N.P. Dover, O.C. Ettlinger, G.S. Hicks, Z. Najmudin, N. Xu, M. Gauthier, S.H. Glenzer, L. Giuffrida, G.D. Glenn, R.J. Gray, M. King, P. McKenna, V. Istokskaia, D. Margarone, C. Parisuaña, F. Treffert

Contact author: B. Loughran (bloughran08@qub.ac.uk)

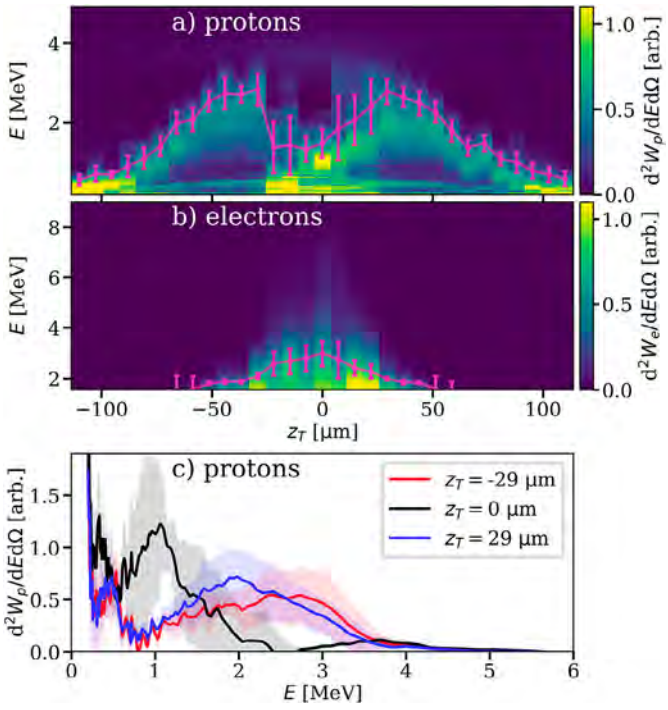

a) Proton and (b) electron energy spectra from the rear side of the target during an automated target position scan (z_T) with a 12 μm Kapton tape and an on-target laser energy of 438±32 mJ. (c) Average proton spectra (and standard deviation) for different z_T positions as indicated in the legend. The proton spectra are recorded by the time-of-flight diamond detector. Each column of the waterfall plots is the average of the 10 shots from each burst. The scan comprises 31 bursts at different target positions spaced at 7.3 μm intervals along the laser propagation axis. Negative values of z_T are when the target plane is closer to the incoming laser pulse and z_T = 0 is the target at the best focus of the laser pulse. The magenta data points, connected with a guideline, indicate the burst-averaged 95th percentile energy as well as the standard deviation of this value across the burst.

Development of a laser driven electron source for radiobiological applications

We report on the characterisation of a laser driven electron source for radiobiological applications. Doses in excess of 3 Gy were generated by a laser driven plasma wakefield accelerator. The electron beam duration is expected to have a duration on the order of 20 fs indicating unprecedented dose-rates in excess of 10^{13} Gy/s are expected. The stability of the source was characterised and its applications to radiobiological research discussed.

Authors: C.A. McAnespie, M.J.V. Streeter, L. Calvin, N. Cavanagh, K. Fleck, G. Sarri, P. Chaudhary, S.J. McMahon, K.M. Prise, B. Kettle, S.W. Botchway, S. Needham, N. Bourgeois

Contact author: C.A. McAnespie (cmcanespie01@qub.ac.uk)

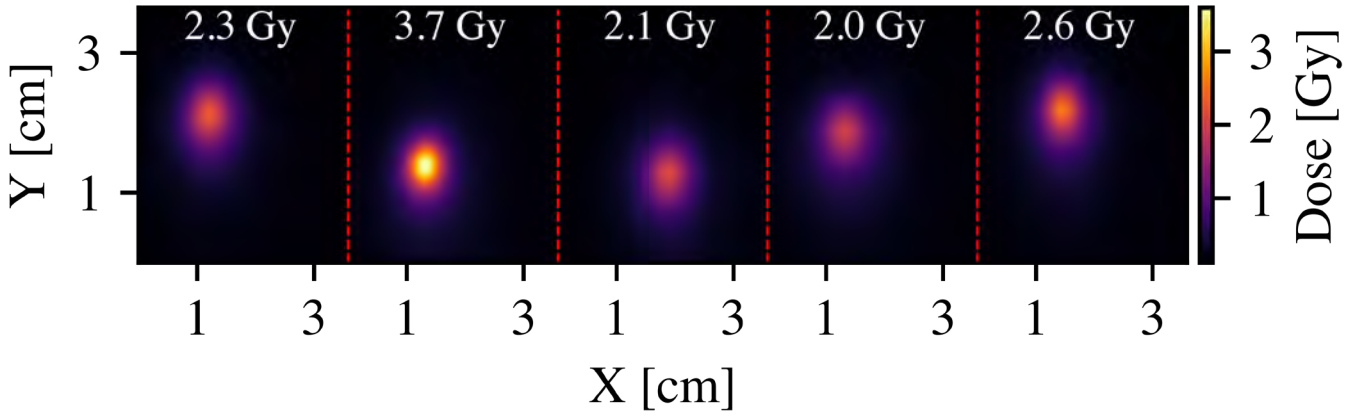

Dose profile and pointing stability for 5 consecutive shots after optimisation. The peak dose for each shot is printed in white. Consecutive shots are separated by a dashed red line.

Characterisation of an all-optical inverse Compton scattering source for industrial imaging

We report on the production of an all-optical inverse Compton scattering (ICS) source for industrial imaging, generated using a two-laser configuration. Successful laser-electron ICS interactions were obtained for electron energies up to ~1 GeV, with numerical estimates suggesting photon energies in the range of approximately 1 - 10 MeV were achieved. The duration of the photon bunch can be estimated as 50 fs, with a source size on the order of 10 μm. Imaging of reference line pairs was used to demonstrate a resolution of 170 μm, highlighting the unique advantages of this source. A copper test object was used to demonstrate the capability for high energy tomographic scanning.

Authors: C.A. McAnespie, M.J.V. Streeter, L. Calvin, N. Cavanagh, K. Fleck, G. Sarri, B. Kettle, O. Finlay, K. Fedorov, C.D. Armstrong, S.J.D. Dann, B. Spiers, D.R. Symes, W. Sun, J.M. Warnett, E. Kiely

Contact author: C.A. McAnespie (cmcanespie01@qub.ac.uk)

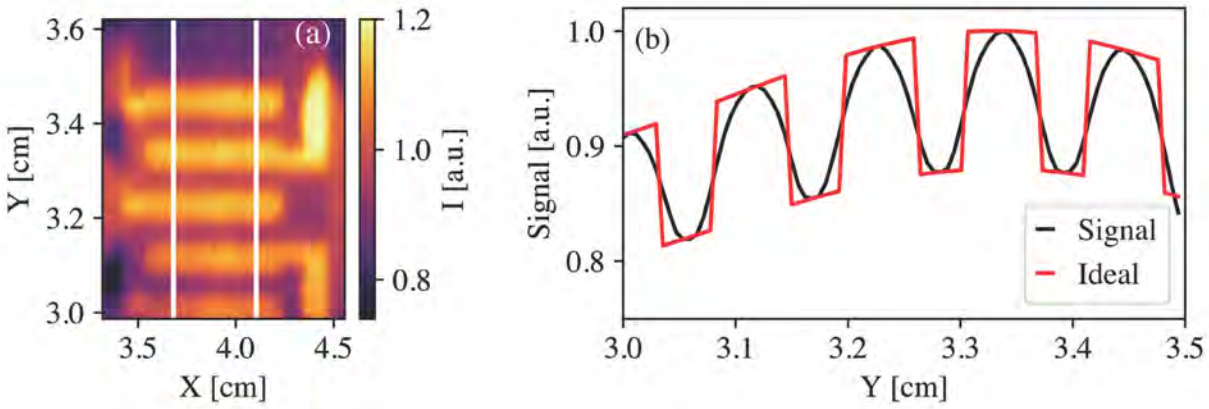

Figure 1: (a): Single shot projection of the resolution grid taken with a magnification of 1.75. The dark and light features highlighted between the two white lines are 400 μm line pairs. (b) The signal (black) averaged between the white banded region of (a). An ideal projection with infinite resolution and zero source size is given in red.

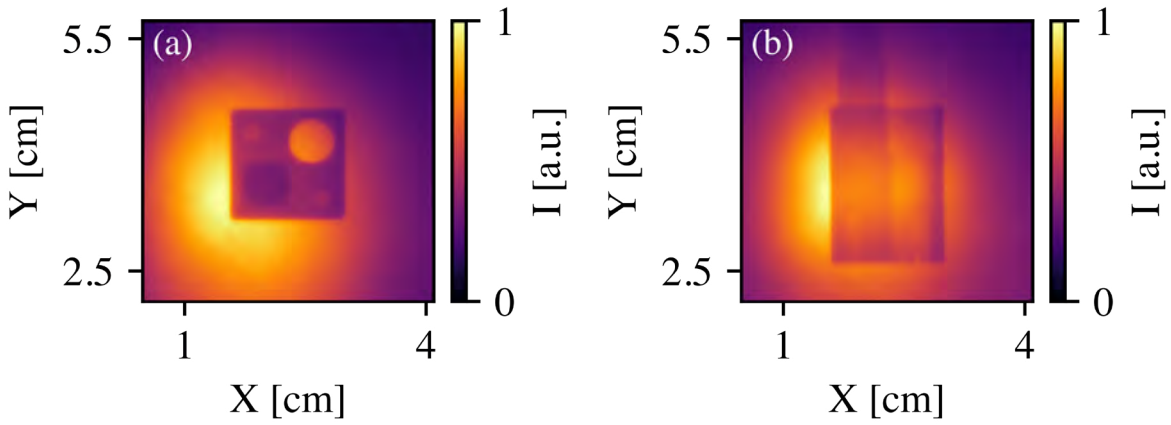

Figure 2: (a) Raw projection at 0 degrees; (b) raw projection at 90 degrees. A filter has been used to remove hot pixels from hard x-ray hits.

Versatile tape-drive for high-repetition-rate laser-driven proton acceleration

We present the development and characterization of a high-stability, multi-material, multi-thickness tape-drive target for laser-driven acceleration at repetition rates of up to 100 Hz. The tape surface position was measured to be stable on the sub-micrometre scale, compatible with the high-numerical aperture focusing geometries required to achieve relativistic intensity interactions with the pulse energy available in current multi-Hz and near-future higher repetition-rate lasers (> kHz). Long-term drift was characterized at 100 Hz demonstrating suitability for operation over extended periods. The target was continuously operated at up to 5 Hz in a recent experiment for 70,000 shots without intervention by the experimental team, with the exception of tape replacement, producing the largest data-set of relativistically intense laser-solid foil measurements to date. This tape drive provides robust targetry for the generation and study of high-repetition-rate ion beams using next-generation high-power laser systems, also enabling wider applications of laser-driven proton sources.

Reproduced from Xu N, Streeter MJV, Ettlinger OC, et al. High Power Laser Sci. Eng. ***11****, e23 (2023), under the terms of the Creative Commons Attribution 4.0 licence doi: 10.1017/hpl.2023.27*

Authors: N. Xu, O.C. Ettlinger, N.P. Dover, G.S. Hicks, Z. Najmudin, M.J.V. Streeter, M. Borghesi, C. Hyland, B. Loughran, O. McCusker, P. Parsons, C.A.J. Palmer, H. Ahmed, S. Astbury, N. Bourgeois, S.J.D. Dann, T. Dzelzainis, J.S. Green, C. Spindloe, D.R. Symes, C.B. Curry, V. Istokskaia, M. Gauthier, S.H. Glenzer, L. Giuffrida, G.D. Glenn, R.J. Gray, M. King, P. McKenna, D. Margarone, C. Parisuaña, F. Treffert

Contact author: C.A.J. Palmer (c.palmer@qub.ac.uk)

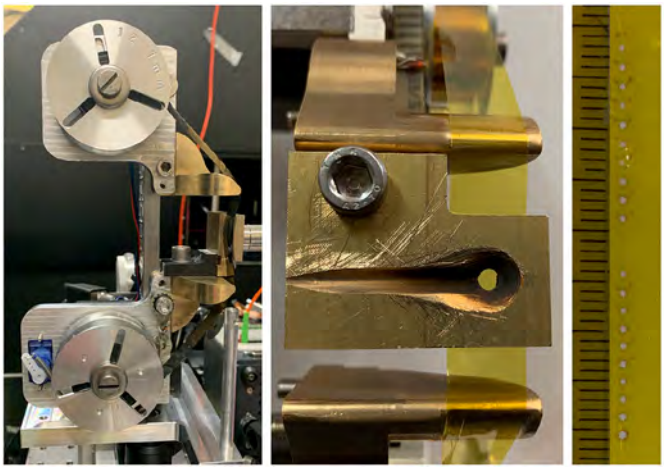

Figure 1: (left) Photograph showing the spools of the drive and the brass frame supporting the tape; (centre) photograph showing tape running vertically on the brass supports. The interaction point is at the centre of the hole, with a groove cut away to provide diagnostic access; (right) photograph of the tape after a series of shots with 400 mJ laser energy. The hole diameters are less than 1 mm diameter and spaced by approximately 2 mm when operating at a linear speed of 2 mm/s. The hardware is capable of speeds exceeding 500 mm/s.

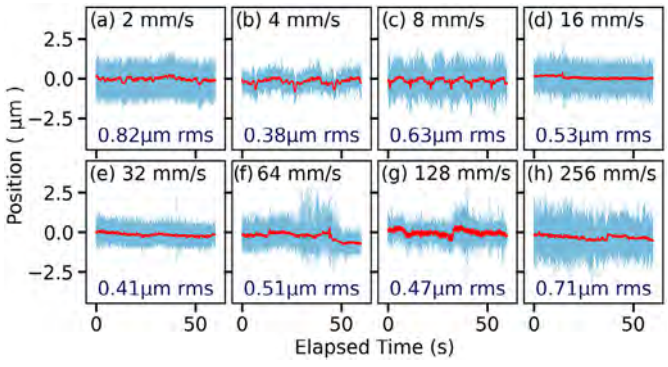

Figure 2: Tape positional jitter across a range of speeds over 1 minute operation. Low frequency movement (< 1 Hz), better representing the tape motion, is shown with the red line and the RMS variation in position is quoted in each subplot. In (c), the oscillations correspond to a resonance of the tape-drive structure. Faster speeds (> 8 mm/s) typically result in lower jitter amplitude because of reduced stepper motor vibration.

Characterization of laser wakefield acceleration efficiency with octave spanning near-IR spectrum measurements

We report on experimental measurements of energy transfer efficiencies in a GeV-class laser wakefield accelerator. Both the transfer of energy from the laser to the plasma wakefield and from the plasma to the accelerated electron beam was diagnosed by simultaneous measurement of the deceleration of laser photons and the acceleration of electrons as a function of plasma length. The extraction efficiency, which we define as the ratio of the energy gained by the electron beam to the energy lost by the self-guided laser mode, was maximized at 19 ± 3% by tuning the plasma density and length. The additional information provided by the octave-spanning laser spectrum measurement allows for independent optimization of the plasma efficiency terms, which is required for the key goal of improving the overall efficiency of laser wakefield accelerators.

*Reproduced from MJV Streeter et al. Phys. Rev. Accel. Beams **25**, 101302 (2022), published by the American Physical Society under the terms of the Creative Commons Attribution 4.0 licence doi: 10.1103/PhysRevAccelBeams.25.101302*

Authors: M.J.V. Streeter, Y. Ma, A.G.R. Thomas, B. Kettle, E. Gerstmayr, J.M. Cole, S.P.D. Mangles, Z. Najmudin, S.J.D. Dann, F. Albert, N. Lemos, N. Bourgeois, P.P. Rajeev, D.R. Symes, S. Cipiccia, I. Gallardo González, O. Lundh, A.E. Hussein, D.A. Jaroszynski, R. Spesyvtsev, G. Vieux , M. Shahzad, K. Falk, K. Krushelnick, R. Sandberg, N.C. Lopes, C. Lumsdon, M. Smid

Contact authors: M.J.V. Streeter (m.streeter@qub.ac.uk)

A.G.R. Thomas (agrt@umich.edu)

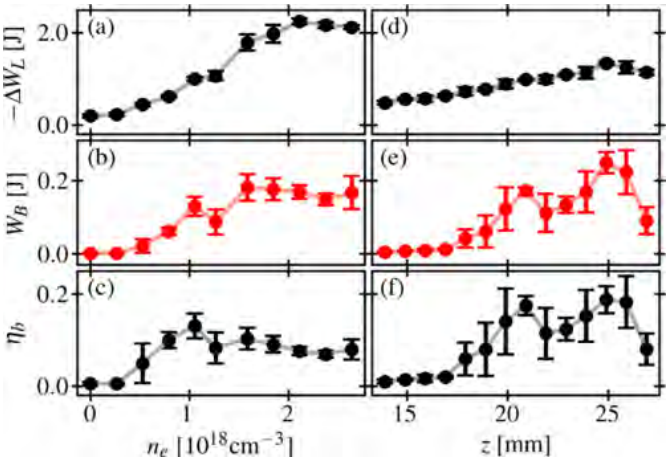

Figure 1: Laser energy loss, electron beam energy, and extraction efficiency as functions of plasma density for z = 27 mm (a)–(c), and length (d)–(f) with n_e = 1.25 x 10^{18} cm^{-3}.

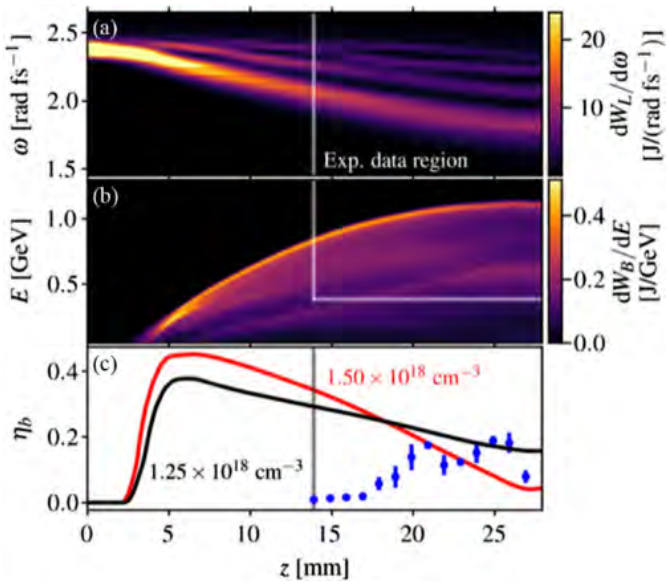

Figure 2: (a) Laser and (b) electron spectra as functions of propagation distance taken from a PIC simulation with a plateau density of n_e = 1.25 x 10^{18} cm^{-3}. (c) The extraction efficiency, calculated as the ratio of the electron beam energy to the laser energy loss, for simulations with n_e = (1.25, 1.5) x 10^{18} cm^{-3} and the experimental measurements (blue points) at n_e = 1.25 x 10^{18} cm^{-3}.

Laser wakefield accelerator modelling with variational neural networks

A machine learning model was created to predict the electron spectrum generated by a GeV-class laser wakefield accelerator. The model was constructed from variational convolutional neural networks, which mapped the results of secondary laser and plasma diagnostics to the generated electron spectrum. An ensemble of trained networks was used to predict the electron spectrum and to provide an estimation of the uncertainty of that prediction. It is anticipated that this approach will be useful for inferring the electron spectrum prior to undergoing any process that can alter or destroy the beam. In addition, the model provides insight into the scaling of electron beam properties due to stochastic fluctuations in the laser energy and plasma electron density.

Reproduced from M.J.V. Streeter et al., High Power Laser Science and Engineering, vol. 11, p. e9, 2023, published by the Cambridge University Press under the terms of the Creative Commons Attribution 4.0 licence doi: 10.1017/hpl.2022.47

Authors: M.J.V. Streeter, L. Calvin, N. Cavanagh, G. Sarri, C. Colgan, E.E. Los, R. Watt, E. Gerstmayr, B. Kettle, Z. Najmudin, S.P.D. Mangles, C.C. Cobo, C. Arran, C.D. Murphy, C.P. Ridgers, N. Bourgeois, S.J.D. Dann, P. Parsons, P.P. Rajeev, D.R. Symes, J. Carderelli, R. Fitzgarrald, Q. Qian, A.G.R. Thomas, A.S. Joglekar, P. Mckenna

Contact author: M.J.V. Streeter (m.streeter@qub.ac.uk)

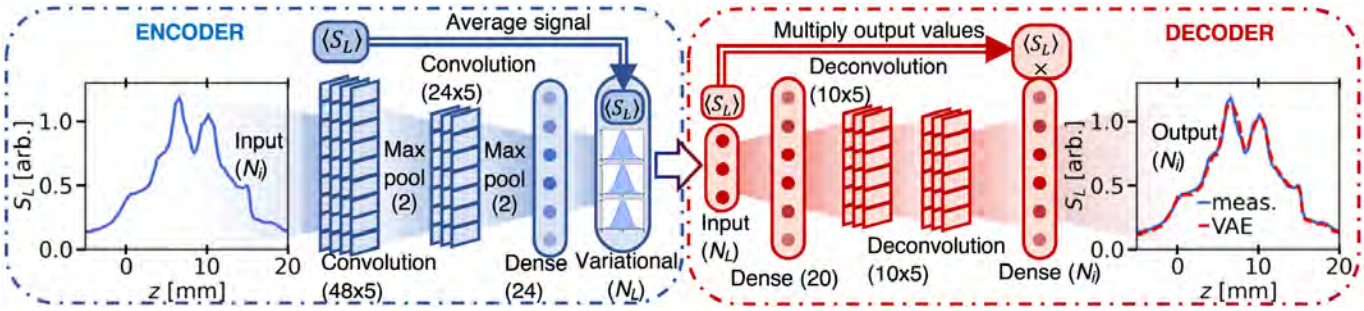

Variational autoencoder (VAE) architecture for determining the latent space representation of the diagnostics. The type and dimension of each layer are indicated in the labels. The inset plots show an example laser scattering signal S_L and the approximation returned by the VAE. The input (and output) size N_i is equal to the data binning of the results for each individual diagnostic. Max pooling was used at the output of each convolution layer, which combined neighbouring output pairs and returned only the maximum of each pair. The average signal, in this case $\langle S_L \rangle$ was passed as an additional latent space parameter for the encoder and was used to scale the output of the decoder. The autoencoder structure was the same for each diagnostic, except for the size of the latent space.

The role of transient plasma photonics structures in plasma-based amplifiers

High power lasers have become useful scientific tools, but their large size is determined by their low damage-threshold optical media. A more robust and compact medium for amplifying and manipulating intense laser pulses is plasma. Here we demonstrate, experimentally and through simulations, that few-millijoule, ultra-short seed pulses interacting with 3.5 J counter-propagating pump pulses in plasma, stimulate back-scattering of nearly 100 mJ pump energy with high intrinsic efficiency, when detuned from Raman resonance. This is due to scattering off a plasma Bragg grating formed by ballistically evolving ions. Electrons are bunched by the ponderomotive force of the beat-wave, which produces space-charge fields that impart phase correlated momenta to ions. They inertially evolve into a volume Bragg grating that backscatters a segment of the pump pulse. This ultra-compact, two-step, inertial bunching mechanism can be used to manipulate and compress intense laser pulses. We also observe stimulated Compton (kinetic) and Raman backscattering.

Reproduced from Vieux, G., Cipiccia, S., Welsh, G.H. et al. The role of transient plasma photonic structures in plasma-based amplifiers. Commun Phys ***6****, 9 (2023) under the terms of the Creative Commons Attribution 4.0 licence doi: 10.1038/s42005-022-01109-5*

Authors: G. Vieux, B. Ersfeld, E. Brunetti, S. Cipiccia, B. Eliasson, C. Picken, G. McKendrick, M.P. Tooley, G.H. Welsh, S.R. Yoffe, D.A. Jaroszynski, F. Gärtner, M-S. Hur, J.M. Dias, T. Kühl, G. Lehmann

Contact authors: G. Vieux (g.vieux@strath.ac.uk)

D.A. Jaroszynski (d.a.jaroszynski@strath.ac.uk)

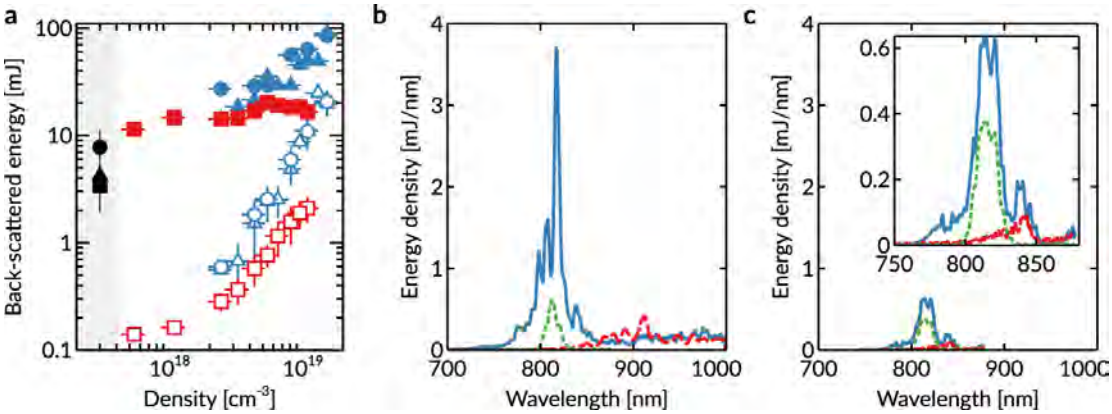

Main experimental results: **a** Back-scattered energy in the seed direction. Combined pump and seed shots are depicted by solid symbols, circle and triangle for positive frequency chirp, and square for negative frequency chirp. Empty symbols represent corresponding shots without the seed pulse i.e. scattering from noise. The different symbol shapes characterise different runs. The energy values are averages of three shots, with the error given as the standard deviation. Error on the inferred plasma density is estimated to be ±20%. Where the error bars are not visible, their lengths are smaller or equal to the symbol sizes. **b**, **c** are single-shot spectra. Solid (blue) line: seed spectrum after interaction; dotted (green) line: initial seed spectrum; dashed (red) line: spectrum of pump back-scattered signal without seed. Areas under the curves have been normalised to the measured energy, assuming that little energy falls outside the spectral window. **b** Pump with a positive frequency chirp, plasma density ~1.5×10^{19} cm^{-3} ($n_p/n_c \approx 8.6 \times 10^{-3}$); **c** Pump with a negative frequency chirp, plasma density ~10^{19} cm^{-3} ($n_p/n_c \approx 5.7 \times 10^{-3}$). The longest observable wavelength is ~880 nm because a different spectrometer grating was used compared to that in **b**. The inset in **c** displays the same data as **c** plotted on a magnified scale.

Laboratory study of the Biermann battery magnetic field compression in laser-produced plasma

In this work we present experimental results related to the collision of parallel magnetic fields and study the compression that ensues between them. For this, we use two dense, spatially separated, targets that are both irradiated by nanosecond laser beams. The generated magnetic fields, due to the Biermann battery effect close to the target surfaces, are clockwise with respect to the plasma expansion axis. The ablating plasmas radially expand and advect the aligned parallel magnetic fields to the interaction region between the targets. By shifting the targets along their normal, we enable these laterally expanding Biermann fields to collide, leading to magnetic field compression and accumulation in the gap between the targets. To resolve in time the topology of the compressed magnetic field we employ the proton deflectometry technique to diagnose each magnetic field and the magnetic field pile-up between the targets.

Authors: W. Yao, R. Lelièvre, J. Fuchs, H. Ahmed, D.C. Carroll, P. Antici, J. Béard, M. Borghesi, C. Fegan, P. Martin, A.F.A. Bott, S.N. Chen, A. Ciardi, E.D. Filippov, E. d'Humières, A. Sladkov, S. Pikuz

Contact author: J. Fuchs (julien.fuchs@polytechnique.edu)

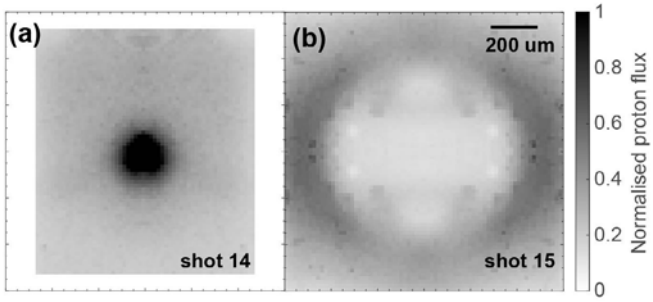

Figure 1: **Proton radiography results:** Experimental RCF measurements probing the single magnetic flux tubes produced on (a) target T2 or (b) target T1. Both images are snapshots taken at 1 ns.

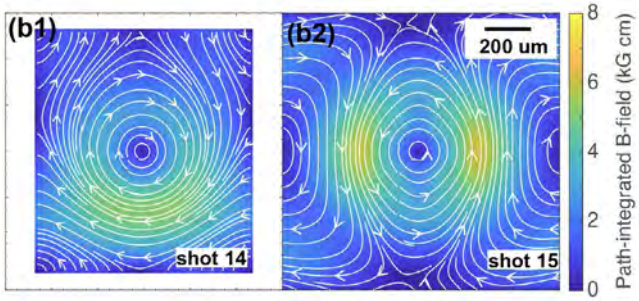

Figure 2: **Analysis of the RCF results:** Path-integrated magnetic field strength analysed via the code PROBLEM.[1] The white-arrow streamlines represent the in-plane magnetic field lines (Bx and By), and the colour-map shows the path-integrated (along the z-axis) strength of the xy-plane magnetic field.

[1] *Bott, A.F.A. et al. (2017) 'Proton imaging of stochastic magnetic fields', Journal of Plasma Physics, 83(6), p. 905830614. doi:10.1017/S0022377817000939*

High dose delivery in radiobiology experiments employing laser-driven protons

High energy protons accelerated by the Vulcan laser have been used, in several campaigns, to irradiate cells and investigate the biological effects of irradiations at ultra-high dose rates.

The use of a novel helical coil target design has enabled the production of highly collimated proton bunches, greatly increasing the dose delivered to the cells in the relevant energy ranges.

We discuss here the irradiation of cell samples using both the standard flat foil and helical coil target configurations, with the latter delivering very high doses to the cells of up to 70 Gy in a single irradiation. This large dose range enables clinically relevant studies of the effects of ultra-high dose rate on various cell types, in studies of potential relevance to the FLASH mechanism of radiotherapy and future approaches to cancer treatment.

Authors: P. Martin, O. Cavanagh, P. Chaudhary, C. Fegan, A. McCay, J. Morrow, S. Kar, M. Borghesi, K. Prise, H. Ahmed

Contact author: M. Borghesi (m.borghesi@qub.ac.uk)

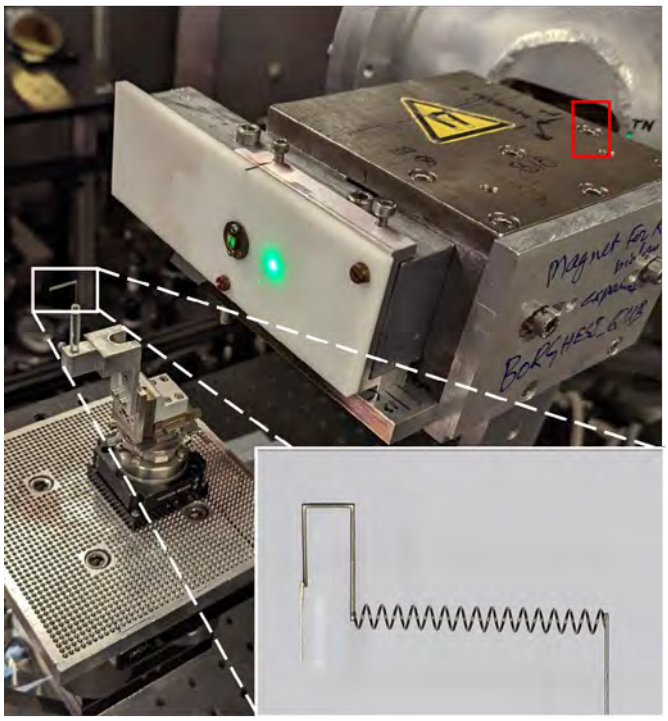

Figure 1: An image of the experimental setup for cell irradiation. A pinhole 8 cm from the target (indicated by the white box) leads into a dipole magnet, separating protons by their energy and leading to a Kapton window, behind which the cells are placed. The red box highlights the cell plane upon which 35 MeV protons were incident. Inset: Side view of a typical helical coil (HC) target used in the campaign, designed to produce a high flux of protons at around 35 MeV.

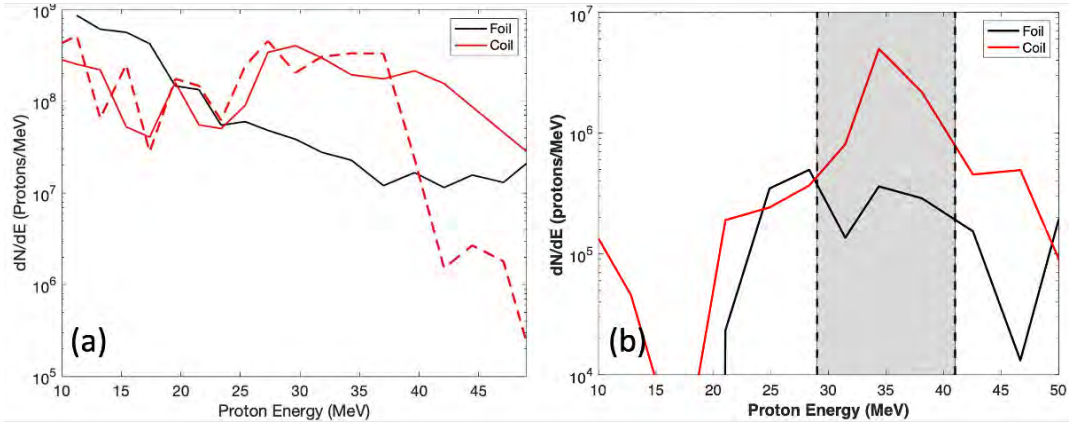

Figure 2: The proton spectrum from radiochromic film (RCF) for flat foils (black) and HC (red), with the RCF stack placed (a) before the magnet (~8 cm from the interaction point), and (b) after the magnet, at the cell plane. The dashed red line is a second HC shot, to demonstrate consistent flux around the 35 MeV point. The grey area indicates the approximate energy range by which the cells were irradiated.

Laser Science and Development

Generation of joule-level green bursts of nanosecond pulses from a DPSSL amplifier

A new approach to generation of a burst of high-energy green pulses by placing a high-energy multi-slab Yb:YAG DPSSL amplifier and SHG crystal inside a regenerative cavity is presented. In a proof-of-concept test, stable generation of a burst of six green (515 nm) pulses, each 10 ns in duration and separated by 29.4 ns (34 MHz), with 2.0 J total energy has been demonstrated at 1 Hz from a non-optimized ring cavity design. A maximum individual green pulse energy of 580 mJ was produced from a 1.78 J circulating infrared (1030 nm) pulse (average fluence 0.9 J/cm^2), corresponding to a SHG conversion efficiency of 32%. Experimental results have been compared with predicted performance from a simple model. Efficient generation of a burst of high energy green pulses offers an attractive pump source for Ti:Sa amplifiers, providing the potential to reduce the impact of amplified stimulated emission by reducing instantaneous transverse gain.

Authors: P.D. Mason, H. Barrett, S. Banerjee, T.J. Butcher, J.L. Collier

Contact author: P.D. Mason (paul.mason@stfc.ac.uk)

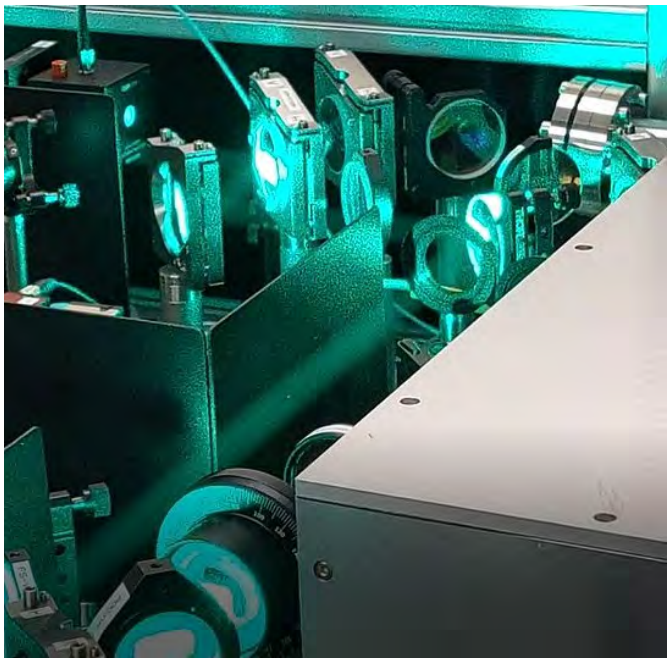

Modelling of thermally-induced stress birefringence in a 10 J, 100 Hz diode-pumped Yb:YAG laser

The high heat loads intrinsically associated with high energy, high repetition rate operation require sophisticated thermal management analyses to minimise the impact of thermal effects on laser performance. In particular, non-uniform heat deposition in optical components can lead to thermal aberrations and thermally-induced stress birefringence. This results in depolarisation of the beam, a deterioration of polarisation purity of a beam passing through the affected optic.

We present an overview and the results of thermal stress-induced depolarisation modelling of Yb:YAG gain medium slabs in a multipass, cryogenically-cooled, nanosecond, diode-pumped solid state laser operating at 10 J, 100 Hz for various input polarisation states. We expect these results to aid in the optimisation of future laser systems.

Authors: G. Quinn, D. Clarke, M. De Vido

Contact author: G. Quinn (gary.quinn@stfc.ac.uk)

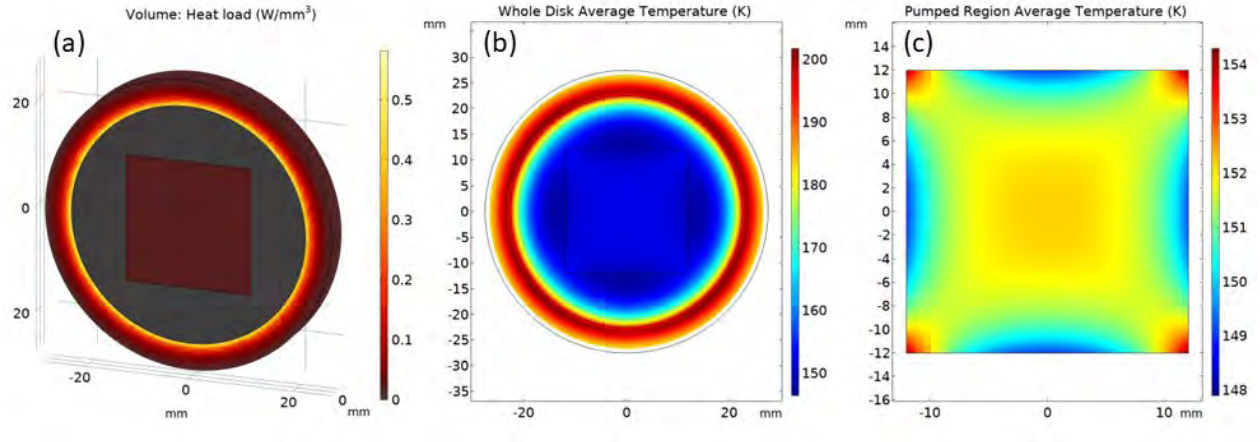

Figure 1: Simulation results showing the heat load distribution within the gain medium slab (a), the temperature distribution in the whole slab averaged over thickness (b), and the temperature distribution in the pumped region averaged over thickness (c)

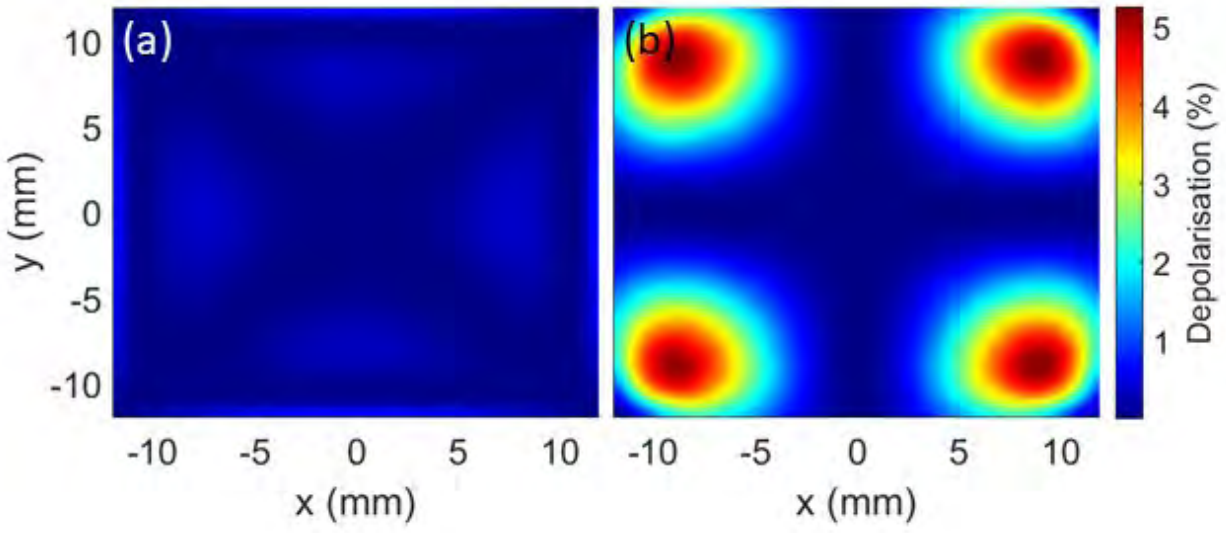

Figure 2: Simulation results showing the single pass depolarisation of a beam propagating through the six gain medium slabs in the amplifier head with an input polarisation state of 45° (a), and 0° (b)

Damage resilience testing of broadband thin-film coating for use in a high-energy Ti:Sa amplifier system

EPAC is a new research facility currently under development at the STFC Central Laser Facility in the UK. It will house a titanium-doped sapphire laser amplifier that will operate at a 10 Hz repetition rate to deliver compressed pulses of PW peak power for applications of laser-driven radiation and particle sources. To achieve this high power, it is key that optics are resilient to laser induced damage. We are performing independent in-house damage resilience tests to ensure that our standards are met.

We report results for broadband highly reflective coatings for the EPAC Ti:Sa amplifier, comparing samples from different suppliers and deposition techniques.

Authors: A.M. Wojtusiak, P.D. Mason, N. Bourgeois, R. Pattathil, C. Hernandez-Gomez

Contact author: A.M. Wojtusiak (agnieszka.wojtusiak@stfc.ac.uk)

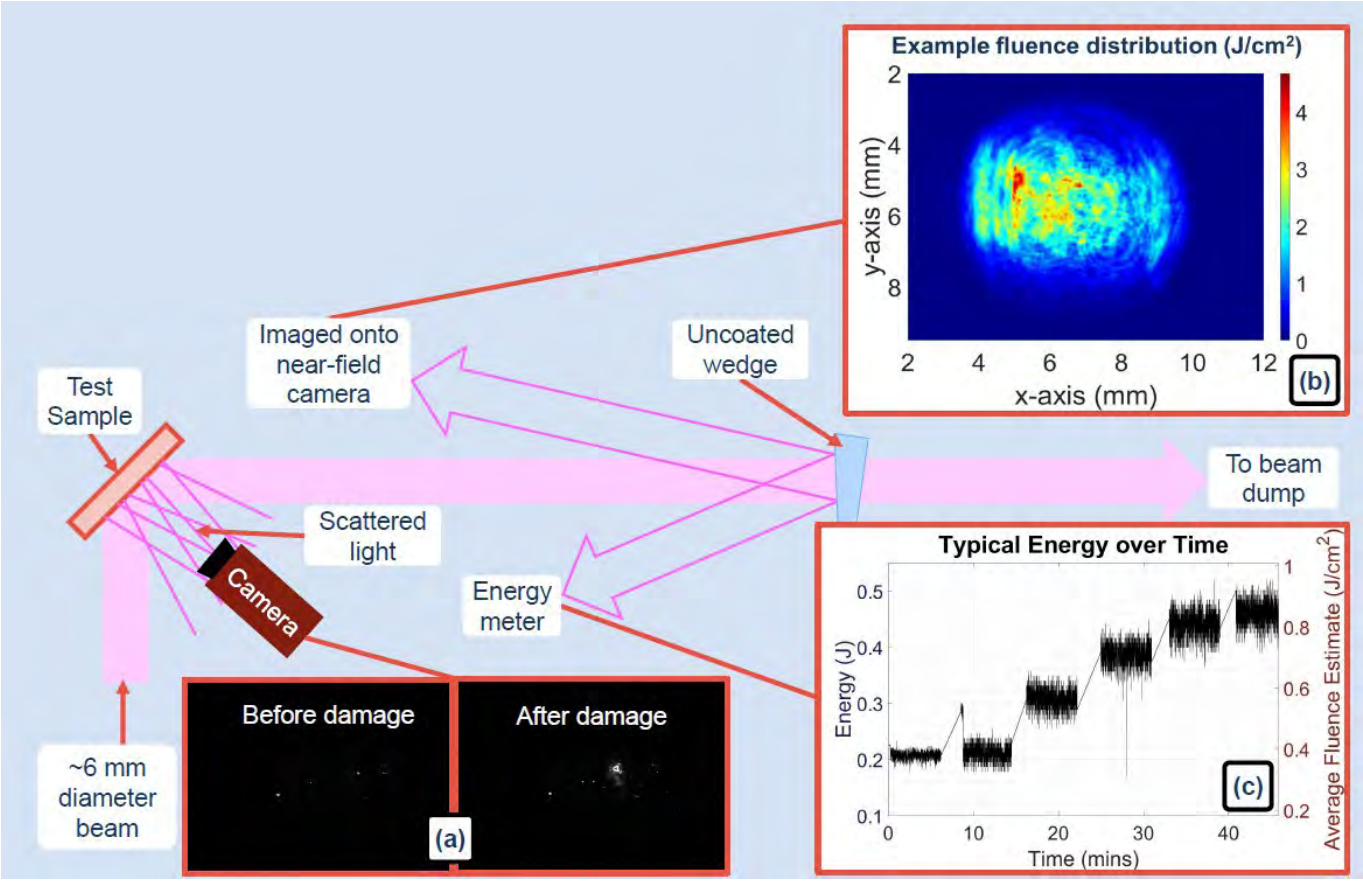

The key components of the test setup are shown here.

A CCD camera imaging light directly scattered from the test sample is used to detect initiation of damage. Insert (a) shows a typical view before and after damage has occurred.

Insert (b) shows an example of the beam profile that is relay imaged from the test sample onto another CCD camera. It also shows the fluence distribution for the maximum incident energy for that sample.

Insert (c) shows a typical graph of pulse energy over time, as well as an estimate of the average fluence – calculated by dividing the pulse energy by an estimate of the beam area.

High-integrity laser safety shutters for personnel interlocks

During the expansion of the Artemis facility, it emerged that innovative beam shutters were required to ensure safety across interconnected spaces. Specifically, wall-mounted shutters were needed to manage and block laser beam propagation between adjacent rooms, and a table/enclosure-mounted shutter variant was also needed for the optical tables. After a detailed specification process, it became apparent that there were no suitable commercial solutions, so a proprietary design was developed.

This new design features compact, lightweight, non-contact switches that are compatible with the CLF's high-integrity laser interlock safety system. These switches are used to monitor the open and closed states of a shutter's actuator. Extensive testing, encompassing nearly 600,000 simulated operations, has demonstrated that the shutters should be able to provide around 287 years of operation without the need for maintenance.

This innovative solution not only enhances operational longevity, but also aligns with the stringent safety requirements of advanced laser facilities.

Authors: S. Spurdle, R. Bickerton, T. Masarira

Contact author: R. Bickerton (richard.bickerton@stfc.ac.uk)

Figure 1: Wall-mounted shutter design

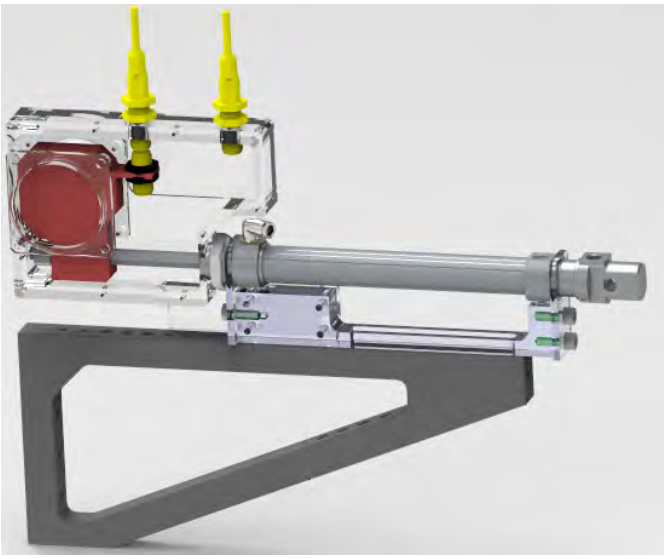

Figure 2: Table/enclosure-mounted shutter design

Laser diagnostic design for the EPAC EA1 beamline

Experimental Area 1 will house a long-focus PW laser beamline primarily designed for laser-wakefield acceleration, as reported in the previous CLF annual report.[1] Here, we describe the diagnostics that will be used to characterise and monitor the laser beam. The first measures the properties of the beam entering EA1, by taking a leakage through the final turning mirror in the beamline. The second characterises the laser pulse exiting the target, to provide spectral and spatial measurements of the beam after the plasma interaction. The optical arrangement attenuates and down-sizes the beam, then relay images onto near-field and far-field cameras, wavefront sensors, spectrometers, and energy meters.

The set-ups have been designed so that they can work both with low-power alignment modes and with the full laser energy. In this way they can be used for daily alignment as well as acting as on-shot references. Zemax software has been used to ensure aberration-free performance of the optical system.

[1] *D.R. Symes et al. EPAC Experimental Areas and Targetry Developments. CLF Ann. Rep. 2021-2022*

Authors: T. Dzelzainis, A. Stallwood, D.R. Symes

Contact author: T. Dzelzainis (thomas.dzelzainis@stfc.ac.uk)

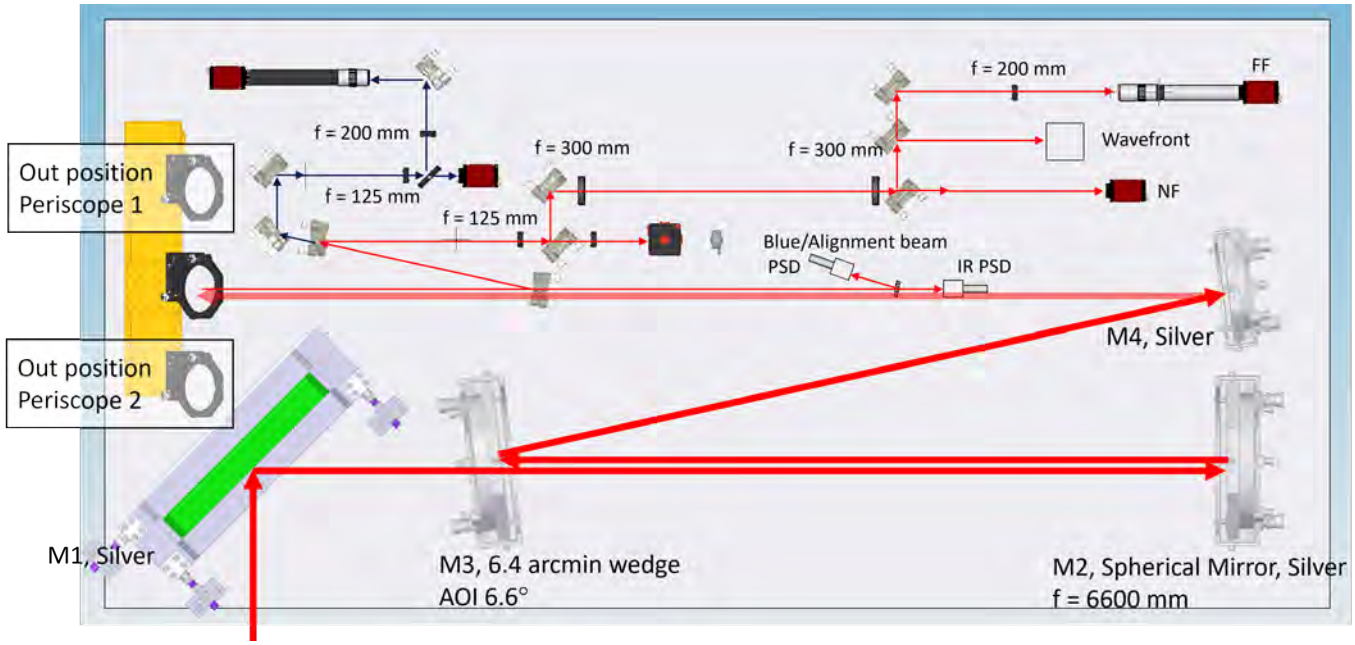

Figure 1: Proposed design for the diagnostic layout used for monitoring the beam entering the EA1 beamline

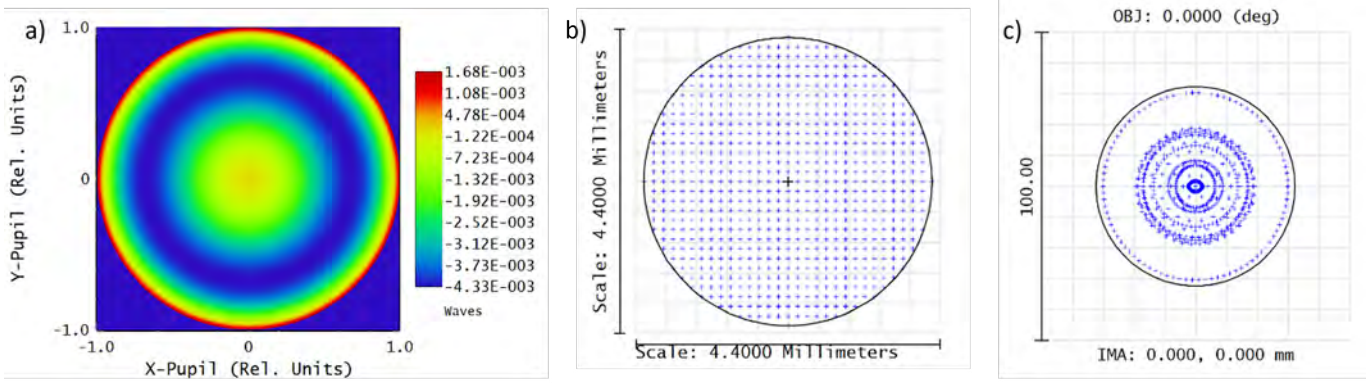

15 mm Aperture
RMS radius = 17 µm

Figure 2: (a) Wavefront map, (b) beam footprint, and (c) raytrace at the image plane of the main beam monitoring diagnostic

Bayesian Optimisation Guided PIC Simulations for EPAC

Experimental Area 1 at the Extreme Photonics Applications Centre (EPAC) will predominantly be used for electron acceleration in underdense plasmas. A mixture of permanent magnet and electromagnetic quadrupoles will be used to collect and transport electrons from the source to the application area or to diagnostics. To aid the design of the magnetic beamline, Particle-In-Cell (PIC) simulations have been performed to generate realistic electron beam outputs from the EPAC laser wakefield accelerator.

A high quality 1 GeV electron beam has been simulated and will be used as the input to magnetic tracking simulations.

Authors: O.J. Finlay, N. Bourgeois, D.R. Symes

Contact author: O. Finlay (oliver.finlay@stfc.ac.uk)

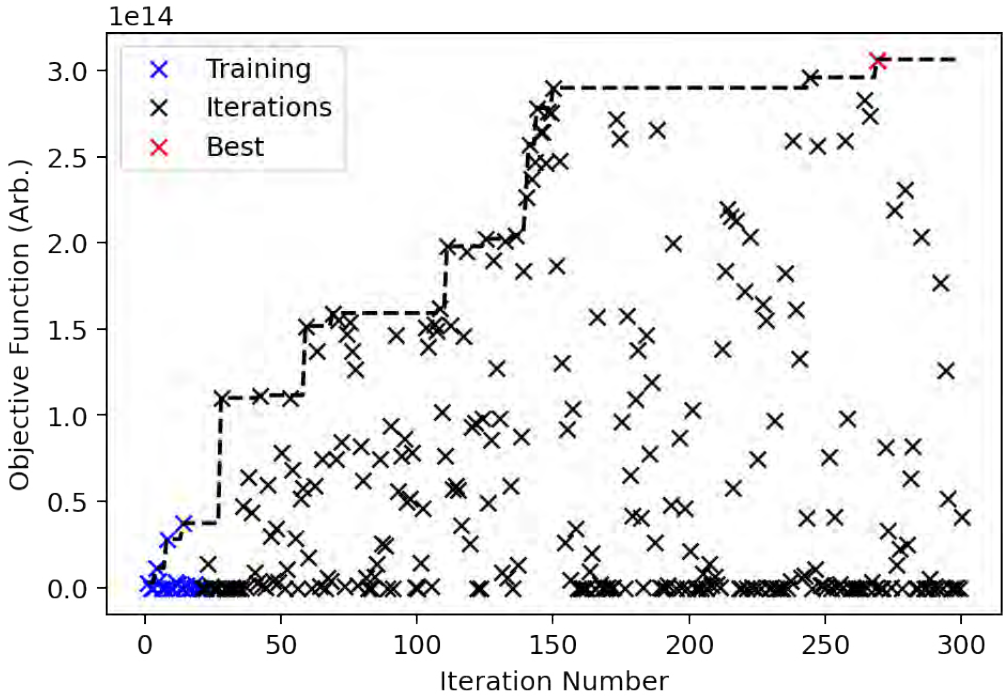

Figure 1: Objective function plotted against iteration number for a PIC simulation optimisation run

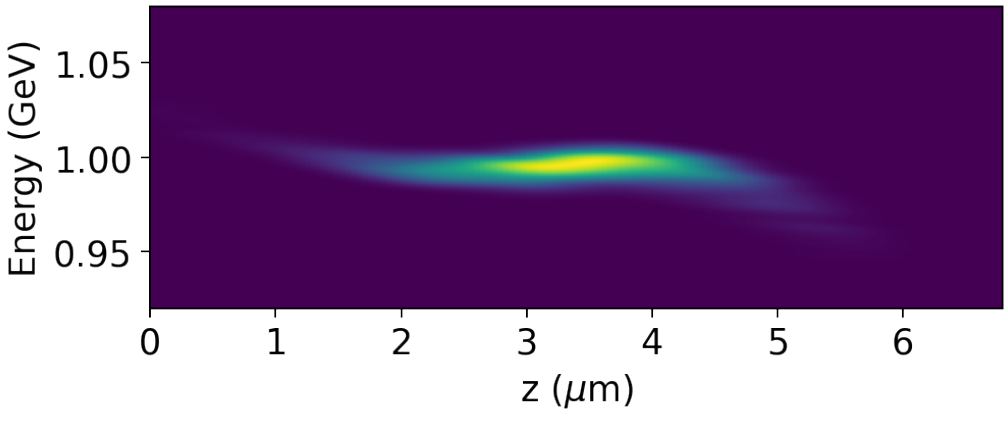

Figure 2: The longitudinal phase space of the optimised electron bunch

Vibration Survey and Analysis on EPAC Support Structures for Stability

This report presents the vibration survey for the new EPAC building, and the structure stability analysis for support structures and breadboards in the EPAC system.

The vibration survey was carried out after the construction of the EPAC building was finished, and before any laser equipment/ instruments were installed. This allowed the vibration of the building to be investigated and provided important data for future analysis in the EPAC system design. In addition, stability analysis was performed for critical structures including the high-level upper chamber and a breadboard for the target chamber. Vibration levels were investigated with the nearby ISIS laser facility both operating and not operating.

The results have enabled engineers to understand the dynamic behaviour of the key structures and evaluate the impact of vibration on the laser systems.

Authors: Z. Pan, S. Tomlinson, J. Bourne, N. Krumpa, A. Stallwood

Contact author: S. Tomlinson (steph.tomlinson@stfc.ac.uk)

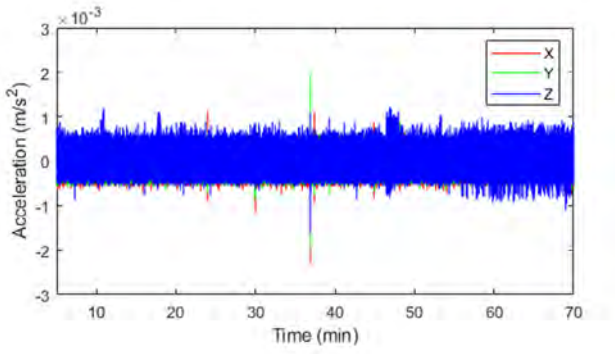

Figure 1: The acceleration of data captured on 26 July 2022 (nearby ISIS facility operating) shows that overall acceleration amplitudes across Experimental Area 1 are low, suggesting that the prevailing background vibration in the building is very low

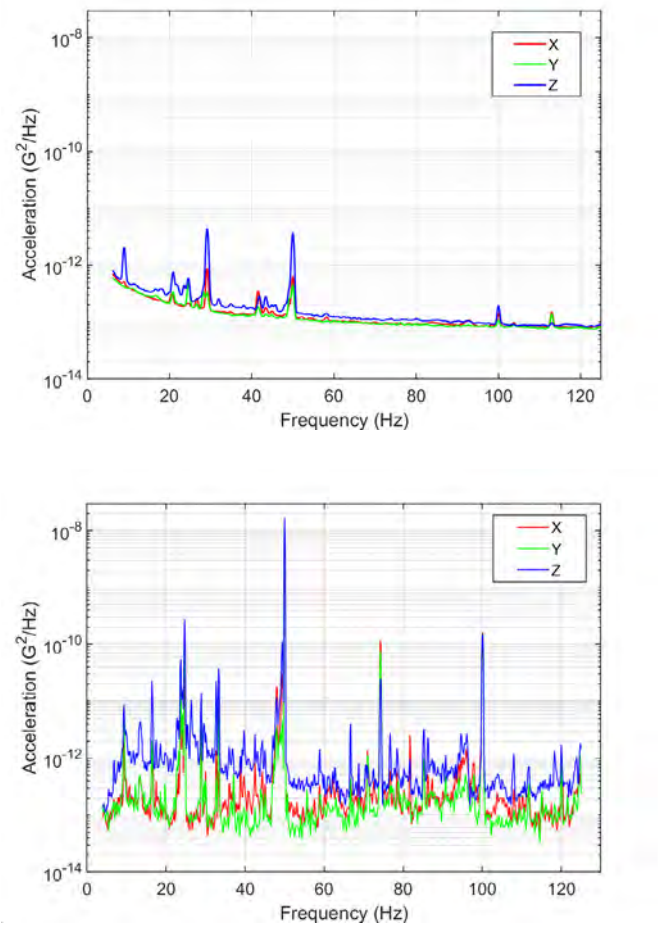

Figure 2: Measured power spectral density (PSD) for (top) Experimental Area 1 and (bottom) the Gemini area, captured with ISIS operational. The spectrum for EPAC is cleaner, with the peaks around 25, 50 and 100 Hz notably lower than those in the Gemini area.

High-repetition rate LWFA system in Gemini Target Area 2

During 2024/2025, in collaboration with our user community, we will use Gemini Target Area 2 (TA2) to carry out research and development necessary for prototyping and delivering EPAC. Construction of the LWFA beamline in TA2 will allow us to test components, and develop new techniques, in an iterative way that is not possible during short access slots on an operational user facility. We aim to continue studies of beam optimization through manipulation of a variety of factors, including plasma density, acceleration length, and laser pulse shape.

In this report, we describe elements of the experimental setup that have been developed for this purpose: the TA2 laser system and laser performance, the LWFA equipment, and available LWFA manipulation mechanisms.

Authors: K. Fedorov, D.R. Symes, C.D. Armstrong, S. Devadesan, O. Finlay, S.J.D. Dann, C. Selig, B. Spiers, N. Bourgeois, T. Dzelzainis. W. Robins, Z. Athawes-Phelps, R. Sarasola, D. Bloemers, I. Symonds, B. Morkot, A. Thomas, R. Lyon, T. Pocock, A. Gunn, T. Pacey, Y. Saveliev, S. Mathisen, A. Bhardwaj, R. Sugumar

Contact author: K. Fedorov (kirill.fedorov@stfc.ac.uk)

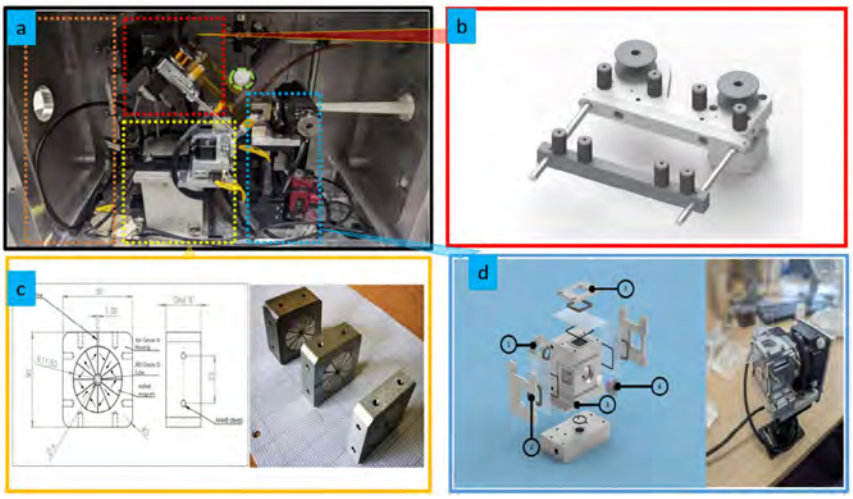

Figure 1: (a) The internal interaction chamber, colour-coded as follows: orange – space reserved for dielectric streaker; red – kapton tape drive/beam dump (shown in (b)); yellow – Halbach quadrupole magnet (shown in (c)) on XYZ translational stage; blue – gas-cell; (d) LEFT: Gas-cell assembly design: 1 – entrance aperture; 2 – probe beam diagnostics window; 3 – gas-cell volume; 4 – replaceable exit aperture MACOR plate; 5 – top view window; RIGHT: Assembly with a motorized stage to control gas-cell length

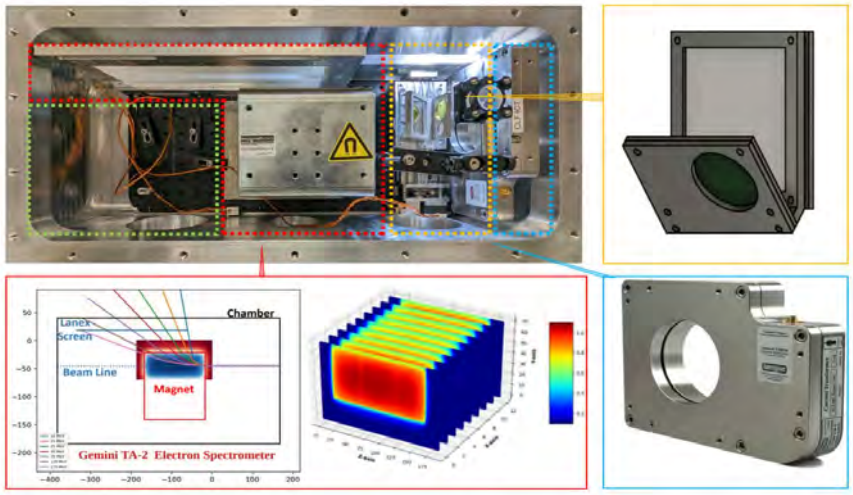

Figure 2: The diagnostics chamber developed to house specific diagnostics, colour-coded as follows: green – space reserved for tomography sample; red – electron spectrometer; orange – YAG:Ce scintillator screen; blue – integrated current transformer (Bergoz turbo-ICT)

Software developments in Gemini

The Gemini laser system's software undergoes upgrades to enhance control measures and facility monitoring. Leveraging EPICS enables the integration of diverter mirrors, pickoffs, and attenuators into the control system, streamlining experiment processes and enhancing safety. Expanded EPICS process variables (PVs) facilitate comprehensive facility-wide parameter monitoring, aiding in system health assessment. The redesigned facility monitoring application, penguin, provides real-time insights into system performance and experiment progress. These advancements optimize control and monitoring, ensuring safer and more efficient experimental operations.

Author: V.A. Marshall

Contact author: V.A. Marshall (victoria.marshall@stfc.ac.uk)

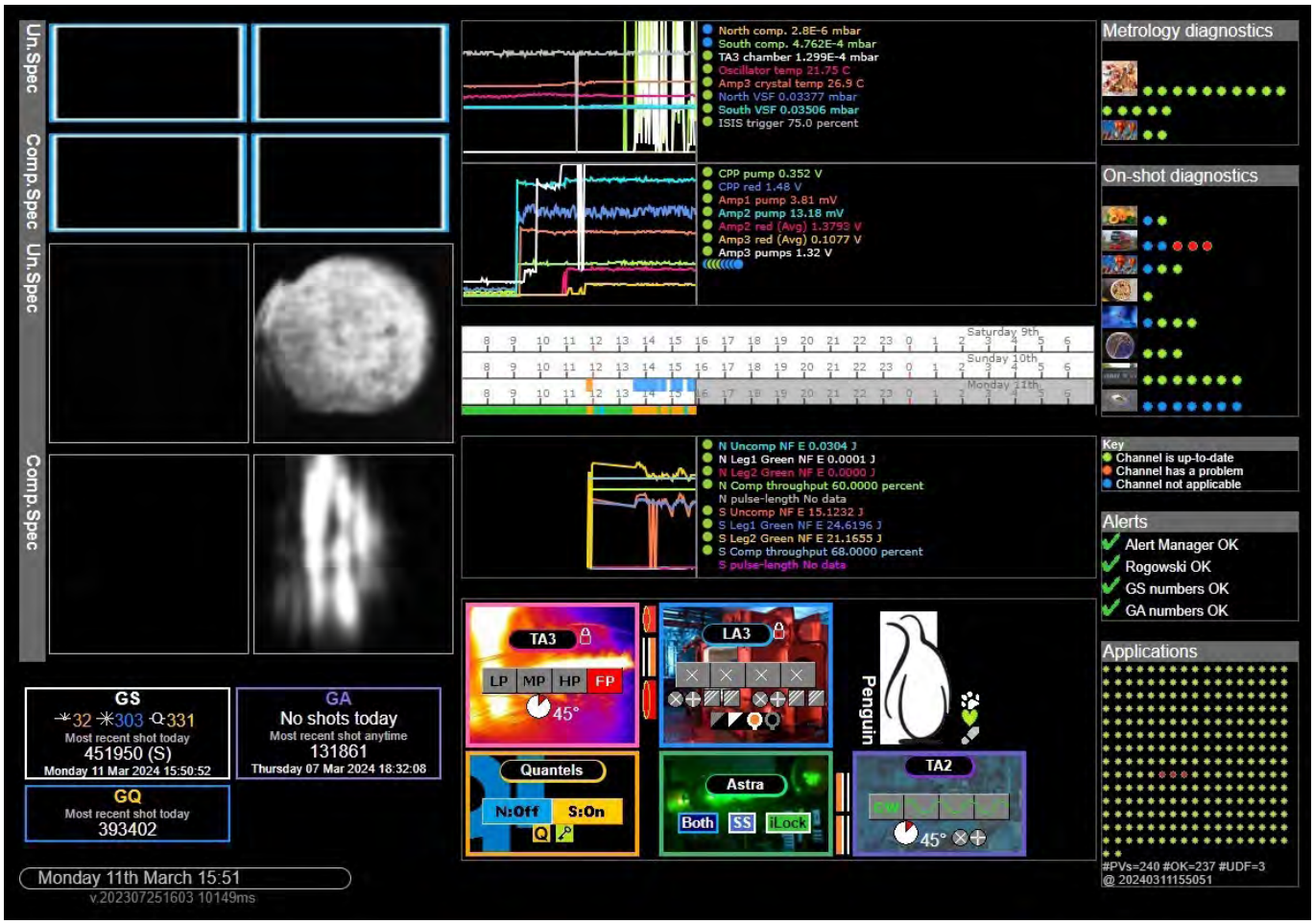

Screenshot of the main facility monitoring application – *penguin* – web page, which has been restructured and rewritten to take advantage of new features

Gemini timing drift stabilisation

A new method of analysis was implemented to improve timing drift stabilisation on Gemini, measuring delay on individual measurements of drift with an uncertainty of 9 fs. Code was written to move the split and delay stage in order to compensate for drift; in typical operating conditions, delay due to drift was kept smaller than delay due to shot-to-shot jitter.

Authors: P. Parsons, N. Bourgeois

Contact author: P. Parsons (pparsons03@qub.ac.uk)

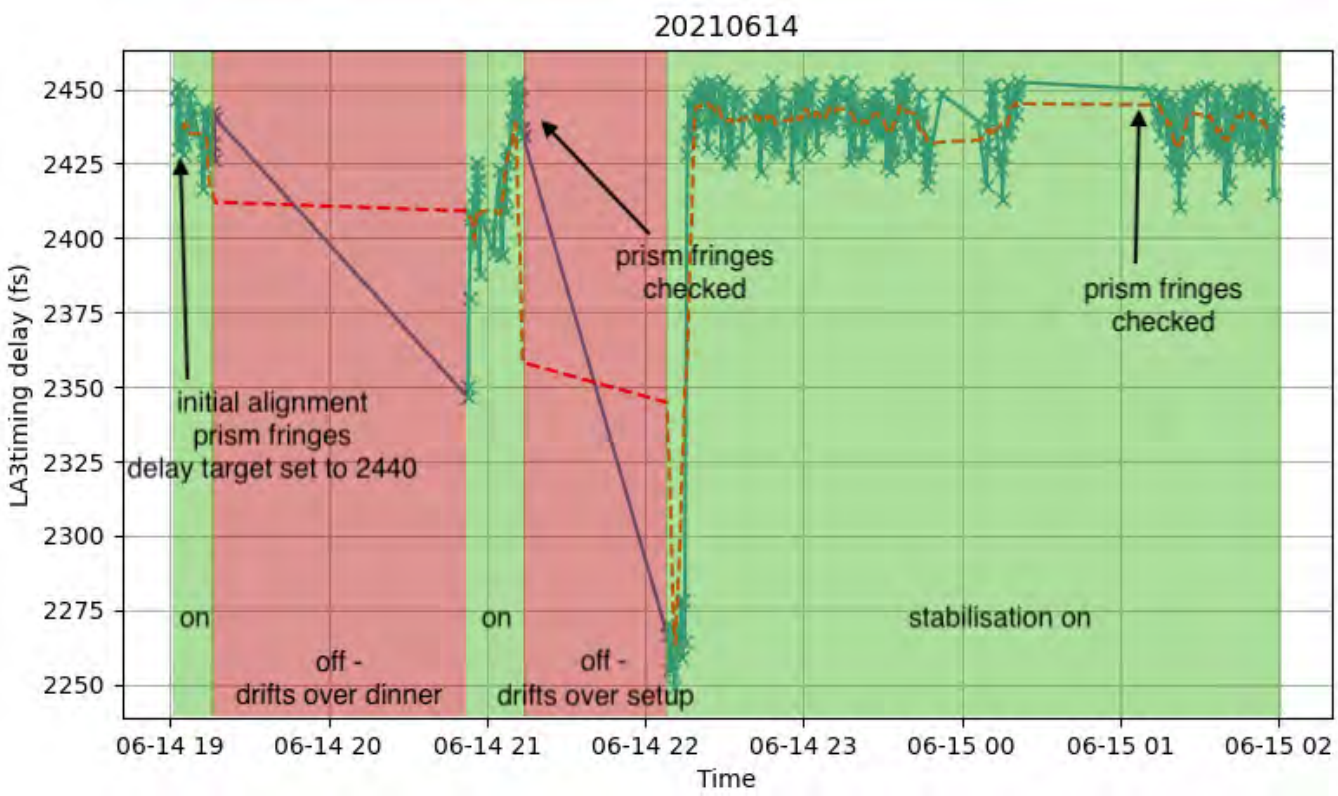

The delay between the two beams as measured in the laser area, LA3, against time. The green crosses are full power shots, and the red line is the 15 shot average. The timing stabilisation code was set to keep the drift at 2440 fs and was running except for the two red sections at about 7:15pm and 9:15pm. 'Prism fringes checked' refers to confirming the delay by measuring it in the target area with using a prism and spatial interference – these gave a similar values to the timing diagnostic in LA3.

Graph courtesy of C. Colgan, Imperial College London

Commissioning Progress of the New Petawatt Beamline in Vulcan

A new, short pulse petawatt beamline was successfully installed into R1 to accompany the Vulcan laser. The layout and progress are discussed, with the various commissioning challenges and accomplishments.

Authors: S. Buck, V. Aleksandrov, P. Oliveira, M. Tobiasiewicz, T. Winstone, M. Woodward, M. Galimberti

Contact author: S. Buck (samuel.buck@stfc.ac.uk)

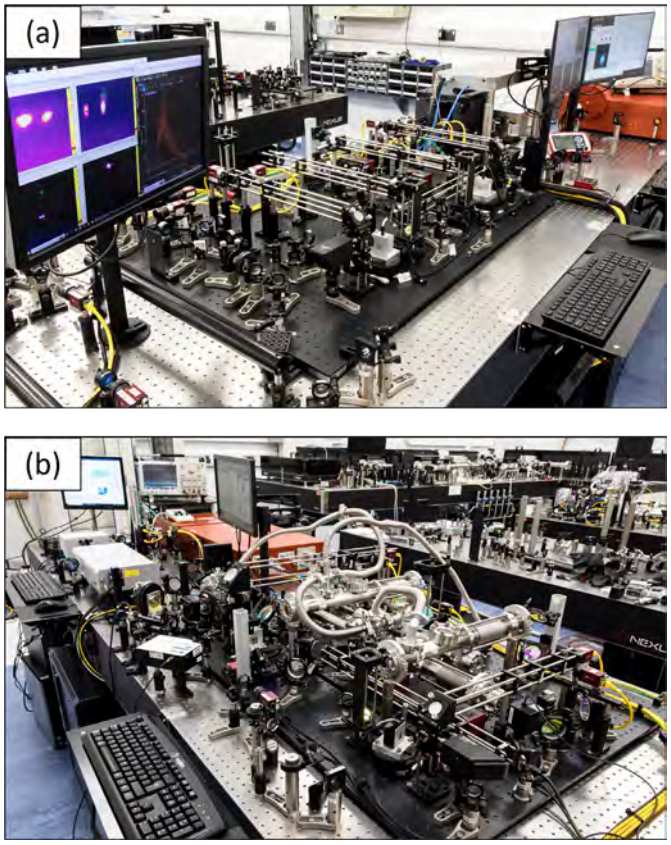

Figure 1: Picosecond front end of the VOPPEL beamline: (a) Stages 1 and 2, (b) Stages 3 and 4

Figure 2: Three-tier table installed in LA4. A large-aperture (90 mm) LBO OPA stage on the bottom level will be pumped by a frequency-converted Vulcan long pulse beam, delivered from the top level.

Single shot autocorrelator for the emPULS laser system

In the Laboratory for Advanced Analytical Technologies of the Swiss Federal Laboratories for Materials Science (Empa), a new terawatt laser facility (emPULS) is under development. The system is a CPA architecture based on Nd:phosphate flash pumped amplifier, similar to the rod chain of the Vulcan laser system. Within the scientific collaboration, a single shot autocorrelator was setup, following the successful design of the pulse front tilt single shot autocorrelator developed at CLF.[1]

[1]*Gonçalo Figueira et al. "Simultaneous measurement of pulse front tilt and pulse duration with a double trace autocorrelator," J. Opt. Soc. Am. B 36, 366-373 (2019). doi: 10.1364/JOSAB.36.000366*

Authors: Y. Hemani, D. Bleiner, M. Galimberti

Contact author: M. Galimberti (marco.galimberti@stfc.ac.uk)

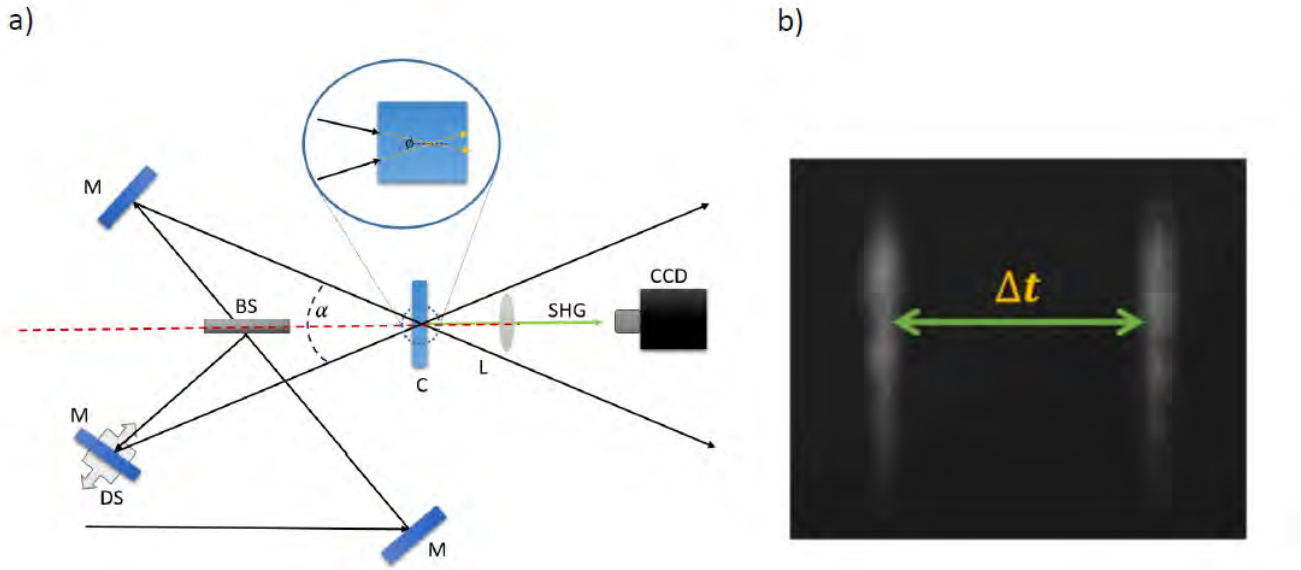

Figure 1: a) Optical design of a single shot auto correlator. It consists of: three mirrors (M), of which one is on a delay stage (DS); a beam splitter (BS); a non-linear crystal (C); a focusing lens (L); and camera (CCD). b) An example of an auto-correlator measurement is shown. The separation between two reflected pulses is indicated.

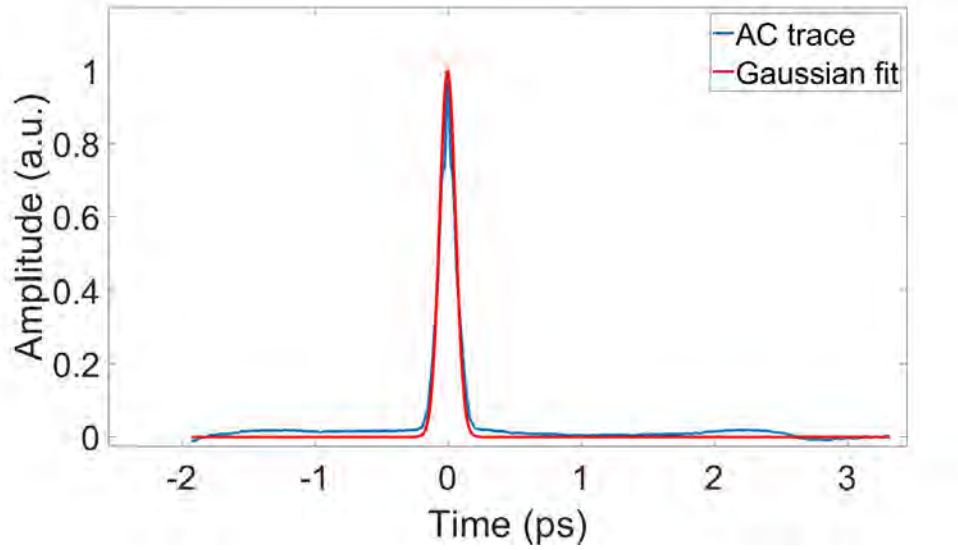

Figure 2: The calibrated autocorrelation trace collected from the camera is shown (in blue), with its Gaussian fit (in red)

Reduction of electrical noise on diode trace measurements via a pulse replicator

A low cost and easy to implement solution to increase the signal to noise ratio in single shot measurements is presented. Pulse replicas are created and redistributed to the same photodiode/oscilloscope combination. Averaging those replicas reduces the electrical noise in the pulse shape. We present simulation and experimental results including a calibration of the instrument.

Authors: A. Mayouf, P. Oliveira

Contact author: P. Oliveira (pedro.oliveira@stfc.ac.uk)

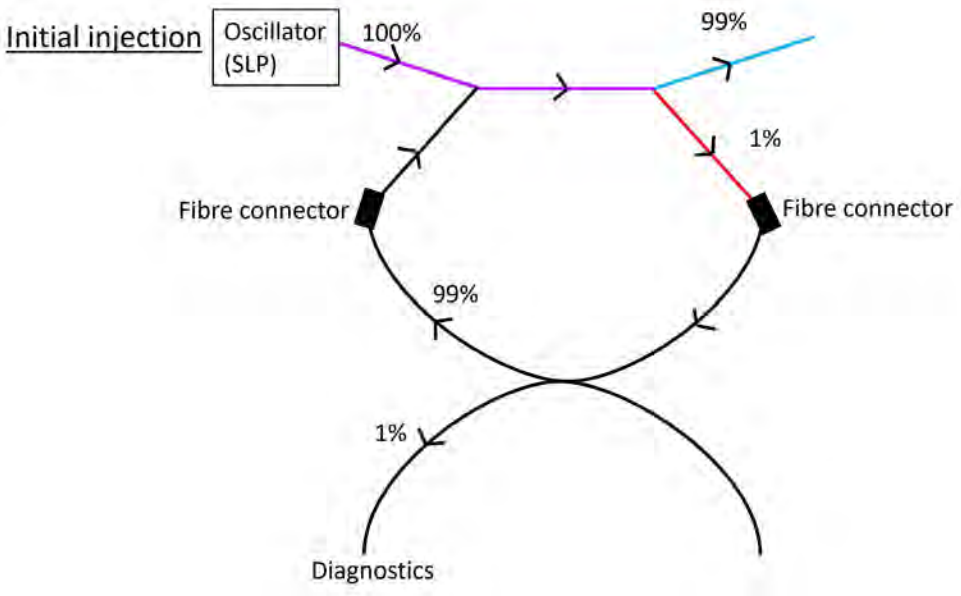

Figure 1: Fibre system setup showing initial injection from the oscillator into the two fibre splitters, which had been connected together then into the diagnostics. The percentages of the intensity of light going through each section of the fibre system are shown.

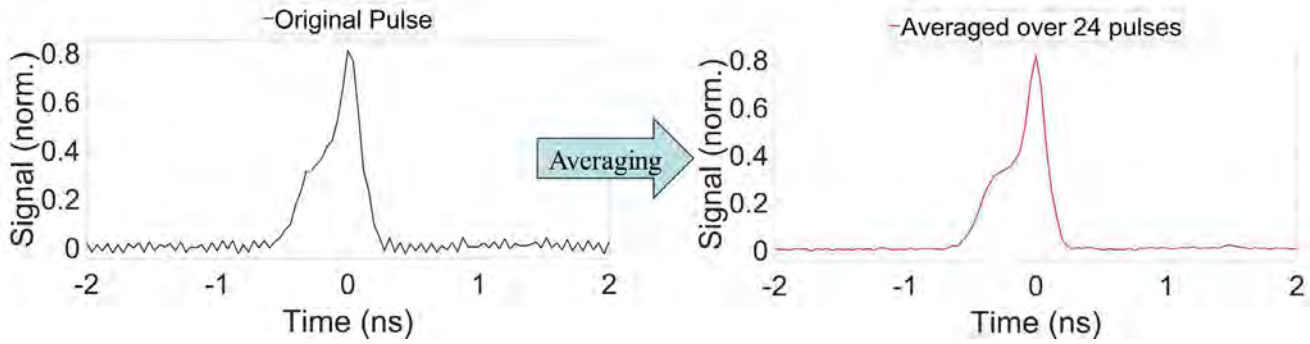

Figure 2: Pulse shape before averaging (left) compared with the pulse shape after optimal averaging (right).

Characterisation of Nested Anti-Resonant Hollow Core Fibre for Ultrafast Synchronisation Applications

In this report, a new nested anti-resonant nodeless (NANF)-type hollow core fibre (HCF) cable has been made and characterised for use in the Vulcan Petawatt Laser Facility. First measurements of the autocorrelation, spectrum and spectral interferogram of light directed through 50 m of the fibre demonstrate its ability to distribute laser pulses with little change over distances relevant to the scale of the Vulcan 20-20 facility. The results support its use as a distributor of optical reference pulses for the Vulcan 20-20 timing system.

Authors: A.C. Aiken, J.R. Henderson, P. Oliveira, J. Morse, M. Galimberti, B. Shi, F. Poletti, R. Slavik

Contact author: P. Oliveira (pedro.oliveira@stfc.ac.uk)

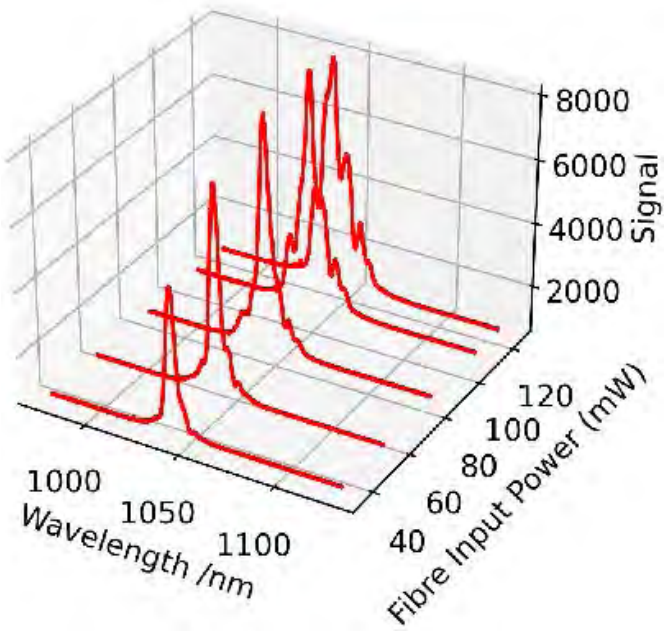

Figure 1: Evolution of the spectral envelope of the light with increasing power coupling into the fibre

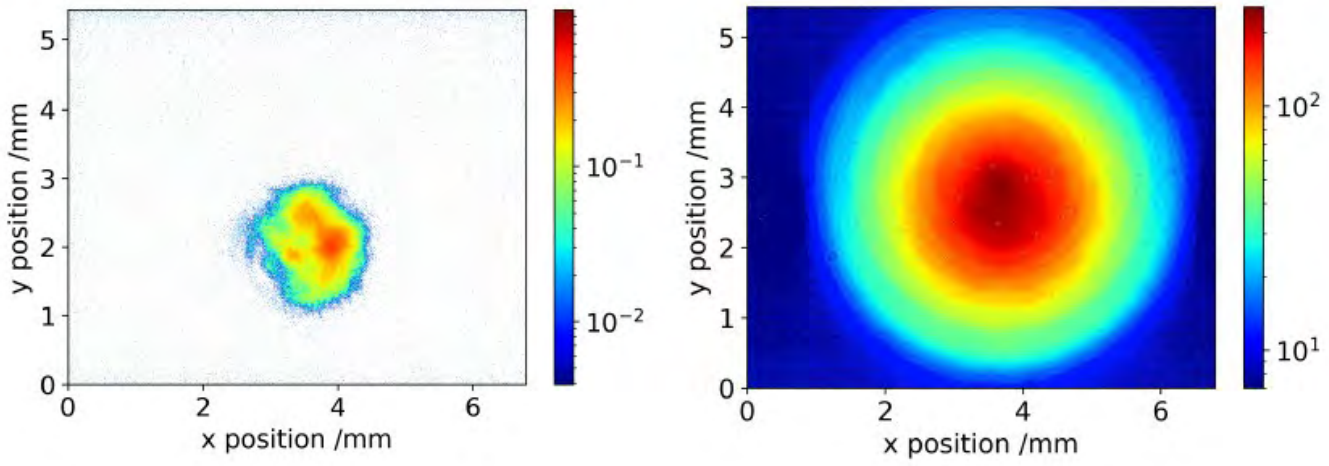

Figure 2: (Left) Spatial profile of the InSight DeepSee ultrafast laser prior to the fibre input. (Right) Spatial profile at the output of the fibre. Image colour scales are arbitrary.

A versatile high-average-power ultrafast infrared driver tailored for high-harmonic generation and vibrational spectroscopy

Ytterbium-based high-average-power lasers are becoming increasingly popular amidst the ultrafast science community. They afford robust and reliable turn-key operation at high repetition rates with sufficient laser pulse energies to drive non-linear phenomena in atoms, molecules and condensed matter. We recently commissioned a tunable infrared femtosecond optical parametric chirped-pulse amplifier, driven by a 200 W (2 mJ at 100 kHz) thin-disk regenerative amplifier at a wavelength of 1 micron. The laser is tailored to suit a wide variety of experimental requirements for Ultra and Artemis, ranging from ultrafast infrared and Raman spectroscopy to transient angle-resolved photoelectron spectroscopy (tr-ARPES) and x-ray absorption spectroscopy (tr-XAS) using high-harmonic generation (HHG). The versatility of the laser design provides a feasible means of investing into a single high-average-power front-end and yet be able to cater to diverse experimental platforms in ultrafast condensed-matter physics, material science, chemistry and biology.

Authors: N. Thiré, Y. Pertot, O. Albert, N. Forget, G. Chatterjee, G. Karras, Y. Zhang, A.S. Wyatt, M. Towrie, E. Springate, G.M. Greetham

Contact author: G. Chatterjee (gourab@slac.stanford.edu)

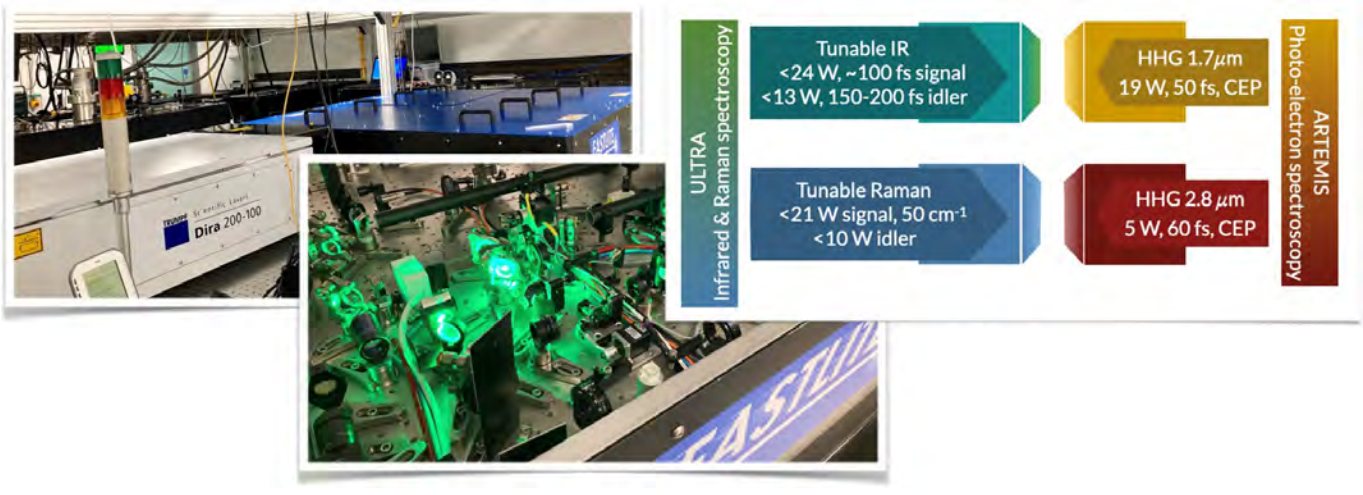

Generation and characterisation of <10 fs pulses for ultrafast spectroscopy in Ultra

Sub-10 fs pulses for driving two-dimensional electronic spectroscopy (2DES) experiments at the Ultra facility have been produced and characterised, using a combination of hollow core fibre pulse broadening and a commercial dispersion scan system. This source will initially be for use in 2DES, but it opens the door to a range of other broadband time-resolved spectroscopies.

Authors: T.B. Avni, G. M. Greetham, I.A. Heisler, S.R. Meech

Contact author: T.B. Avni (timur.avni@stfc.ac.uk)

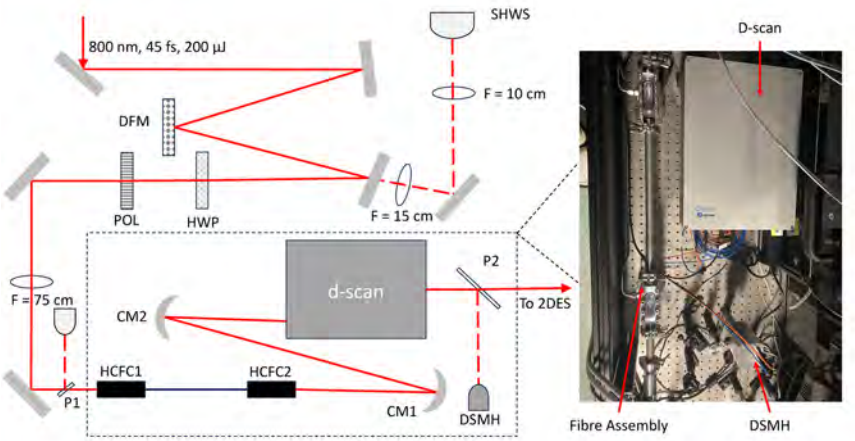

Figure 1: (Left) Schematic of the beam path to the hollow core fibre and the diagnostics before and after it to prepare the beam for use in 2DES experiments. The solid lines represent the primary beam path, and the dashed lines are leak-through and pickoff beams for diagnostics. (Right) The fibre and d-scan as installed in Ultra-B.

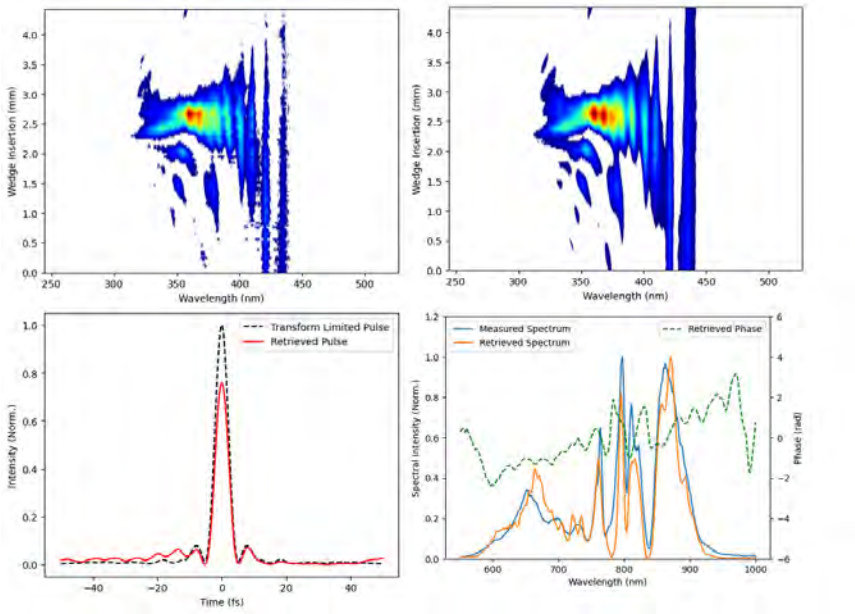

Figure 2: Diagnostic data from measurements taken with the d-scan. Top-left: The measured d-scan trace, showing spectrum vs thickness of glass insertion, with optimal compression seen at 2.8 mm wedge insertion. Top-right: The reconstruction of the measured trace using proprietary reconstruction algorithms. Bottom-left: The reconstructed (orange) vs measured (blue) spectrum at the point of optimal pulse compression, overlayed with the retrieved spectral phase (green, dashed). Bottom-right: The retrieved temporal intensity of the pulse (red) and the ideal transform limited pulse (black, dashed). The reconstruction gives a pulse duration of 4.75 fs, with a transform limit of 4.68 fs and a reconstruction error of 1.9%.

Half-broadband two-dimensional electronic spectroscopy with active noise reduction

Two-dimensional electronic spectroscopy (2DES) provides detailed insight into coherent ultrafast molecular dynamics in the condensed phase. Here we report a referenced broadband pump-compressed continuum probe half-broadband 2DES spectrometer in a partially collinear geometry. To optimise signal-to-noise ratio (SNR) we implement active noise reduction referencing. The method is calibrated against the well characterised 2DES response of the oxazine dye cresyl violet and demonstrated at visible wavelengths on the photochromic photoswitch 1,2-Bis(2- methyl-5-phenyl-3-thienyl)perfluorocyclopentene (DAE). The SNR is improved by a factor of ~2 through active referencing. We further show that active noise reduction referencing, coupled with the rapid data collection, allows the extraction of weak vibronic features, most notably a low frequency mode in the excited electronic state of DAE.

Authors: G. Bressan, S.R. Meech, I.A. Heisler, G.M. Greetham, A.E.D. Meades

Contact author: S.R. Meech (s.meech@uea.ac.uk)

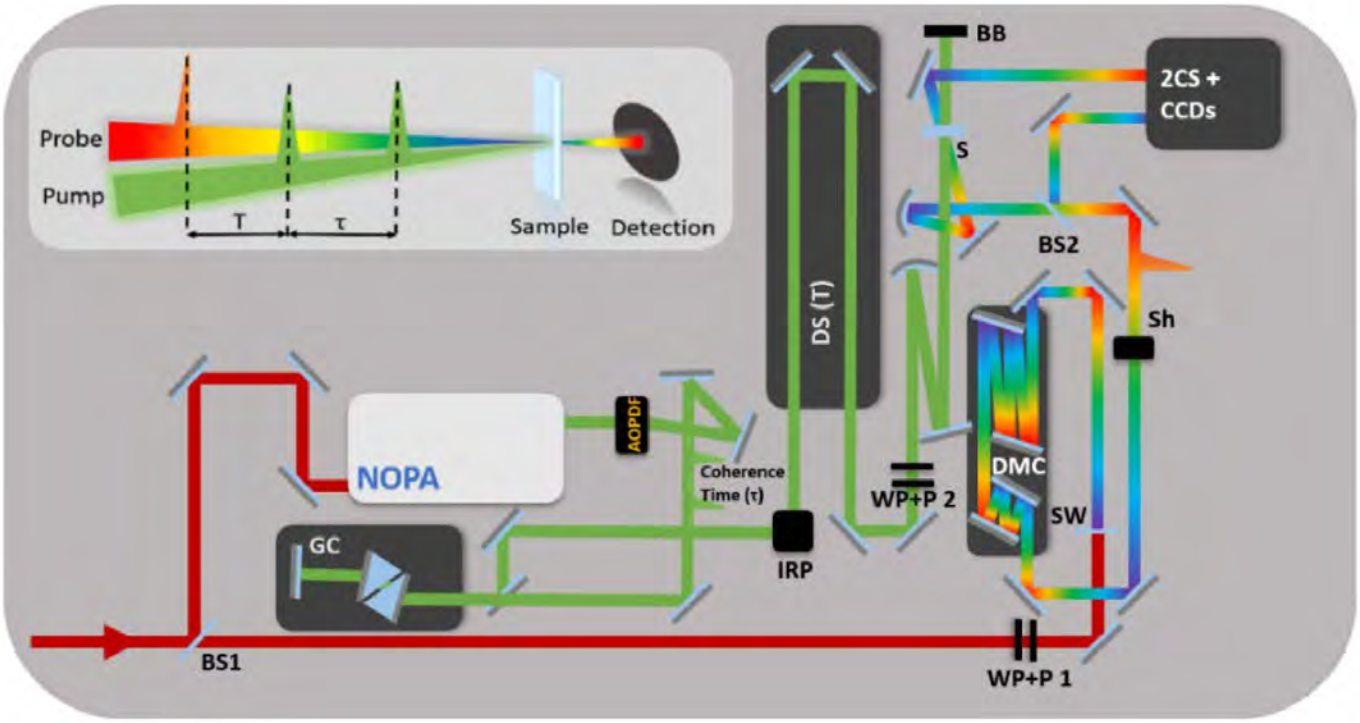

Complex Micro-Target Fabrication to Study Shock Compression

Recent years have seen target complexity increase due to the availability of a greater range of diagnostic techniques, and also because of the general growth in sophistication of experiments that are conducted. Target fabrication for such experiments typically requires integration of a range of techniques to make one target cluster. To meet demand, there has been a rapid development in advanced target fabrication techniques such as robotic assembly, micro 3D printing, single-point diamond turning, laser micromachining and (MEMS-based) lithography.

This annual report details one complex target fabrication programme that was carried out for an experiment in Target Area West on the Vulcan facility.

Authors: P. Ariyathilaka, D. Wyatt, C. Spindloe, M. Tolley, M. Oliver, L. Sparkes, B.C. Bateman

Contact author: P. Ariyathilaka (pawala.ariyathilaka@stfc.ac.uk)

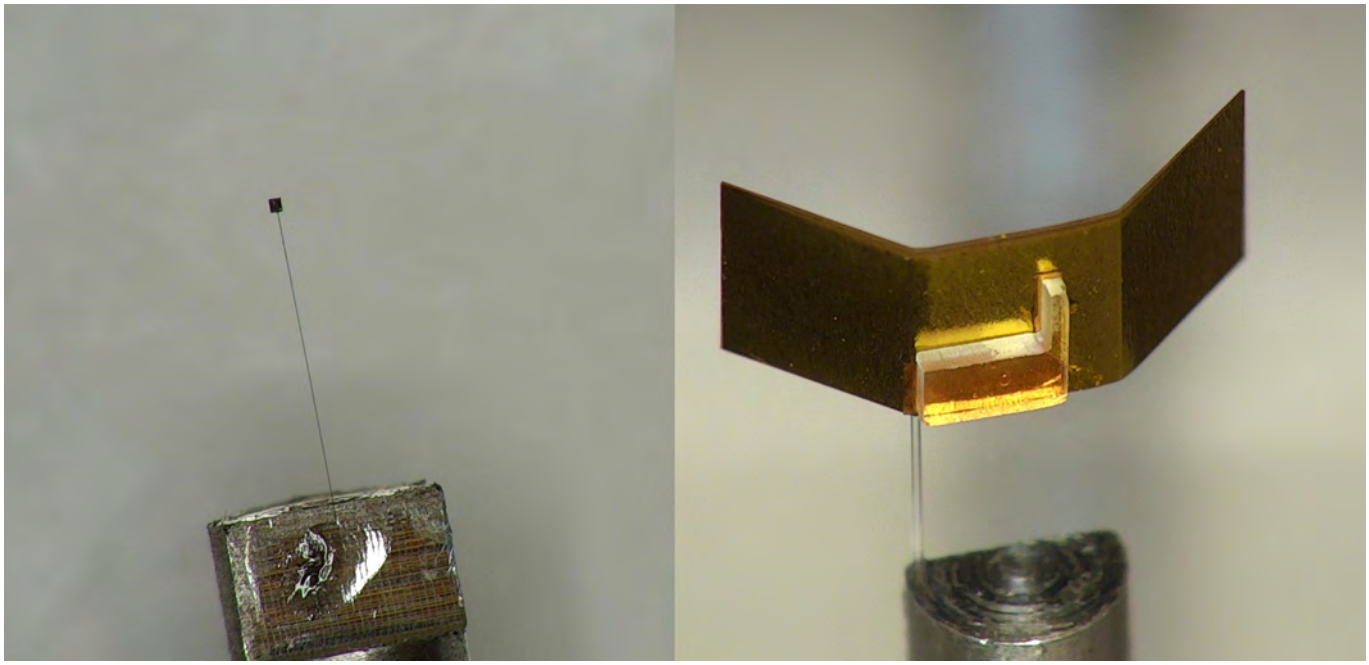

Two of the three targets used in the final target cluster: (left) Zinc backlighter foil 100 µm x 100 µm, and (right) lithium fluoride sample assembled to gold shield

Liquid Targetry Development for High Repetition Rate Experiments

The demands of modern high repetition rate, high power lasers have ushered in new challenges for laser targetry. For applications in X-ray free electron lasers and for plasma mirror experiments, thin liquid sheet targets have proven themselves to be perfect candidates due to their low debris and ability to rapidly self-replenish. The Extreme Photonics Applications Centre (EPAC) will come online within the next couple of years, and we face the need to develop larger and thinner sheets than previous studies have achieved. However, fine tuning nozzles via a system of trial and error is a long and costly process.

Here, we propose an efficient pipeline from conception of a design through simulation and optimisation, prototyping and testing, and finally production of a functioning part ready for application in high power laser experiments. We outline the progress made so far and the next steps required to make this a functioning process ready for implementation.

Authors: D.E. Crestani, S. Astbury, H. Edwards, W. Robins, C. Spindloe, M. Beardsley, L. Bushnell, C. Palmer, P. Parsons

Contact author: D. Crestani (dominic.crestani@stfc.ac.uk)

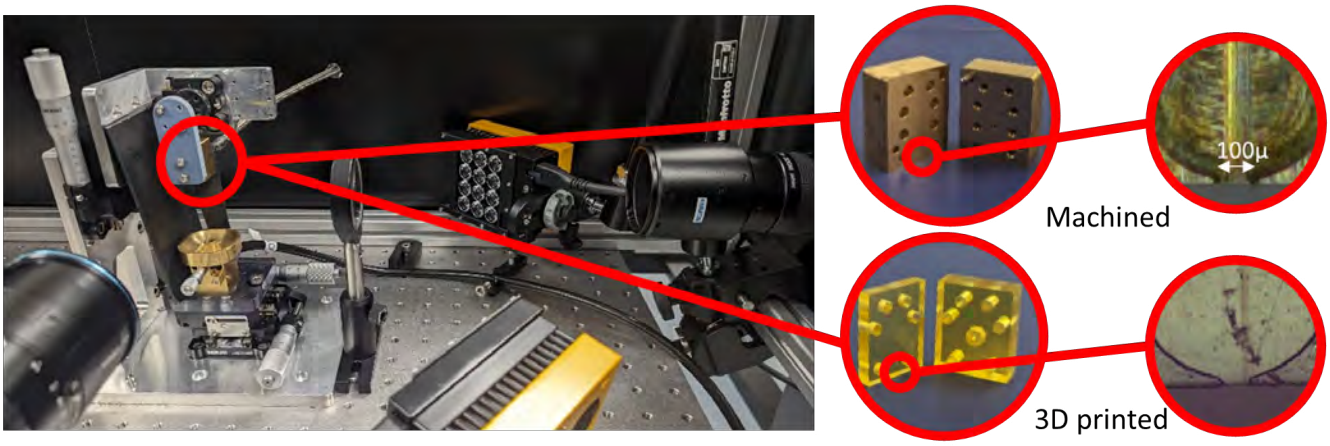

Figure 1: Experimental setup of the liquid target system, with magnified images of a high precision machined brass nozzle and a resin 3D printed nozzle

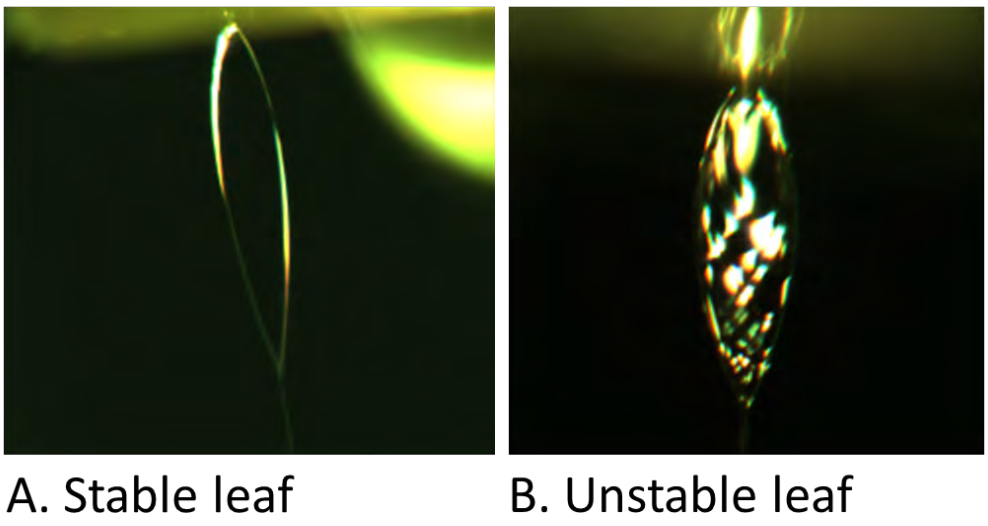

Figure 2: White light reflectance interferometry of a stable and an unstable liquid leaf

Using Additive Manufacturing to Aid the Manufacture of Complex 3D Microtargets

This article discusses the recent upgrades to the Target Fabrication group's suite of 3D printers, with the purchase and commissioning of a new micro additive manufacturing system and will give examples of where it has been used for target production.

The capability to print components with high resolution has opened many opportunities in target design. It has enabled more complex and, simultaneously, more flexible geometries to be made.

Moreover, it has often reduced or eliminated the need for assembly fixtures by producing multi-component assemblies in one print. Sets of components and complete laser microtarget assemblies have been printed.

Authors: C. Dobson, P. Ariyathilaka, D. Crestani, C. Spindloe, J. Robinson

Contact author: C. Dobson (claire.dobson@stfc.ac.uk)

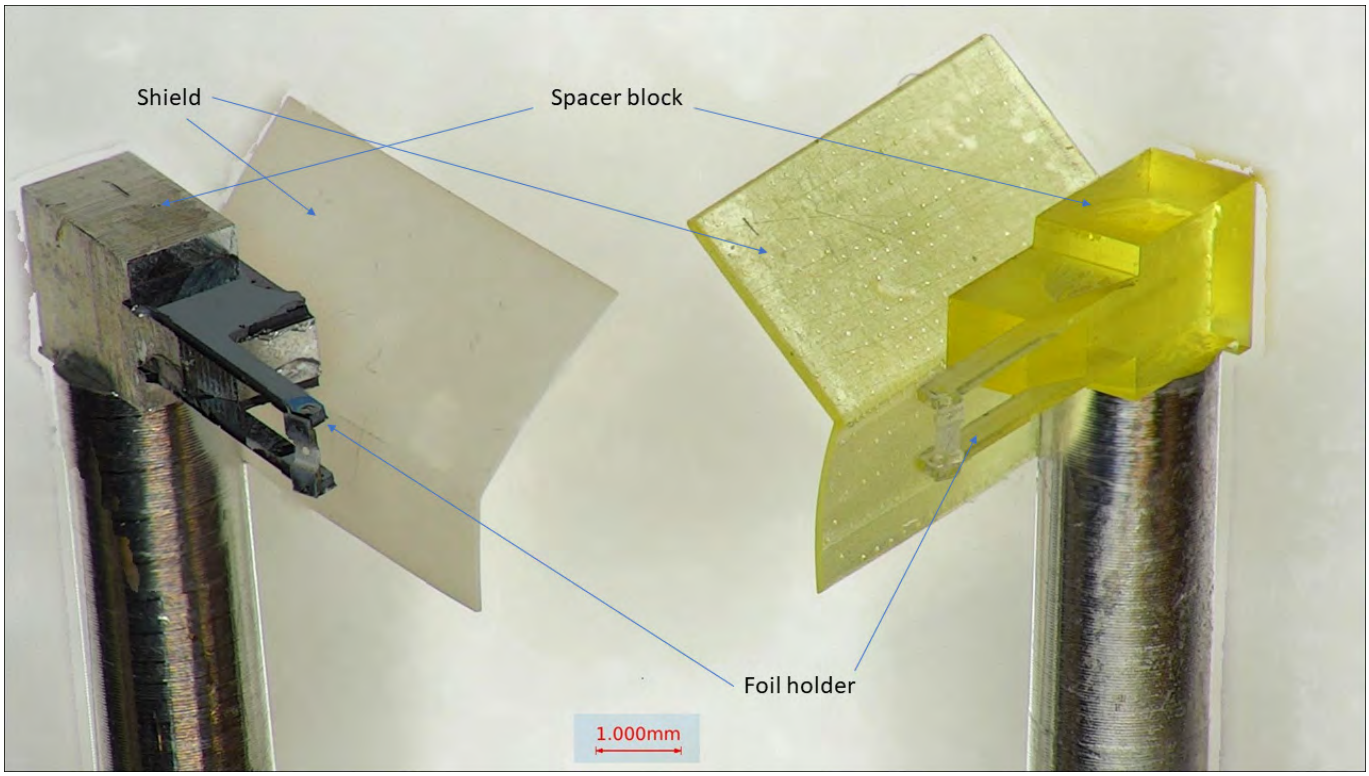

Traditionally made (multi-component) experimental target (left) and proof of concept 3D printed target (right). In this example, it was possible to print up to 90% of the target using the printer – including the spacer block, the foil mounts, and the shield on the rear of the target.
Photo: P. Ariyathilaka

Current developments in the Target Array Assembly System

The Target Array Assembly System (TAAS) is a robotic system that is being developed by the Target Fabrication Group of the Central Laser Facility to autonomously assemble microtarget arrays. The project is being developed to support the future solid target demands of the Extreme Photonics Applications Centre (EPAC) facility, which will be operational in 2025 [1].

Currently, the TAAS can automatically assemble an array target containing 32 foils in 27 minutes. This milestone provided an opportunity to review the abilities and future development plans for the TAAS. In this article, the functional requirements for the system are set out, as well as the current layout of the system. The target assembly methodology and system design are described, before highlighting areas for future development work.

[1]P. Umesh et al, "A Systems Engineering Architecture for Robotic Microtarget Production", CLF Annual Report 2019-20

Authors: J. Fields, P. Ariyathilaka, S. Astbury, M. Tolley, C. Spindloe

Contact authors: J. Fields (jfields1@sheffield.ac.uk)

P. Ariyathilaka (pawala.ariyathilaka@stfc.ac.uk)

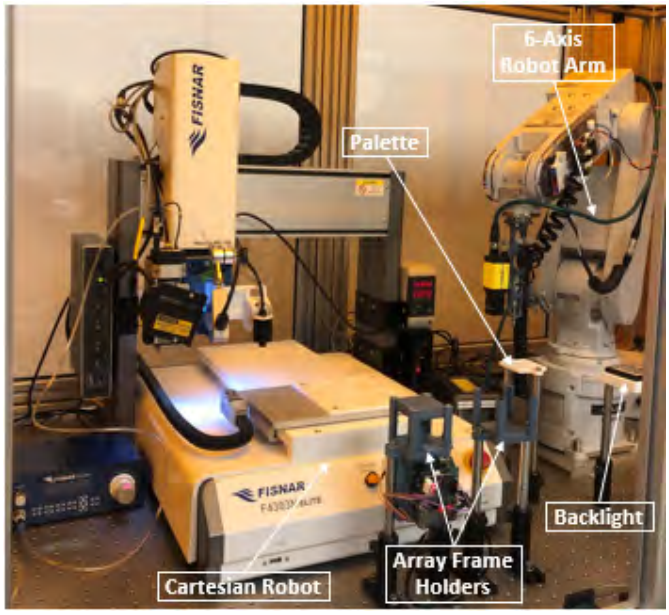

Figure 1: The Target Array Assembly System (TAAS), showing the robot arm, cartesian robot, array frame holders, backlight and palette

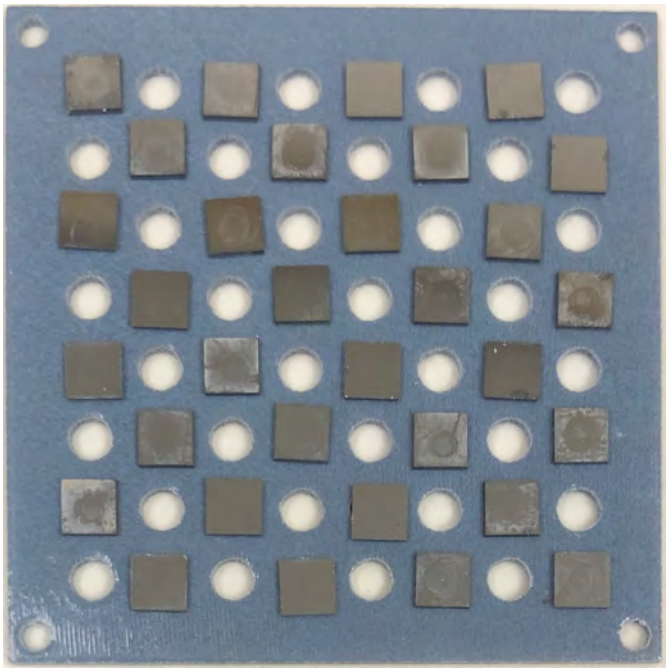

Figure 2: A '32-foil' array target

Investigating sources of inaccuracy within the Target Array Assembly System

The Target Array Assembly System (TAAS) is a robotic system that is being developed by the Central Laser Facility's Target Fabrication group to autonomously assemble microtarget arrays. A MELFA 'RV-2FRLB' industrial robot is used to manipulate target foils for the assembly of array targets. During system development, a coordinate drift was observed in this robot, causing unreliable and inaccurate foil placement. After initial experimentation, an investigation into the effect of thermal expansion on the robot arm was conducted.

The position change with respect to temperature was quantified using chromatic confocal distance sensors. By measuring the relative distance between set positions on the robot and fixed reference positions, any position changes could be observed.

The investigation showed that thermal expansion caused a significant, yet repeatable, position change. This led to the development of a 'warm-up' routine for the arm, to ensure it was at an operation temperature before use. This experiment also provided a greater understanding of inaccuracies within the TAAS.

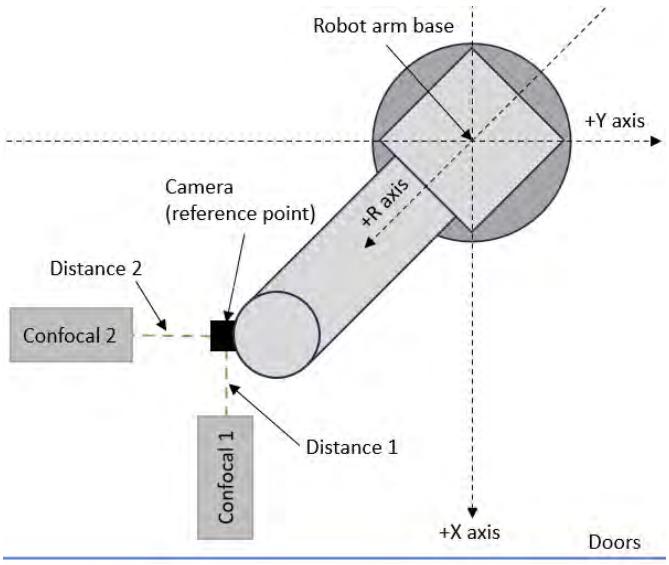

Figure 1: A simplified representation of the experimental setup

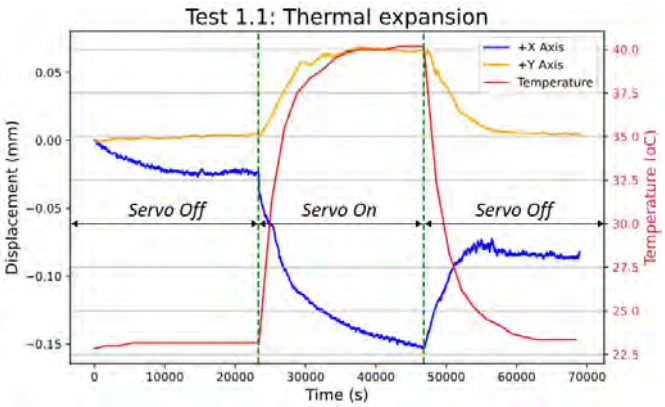

Figure 2: Change in position and temperature over time during one of the tests

Authors: J. Fields, P. Ariyathilaka, S. Astbury, M. Tolley, C. Spindloe

Contact authors: J. Fields (jfields1@sheffield.ac.uk)

P. Ariyathilaka (pawala.ariyathilaka@stfc.ac.uk)

Embedding of Ruby Microspheres in Low Density Foam Targets

Trimethylolpropane triacrylate monomer was used to create low density, polymeric structures by a supercritical fluid drying process to hold ruby microspheres for shock experiments. The design and manufacture of the target, and the initial results of the laser shock experiment, are covered by this article.

Ruby was chosen due to its density and average Z; challenges to ensure placement and fixing are covered. Full characterisation of the external and internal morphology of the target was conducted, with a combination of optical microscopy and x-ray radiographic measurements. The targets were successfully shot on the PHELIX laser in GSI.

Authors: S. Irving, P. Ariyathilaka, C. Spindloe, J. Robinson, P. Neumayer, L. Wegert

Contact author: S. Irving (samuel.irving@stfc.ac.uk)

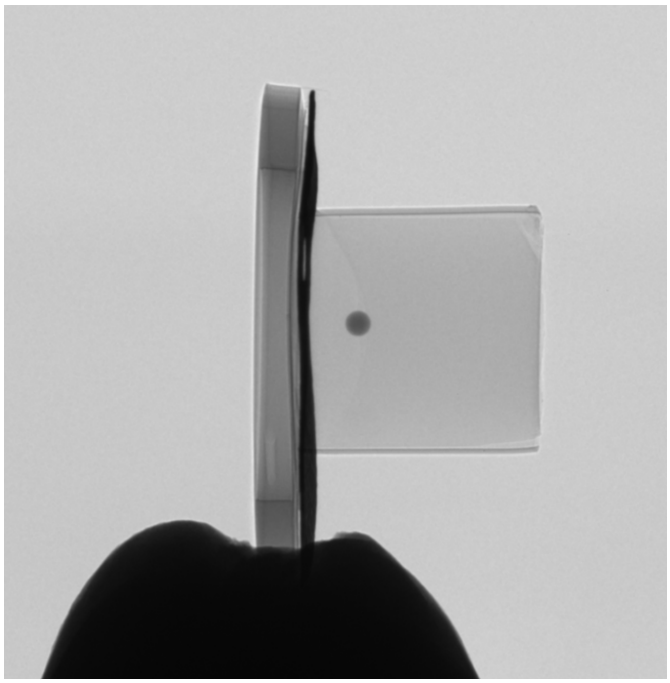

Figure 1: Side on radiograph with a much-reduced interfacial membrane

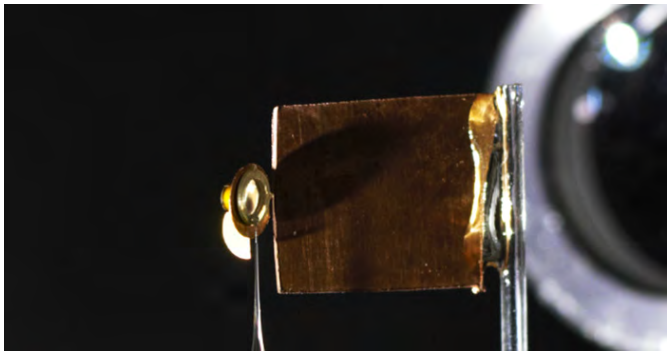

Figure 2: The target in the chamber (left) with additional shielding (right)

Plasma Diagnostics

An Active Multi-Channel Ion Beam Profiler for Laser-Driven Ion Beams

An optical imaging system for an ion beam profiler was designed and successfully tested in an experiment at Vulcan Petawatt. Several different optical components were tested as well as different designs for the optical setup to maximise the resolution. The spatial resolution that can be achieved by the optical system itself was ~ 4 lp/mm. Several scintillator stack designs were used throughout the experiment for comparisons of brightness and resolution. It was found that, out of commonly used plastic scintillators, EJ 260 was the brightest, yet it was still an order of magnitude dimmer than Gadox-based phosphor screens, viz. the Lanex screen and P43 screens. The response of the P43 screen was calibrated against radiochromic film (RCF), giving a conversion factor of ~ 170 counts/Gy.

Authors: T.H. Hall, H. Ahmed, C. Armstrong, C. Baird, D.C. Carroll, J. Green, R.J. Clarke, P. Martin, O. Cavanagh, C. Fegan, S. Kar, A. McCay, C. Palmer, M. Borghesi

Contact author: H. Ahmed (hamad.ahmed@stfc.ac.uk)

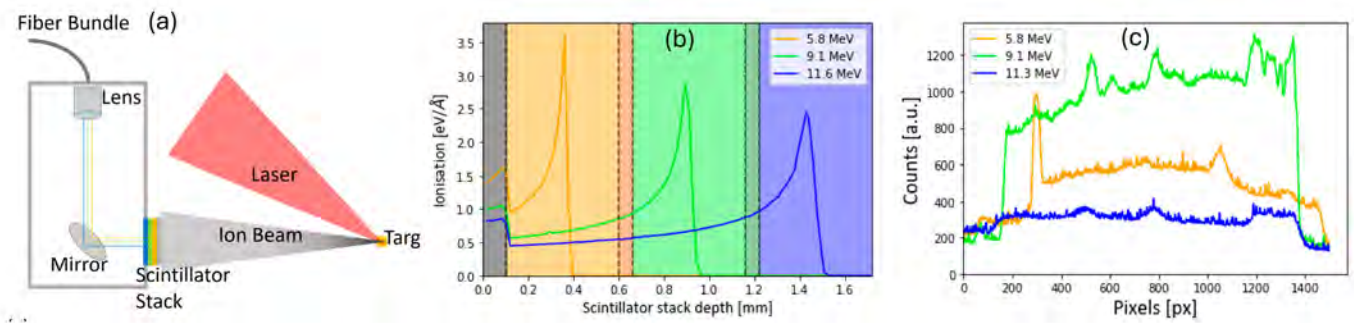

(a) The setup of the ion beam profiler inside the vacuum chamber; the image was transported away from the interaction region using a fibre bundle. (b) The Bragg peak in each layer of the scintillators stack deployed in the experiment. (c) A comparison of the brightness of light output from the scintillators.

Imaging and Dynamics for Physical and Life Sciences

Exploring the Charge Density Wave Phase of 1*T*–$TaSe_2$: Mott or Charge-Transfer Gap?

The quest for finding quantum materials with unconventional electronic structures and on demand electrical switching has highlighted 2D tantalum-based dichalcogenides as systems with interesting metal to insulator transitions. 1*T*–$TaSe_2$ is widely believed to host a Mott metal-insulator transition in the charge density wave (CDW) phase according to the observation of a band gap that extends across all momentum space. At CLF-Artemis we combined time- and angle-resolved photoemission spectroscopy to gain new insights on the electronic structure and dynamics of this material. Our experiment probes the conduction band, previously ascribed to the upper Hubbard band, and a band gap of ~0.7 eV. We demonstrate that the origin of the gap rests on band structure modifications induced by the CDW phase alone, without the need for Mott correlation effects. The results contribute towards the understanding and design of material platforms for memristors and low-energy devices in computing and data storage applications.

Authors: C.J. Sayers, G. Cerullo, Y. Zhang, C.E. Sanders, R.T. Chapman, A.S. Wyatt, G. Chatterjee, E. Springate, D. Wolverson, E. Da Como, E. Carpene

Contact author: E. Da Como (edc25@bath.ac.uk)

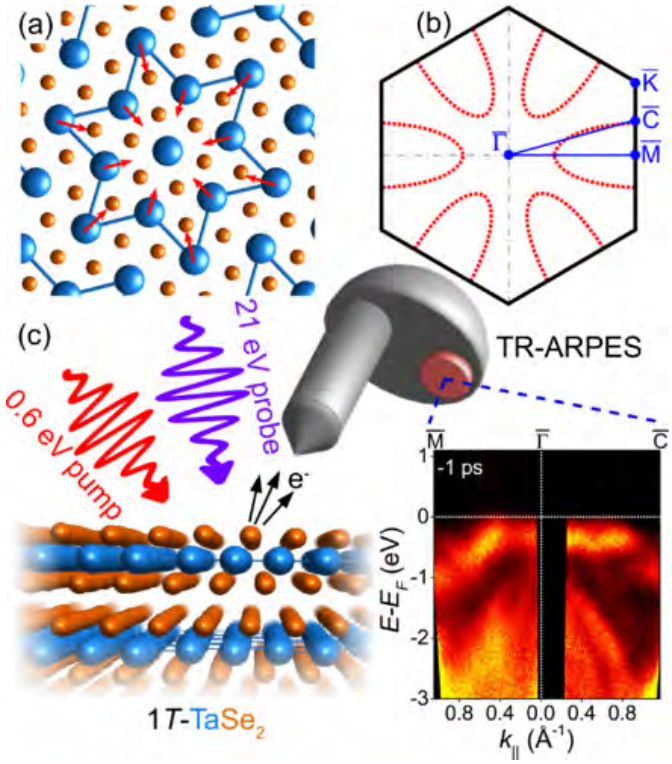

(a) Illustration of the starlike lattice reconstruction in the CDW phase of 1*T*-$TaSe_2$. (b) Surface-projected Brillouin zone (BZ) of the undistorted "normal" state. The red dashed lines mimic the Fermi surface and the blue solid line indicates the experimental path through the BZ as measured by time- and angle-resolved photoemission spectroscopy (TR-ARPES) at Artemis (c) Sketch of the TR-ARPES experiment with laser photon energies.

Ultrafast Rydberg-Valence Interactions and Photodissociation Dynamics of Trimethylamine: A Time-Resolved XUV Photoelectron Spectroscopy Experiment

The photodissociation dynamics of trimethylamine (TMA) have been studied using extreme ultraviolet (XUV) photoelectron spectroscopy. The XUV probe allows us to monitor the initial dynamics in the electronically excited Rydberg states, and how these correlate with the dissociation products formed.

Measurements show that following excitation into the 3p Rydberg state, competing internal conversion and dissociation processes occur leading to the 3p state lifetime of 4.4 ps. Dissociation directly from the 3p state leads to the formation of vibrationally hot methyl fragments in conjunction with ground state dimethyl amidogen (DMA), while internal conversion leads to population of the 3s Rydberg state. Once in the 3s state, the Rydberg state couples to a dissociative valence state leading to the formation of a vibrationally cold methyl radical and an electronically excited DMA on a 70 ps timescale.

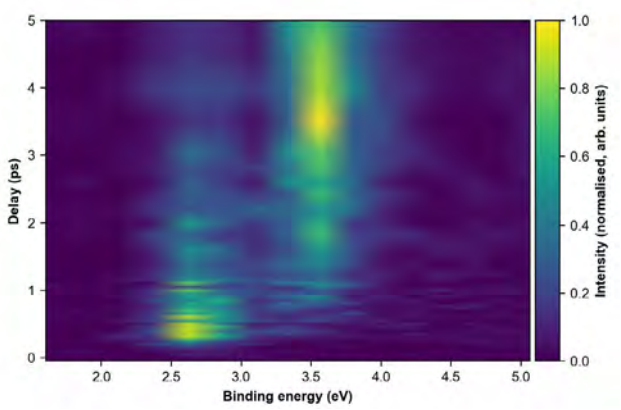

Time-resolved photoelectron spectrum of trimethylamine measured following excitation with a 6.1 eV pump and a 21.5 eV probe. The spectrum plotted highlights the initial Rydberg state dynamics involving internal conversion from the initially excited 3p Rydberg state, to the 3s Rydberg state.

Authors: D.J. Hughes, H.J. Thompson, R.S. Minns, P. Krüger, D.A. Horke, M.A. Parkes, R.T. Chapman, E. Springate, J.O.F. Thompson

Contact author: R.S. Minns (r.s.minns@soton.ac.uk)

Access to the full three-dimensional Brillouin zone with time resolution, using a new tool for pump-probe photoemission spectroscopy

Artemis has reported on time- and angle-resolved photoemission spectroscopy (TR-ARPES) results that were acquired from solid-state samples using the new Fermiologics "FeSuMa" analyser. As the authors explain in their manuscript, which has recently been posted to the arXiv, the FeSuMa offers several advantages for TR-ARPES. The paper explores some of the ways in which the new analyser's capabilities relate to those of hemispherical analysers and momentum microscopes. Artemis has integrated both the FeSuMa and a hemispherical analyser into a fully optimised pump-probe beamline that permits efficient photon-energy scanning for fully three-dimensional measurements, using probe energies generated from high harmonics in a gas jet. The advantages of using the FeSuMa in this situation include the possibility of taking advantage of its "fisheye" mode of operation.

Full information can be found in the manuscript, arXiv:2309.11535 [cond-mat.mtrl-sci], at https://doi.org/10.48550/arXiv.2309.11535

Authors: P. Majchrzak, P. Hofmann, A. Kuibarov, S. Borisenko, B. Büchner, Y. Zhang, R. Chapman, A. Wyatt, E. Springate, C.E. Sanders

Contact author: C.E. Sanders (charlotte.sanders@stfc.ac.uk)

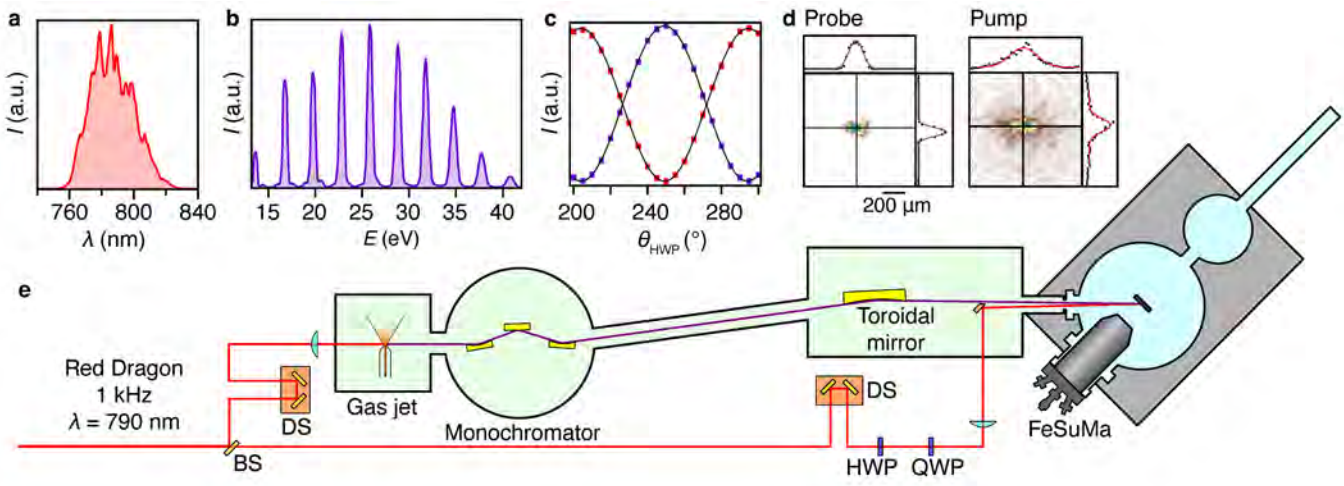

(a) The spectrum of the 1-kHz titanium-sapphire (Ti:sapp) laser that was used to make the measurements reported in the new work. (b) The high-harmonics spectrum, driven by the Ti:sapp laser in an argon gas jet. (c) Calibration curves for pump polarisation, measured as intensity through a polariser after the beam passes through a quarter- and a half-wave plate (QWP and HWP, respectively). The intensity is shown as a function of rotation of the HWP. Control of the pump polarisation means that dichroic effects can be probed. (d) Spot sizes of the probe and pump beams. (e) Schematic of the experimental setup. "DS" indicates "delay stage." "BS" indicates a beam splitter.

The guidance and adhesion protein FLRT2 dimerizes in *cis* via dual small-X_3-small transmembrane motifs

Fibronectin Leucine-rich Repeat Transmembrane (FLRT 1–3) proteins are a family of broadly expressed single-spanning transmembrane receptors that play key roles in development. Their extracellular domains mediate homotypic cell-cell adhesion and heterotypic protein interactions with other receptors to regulate cell adhesion and guidance. These *in trans* FLRT interactions determine the formation of signaling complexes of varying complexity and function. Whether FLRTs also interact at the surface of the same cell, *in cis*, remains unknown. Here, molecular dynamics simulations reveal two dimerization motifs in the FLRT2 transmembrane helix. Single particle tracking experiments show that these Small-X_3-Small motifs synergize with a third dimerization motif encoded in the extracellular domain to permit the cis association and co-diffusion patterns of FLRT2 receptors on cells. These results may point to a competitive switching mechanism between *in cis* and *in trans* interactions, which suggests that homotypic FLRT interaction mirrors the functionalities of classic adhesion molecules.

Reproduced from Jackson, V. et al. (2022). The guidance and adhesion protein FLRT2 dimerizes in cis via dual small-X_3-small transmembrane motifs. Structure 30, 1354–1365.e5 © Elsevier Ltd under an Elsevier user license. doi: 10.1016/j.str.2022.05.014

Authors: V. Jackson, R.A. Corey, A.L. Duncan, A. Chu, M.S.P. Sansom, E. Seiradake, J. Hermann, C.J. Tynan, D.J. Rolfe, M.L. Martin-Fernandez, M. Noriega, M. Chavent, A.C. Kalli, E.Y. Jones

Contact authors: M.L. Martin-Fernandez (marisa.martin-fernandez@stfc.ac.uk)

E. Seiradake (elena.sieradake@bioch.ox.ac.uk)

M. Chavent (matthieu.chavent@ipbs.fr)

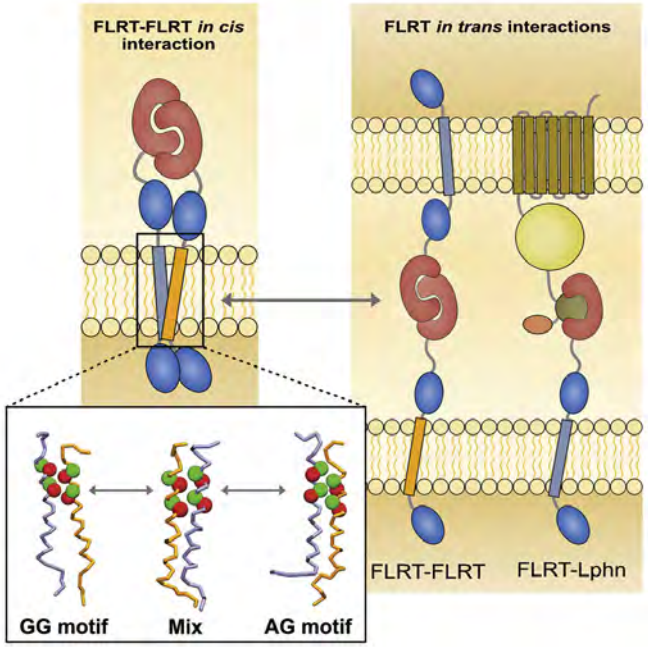

Instantaneous 4D micro-particle image velocimetry (μPIV) via multifocal microscopy (MUM)

Multifocal microscopy (MUM), a technique to capture multiple fields of view (FOVs) from distinct axial planes simultaneously and on one camera, was used to perform micro-particle image velocimetry (μPIV) to reconstruct velocity and shear stress fields imposed by a liquid flowing around a cell. A diffraction based multifocal relay was used to capture images from three different planes with 630 nm axial spacing from which the axial positions of the flow-tracing particles were calculated using the image sharpness metric. It was shown that MUM can achieve an accuracy on the calculated velocity of around (0.52 ± 0.19) μm/s. Using fixed cells, MUM imaged the flow perturbations at subcellular level, which showed characteristics similar to those observed in the literature. Using live cells as an exemplar, MUM observed the effect of changing cell morphology on the local flow during perfusion. Compared to standard confocal laser scanning microscope, MUM offers a clear advantage in acquisition speed for μPIV (over 300 times faster). This is an important characteristic for rapidly evolving biological systems where there is the necessity to monitor in real time entire volumes to correlate the sample responses to the external forces.

doi:10.1038/s41598-022-22701-3

Authors: M.G.R. Guastamacchia, W.T.E. Pitkeathly, P.A. Dalgarno, R. Xue, P.D. Lee, S.H. Cartmell, K. Madi, S.E.D. Webb

Contact author: P.A. Dalgarno (p.a.dalgarno@hw.ac.uk)

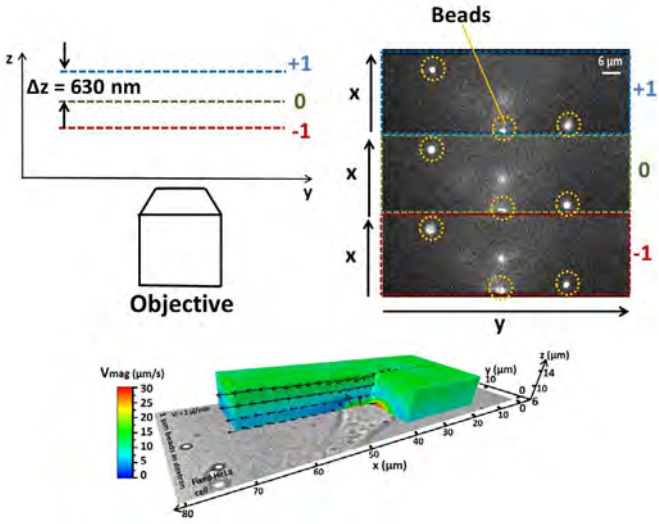

Top panels: In multifocal fluorescence microscopy, images of different axial planes of the same area are collected simultaneously in different regions of a single camera. For this paper, we used a diffraction grating that placed the planes 630 nm apart. The differing sharpness of an object within the three sub-images is used to determine its axial position, with fluorescent beads used to calibrate the microscope.

Bottom panel: By acquiring a time series of images of fluorescent beads flowing over a cell, the magnitude (colour) and direction (arrows) of bead velocities can be mapped in 3D. Here, we used 1 μm beads in dextran flowing over a fixed HeLa cell to image the cell-induced perturbation of the flow. The white light transmission image of the cell was collected using a second camera via an image splitter.

Ultraviolet refractive index values of organic aerosol extracted from deciduous forestry, urban and marine environments

The refractive index values of atmospheric aerosols are required to address the large uncertainties in the magnitude of atmospheric radiative forcing and measurements of the refractive index dispersion with wavelength of particulate matter sampled from the atmosphere are rare over ultraviolet wavelengths. An ultraviolet-optimized spectroscopic system illuminates optically-trapped single particles from a range of tropospheric environments to determine the particle's optical properties. Aerosol from remote marine, polluted urban, and forestry environments is collected on quartz filters, and the organic fraction is extracted and nebulized to form micron-sized spherical particles. The radius and the real component of refractive index dispersion with wavelength of the optically trapped particles are determined to a precision of 0.001 μm and 0.002 respectively over a near-ultraviolet-visible wavelength range of 0.320–0.480 μm. Remote marine aerosol is observed to have the lowest refractive index (n = 1.442 (λ = 0.350 μm)), with above-canopy rural forestry aerosol (n = 1.462–1.481 (λ = 0.350 μm)) and polluted urban aerosol (n = 1.444–1.485 (λ = 0.350 μm)) showing similar refractive index dispersions with wavelength.

In-canopy rural forestry aerosol is observed to have the highest refractive index value (n = 1.508 (λ = 0.350 μm)). The study presents the first single particle measurements of the dispersion of refractive index with wavelength of atmospheric aerosol samples below wavelengths of 0.350 μm. The Cauchy dispersion equation, commonly used to describe the visible refractive index variation of aerosol particles, is demonstrated to extend to ultraviolet wavelengths below 0.350 μm for the urban, forestry, and atmospheric aerosol water-insoluble extracts from these environments. A 1D radiative-transfer calculation of the difference in top-of-the-atmosphere albedo between atmospheric core–shell mineral aerosol with and without films of this material demonstrates the importance of organic films forming on mineral aerosol.

Reproduced from Environ. Sci.: Atmos., 2023,3, 1008-1024, under the terms of a Creative Commons Attribution 3.0 Unported licence. doi: 10.1039/d3ea00005b

Authors: C.R. Barker, E.J. Stuckey, M.L. Poole, M.D. King, M. Wilkinson, J. Morison, A. Wilson, G. Little, R.J.L. Welbourn, A.D. Ward

Contact author: M.D. King (m.king@rhul.ac.uk)

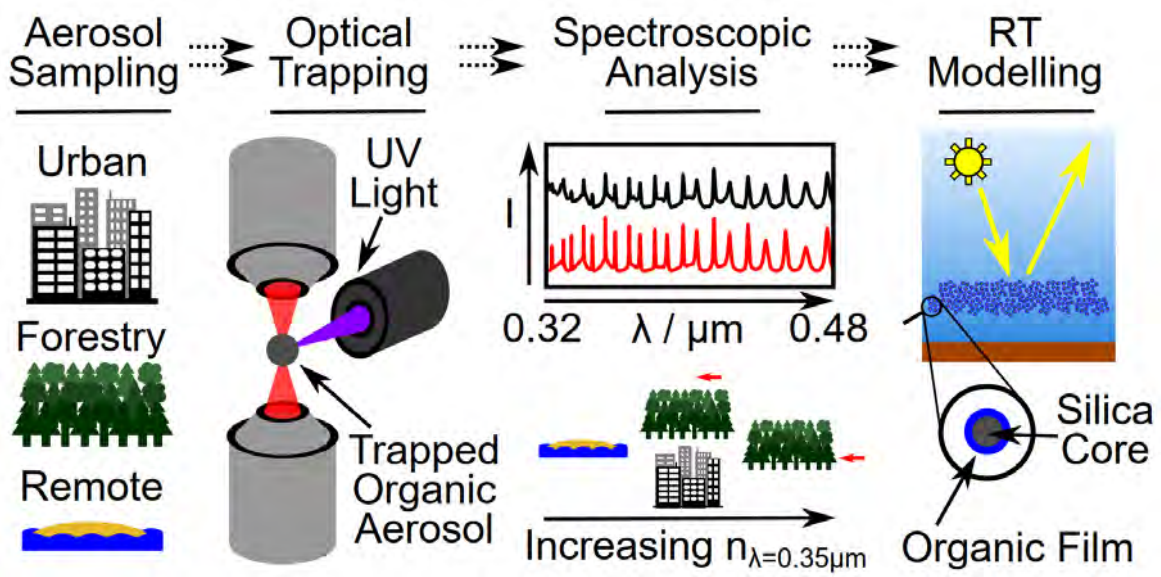

FRET-FLIM to determine protein interactions and membrane topology of enzyme complexes

Determining protein-protein interactions is vital for gaining knowledge on cellular and metabolic processes including enzyme complexes and metabolons. Förster resonance energy transfer with fluorescence lifetime imaging microscopy (FRET-FLIM) is an advanced imaging methodology that allows for the quantitative detection of protein-protein interactions. In this method, proteins of interest for interaction studies are fused to different fluorophores such as enhanced green fluorescent protein (eGFP; donor molecule) and monomeric red fluorescent protein (mRFP; acceptor molecule). Energy transfer between the two fluorophore groups can only occur efficiently when the proteins of interest are in close physical proximity, around ≤10 nm, and therefore are most likely interacting. FRET-FLIM measures the decrease in excited-state lifetime of the donor fluorophore (eGFP) with and without the presence of the acceptor (mRFP) and can therefore give information on protein-protein interactions and the membrane topology of the tested protein. Here we describe the production of fluorescent protein fusions for FRET-FLIM analysis in tobacco leaf epidermal cells using Agrobacterium-mediated plant transformation and a FRETFLIM data acquisition and analysis protocol in plant cells. These protocols are applicable and can be adapted for both membrane and soluble proteins in different cellular localizations.

Reproduced from Spatola Rossi, T., Pain, C., Botchway, S. W., & Kriechbaumer, V. (2022). FRET-FLIM to determine protein interactions and membrane topology of enzyme complexes. Current Protocols, 2, e598, under the terms of a Creative Commons Attribution License. doi: 10.1002/cpz1.598

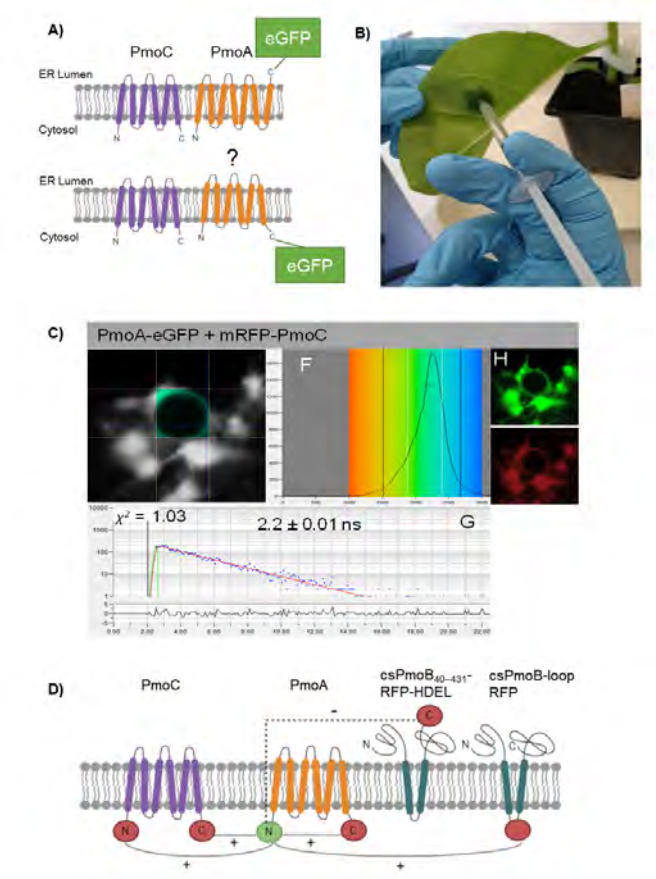

FRET-FLIM interactions can resolve membrane topologies: the bacterial pMMO enzyme complex as an example. (A) Schematic diagram of topology predictions for the enzymes PmoC and PmoA. PmoC is predicted to feature six TMDs. Predictions for PmoA differ between six and seven TMDs, and the C-terminus could therefore either face the ER lumen (top) or the cytosol (bottom). (B) Agrobacterium-mediated tobacco leaf infiltration is carried out to produce the proteins in planta with fluorescent tags. (C) FRET-FLIM analysis is carried out, here as an example PmoA-eGFP with mRFP-PmoC. Different combinations reveal that PmoA features 6 TMDs with both termini in the cytosol.

Authors: V. Kreichbaumer, T.S. Rossi, C. Pain, S.W. Botchway

Contact author: V. Kreichbaumer (vkriechbaumer@brookes.ac.uk)

High-yield vesicle-packaged recombinant protein production from *E. coli*

We describe an innovative system that exports diverse recombinant proteins in membrane-bound vesicles from *E. coli*. These recombinant vesicles compartmentalize proteins within a micro-environment that enables production of otherwise challenging insoluble, toxic, or disulfide-bond containing proteins from bacteria. The release of vesicle-packaged proteins supports isolation from the culture and allows long-term storage of active protein. This technology results in high yields of vesicle-packaged, functional proteins for efficient downstream processing for a wide range of applications from discovery science to applied biotechnology and medicine.

Reproduced from Eastwood, Tara A et al. "High-yield vesicle-packaged recombinant protein production from E. coli." Cell Reports Methods 3, 100396, 2023, doi:, under the terms of a Creative Commons Attribution License. doi: 10.1016/j.crmeth.2023.100396

Authors: T.A. Eastwood, K. Baker, B.R. Streather, I.R. Brown, D.P. Mulvihill, N. Allen, L. Wang, S.W. Botchway, J.R. Hiscock, C. Lennon

Contact author:
D.P. Mulvihill (d.p.mulvihill@kent.ac.uk)

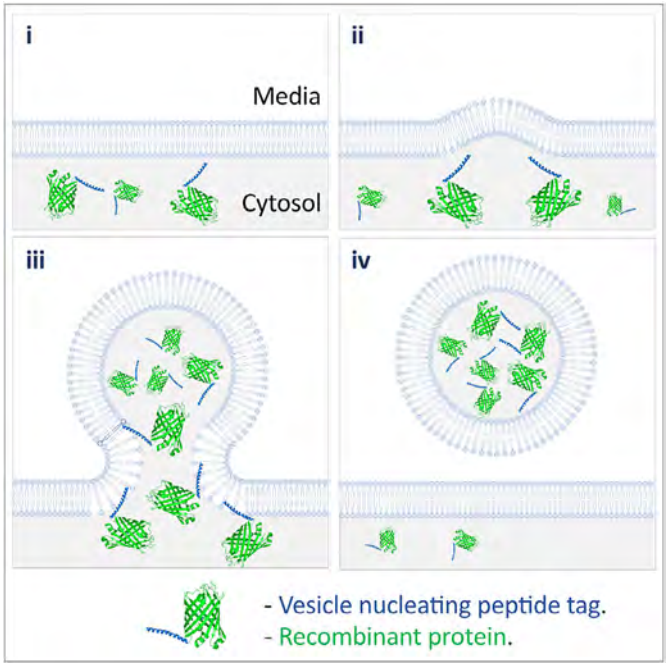

A simple peptide tag generates recombinant-protein-filled vesicles from *E. coli*. This approach allows simplified production of recombinant protein at high yields.

Microsphere-supported gold nanoparticles for SERS detection of malachite green

Supported metal nanoparticles are attractive for wide ranging applications including catalysis and imaging. In this work we prepare surface-enhanced Raman scattering (SERS) active materials by exploiting the high surface area of porous carbon microspheres (CμP) to assemble high loadings of gold nanoparticles (AuNPs). The specific surface functionalization of CμPs is exploited to prepare composites by two approaches, (1) carboxylic acid surface groups are used to attract positively charged AuNPs and (2) a thiol functionalized surface is used to immobilize AuNPs. Ripening of the surface immobilized gold nanoparticles through hydroquinone treatment results in the preparation of a roughened gold surface with a 22-fold increase in the Au loading from 0.3 to 7.0 (mass Au/mass C). The materials were thoroughly characterized by UV-vis, Infrared and Raman spectroscopy, DLS, zeta potential, TEM and SEM.

The SERS capacity of individual particles to detect malachite green, a mutagenic fungicide used in fish farming, was investigated using Raman optical tweezers. The challenges to trapping these materials due to the significant reflection, refraction and scattering properties of the Au-coated surfaces was overcome using a pinning approach. The measurements revealed the detection of malachite green at nM concentration and showed the potential of the porous carbon particles to act as versatile scaffolds for SERS applications.

Authors: D.T. Hinds, P.E. Colavita, S.J. Quinn, S.A. Belhout, A.D. Ward

Contact author: S.J. Quinn (susan.quinn@ucd.ie)

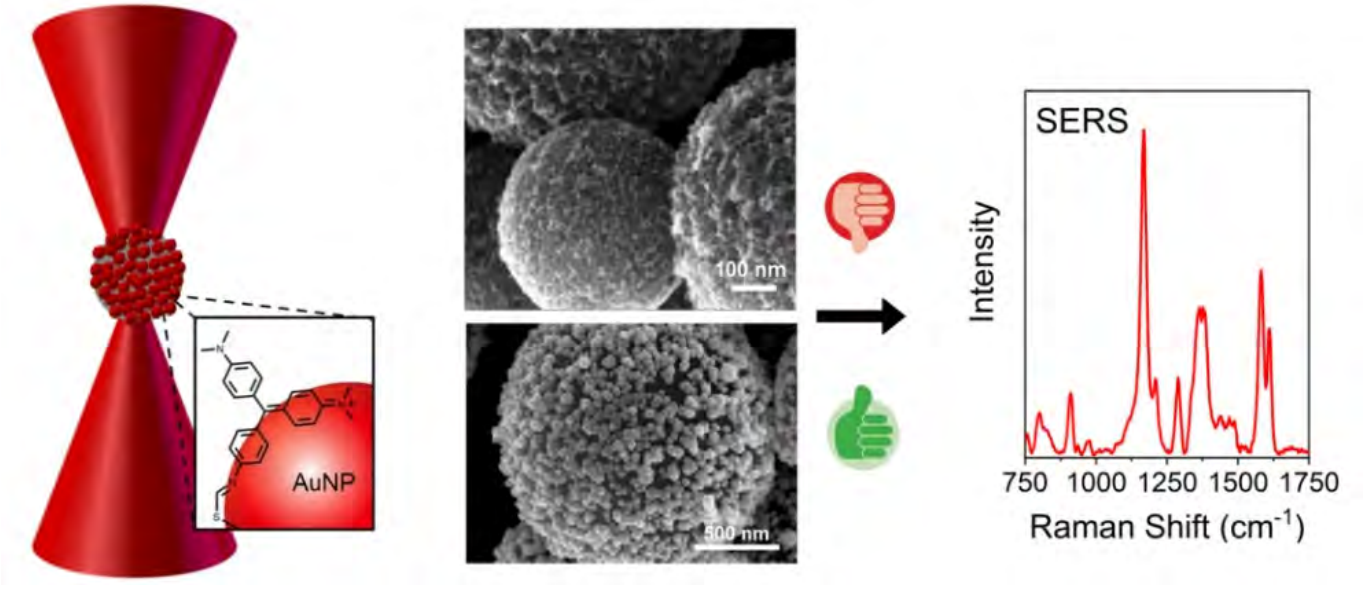

A porous carbon microsphere decorated with gold nanoparticles has been shown to act as a sensitive SERS substrate for the detection of malachite green. The use of an optical trap allows exclusive probing of individual composite particles and reveals the impact of the roughened gold surface on detection.

From Chemotherapy to Phototherapy – Changing the Therapeutic Action of a Metallo-Intercalating Ru^{II}-Re^{I} Luminescent System by Switching its Sub-Cellular Location

The synthesis of a new heterodinuclear $Re^{I}Ru^{II}$ metallointercalator containing Ru^{II}(dppz) and Re^{I}(dppn) moieties is reported. Cell-free studies reveal that the complex has similar photophysical properties to its homoleptic M(dppz) analogue and it also binds to DNA with a similar affinity. However, the newly reported complex has very different in-cell properties to its parent. In complete contrast to the homoleptic system, the Ru^{II}(dppz)/Re^{I}(dppn) complex is not intrinsically cytotoxic but displays appreciable phototoxic, despite both complexes displaying very similar quantum yields for singlet oxygen sensitization. Optical microscopy suggests that the reason for these contrasting biological effects is that whereas the homoleptic complex localises in the nuclei of cells, the Ru^{II}(dppz)/Re^{I}(dppn) complex preferentially accumulates in mitochondria. These observations illustrate how even small structural changes in metal based therapeutic leads can modulate their mechanism of action.

*Reproduced from Chem. Eur. J. 2023, **29**, e202300617, under the terms of a Creative Commons Attribution License. doi: 10.1002/chem.202300617*

Authors: H.K. Saeed, A.J. Auty, A.A.P. Chauvet, J.A. Thomas, P.J. Jarman, R. Mowll, C.G.W. Smythe, S. Sreedharan, J. Bernardino de la Serna

Contact authors: J.A. Thomas (james.thomas@sheffield.ac.uk)

J. Bernardino de la Serna (j.bernardino-de-la-serna@imperial.ac.uk)

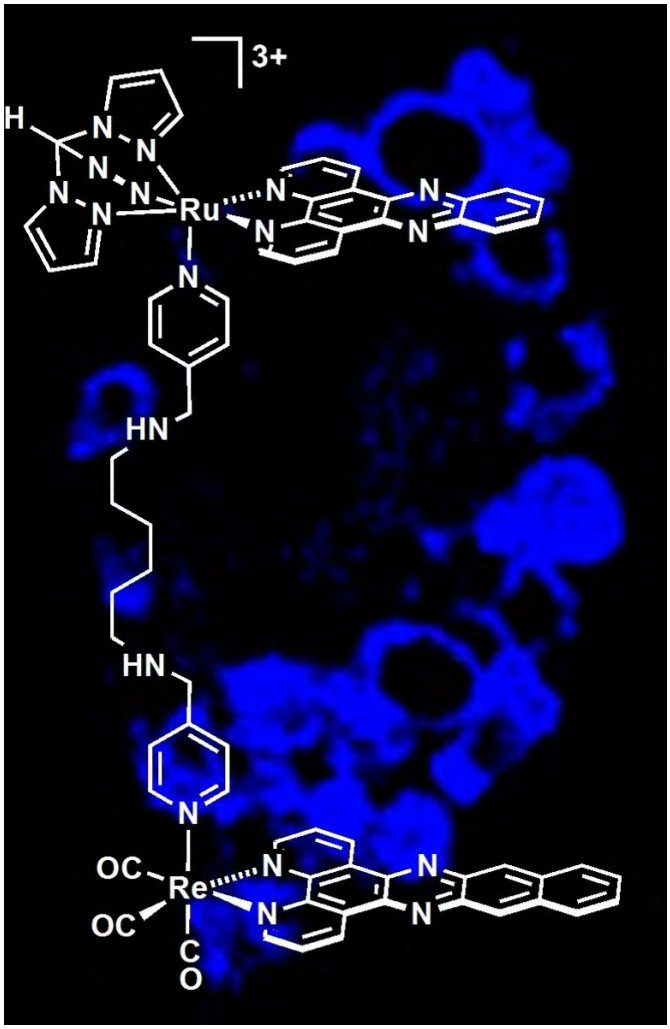

Binding partners regulate unfolding of myosin VI to activate the molecular motor

Myosin VI is the only minus-end actin motor and it is coupled to various cellular processes ranging from endocytosis to transcription. This multi-potent nature is achieved through alternative isoform splicing and interactions with a network of binding partners. There is a complex interplay between isoforms and binding partners to regulate myosin VI. Here, we have compared the regulation of two myosin VI splice isoforms by two different binding partners. By combining biochemical and single-molecule approaches, we propose that myosin VI regulation follows a generic mechanism, independently of the spliced isoform and the binding partner involved. We describe how myosin VI adopts an autoinhibited backfolded state which is released by binding partners. This unfolding activates the motor, enhances actin binding and can subsequently trigger dimerization.

We have further expanded our study by using single-molecule imaging to investigate the impact of binding partners upon myosin VI molecular organization and dynamics.

*Reproduced from Dos Santos Á, Fili N, Hari-Gupta Y, et al. Binding partners regulate unfolding of myosin VI to activate the molecular motor. Biochem J. 2022;**479**(13):1409-1428, published by Portland Press Limited, under the terms of a Creative Commons Attribution 4.0 International License. doi:10.1042/BCJ20220025*

Authors: Á. dos Santos, N. Fili, R.E. Gough, C.P. Toseland, Y. Hari-Gupta, L. Wang, M. Martin-Fernandez, J. Aaron, E. Wait, T-L, Chew

Contact author: C.P. Toseland (c.toseland@sheffield.ac.uk)

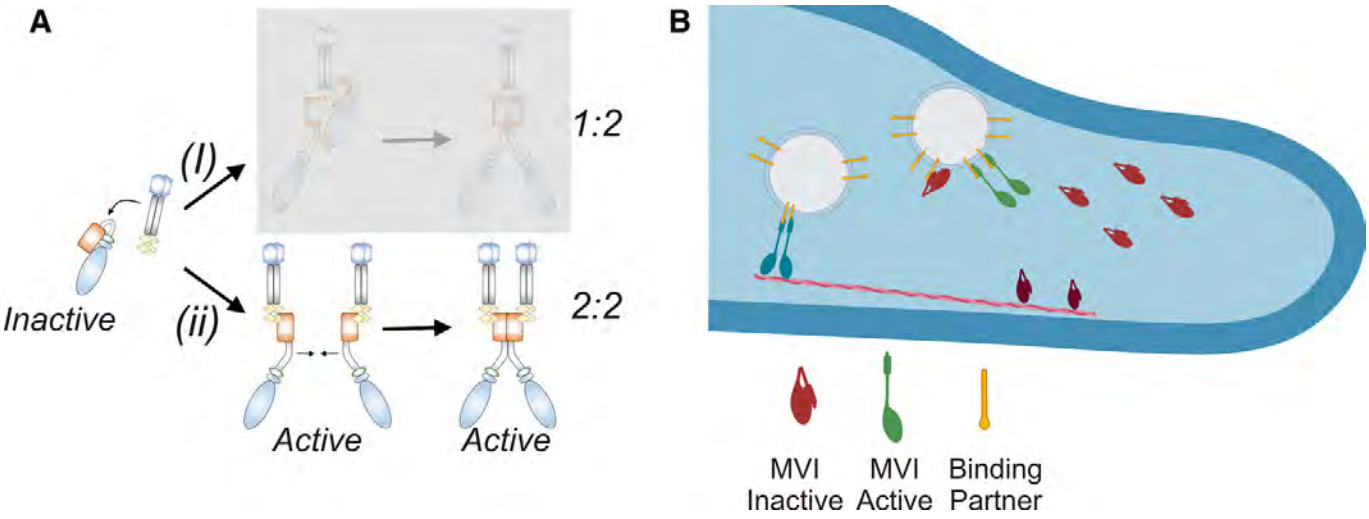

Model describing the activation of myosin VI by binding partners. (A) Two routes of binding partner dependent dimerization of MVI. (B) Recruitment and activation of myosin VI to cellular cargo by binding partners.

Structure and activity of particulate methane monooxygenase arrays in methanotrophs

Methane-oxidizing bacteria play a central role in greenhouse gas mitigation and have potential applications in biomanufacturing. Their primary metabolic enzyme, particulate methane monooxygenase (pMMO), is housed in copper-induced intracytoplasmic membranes (ICMs), of which the function and biogenesis are not known. We show by serial cryo-focused ion beam (cryoFIB) milling/scanning electron microscope (SEM) volume imaging and lamellae-based cellular cryo-electron tomography (cryoET) that these ICMs are derived from the inner cell membrane. The pMMO trimer, resolved by cryoET and subtomogram averaging to 4.8 Å in the ICM, forms higher-order hexagonal arrays in intact cells. Array formation correlates with increased enzymatic activity, highlighting the importance of studying the enzyme in its native environment. These findings also demonstrate the power of cryoET to structurally characterize native membrane enzymes in the cellular context.

Reproduced from Zhu, Y., Koo, C.W., Cassidy, C.K. et al. Structure and activity of particulate methane monooxygenase arrays in methanotrophs. Nat Commun 13, 5221 (2022), under the term of a Creative Commons Attribution 4.0 International License. doi: 10.1038/s41467-022-32752-9

Authors: Y. Zhu, T. Ni, J. Shen, C.W. Koo, A.C. Rosenzweig, C.K. Cassidy, M.C. Spink, Y. Sheng, Y. Song, Z. Yang, L.C. Zanetti-Domingues, B.C. Bateman, M. L. Martin-Fernandez, P. Zhang

Contact authors: A.C. Rosenzweig (amyr@northwestern.edu)

P. Zhang (peijun.zhang@strubi.ox.ac.uk)

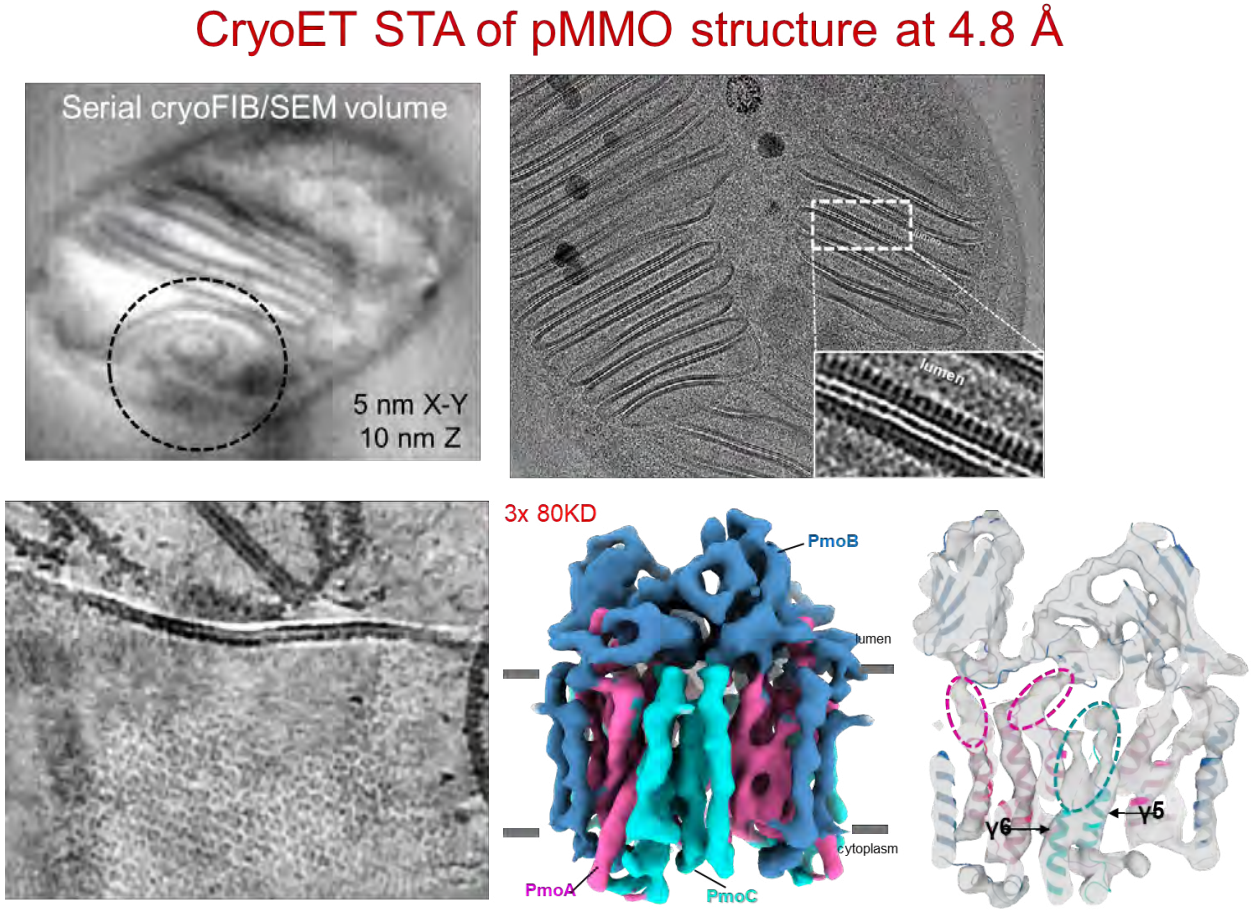

Kerr-gated Raman investigations to understand LDPE decomposition by zeolites

This work uses an optical time gating technique to collect Raman spectra during the catalytic conversion of low-density polyethylene on different zeolites. The chemical recycling of "non-recyclable" plastics is an important step towards a circular carbon economy.

In applying Raman spectroscopy during plastic conversion, we can relate spectral changes with the catalytic activity, to understand further our separately collected catalytic testing data. Intermediate species have been identified, and primary decomposition is separated from secondary reactions taking place, for example to give aromatic side products. Studying such a system under real operando conditions up to 400°C in temperature is extremely challenging, but thanks to the Kerr-gated spectrometer, we can reject fluorescence that otherwise interferes with the Raman signals being collected.

The work highlights zeolite characteristics that are the most and least useful for the process of LDPE pyrolysis, for conversion back to pyrolysis oils for the synthesis of new virgin-grade plastic.

Authors: E. Campbell, S. Wallbridge, S. Dann, S. Kondrat, I. V. Sazanovich, P. Moreau, A. M. Beale

Contact author: E. Campbell (Campbelle3@cardiff.ac.uk)

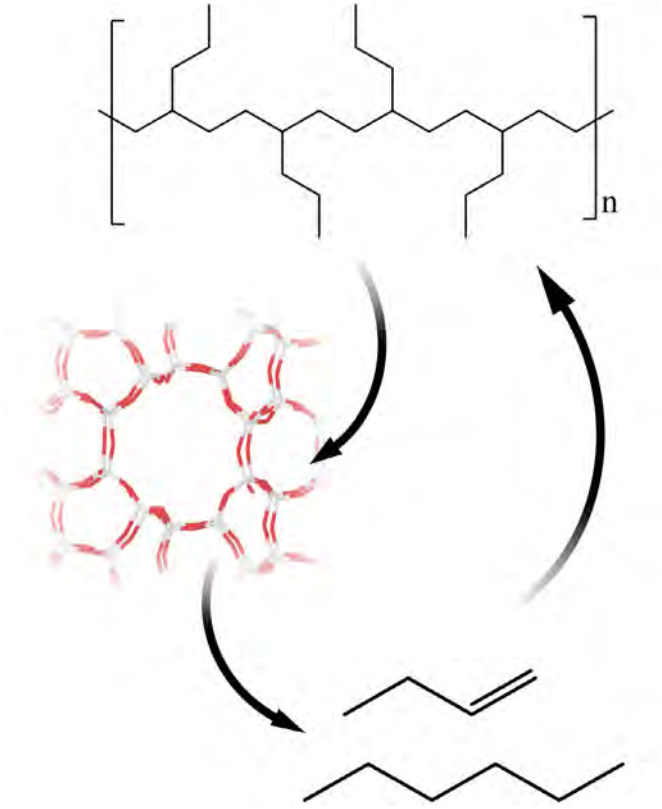

Figure 1: Figure of circularity of the process of chemically recycling LDPE with zeolite catalyst

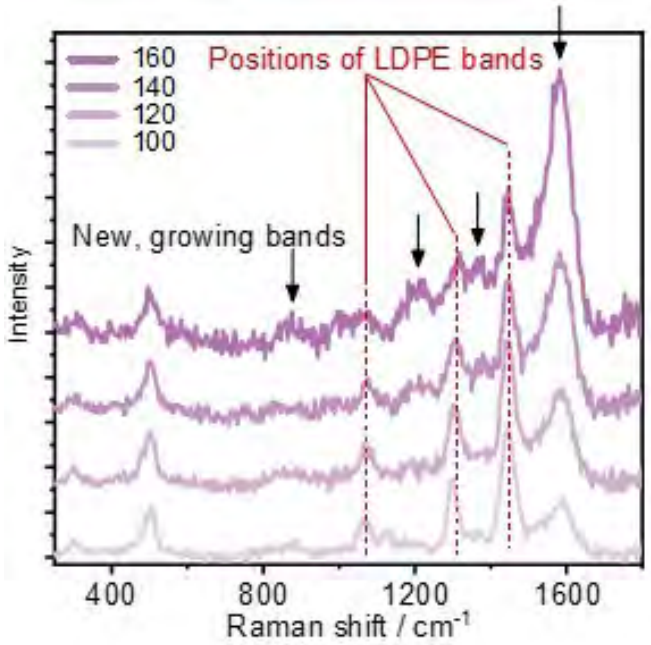

Figure 2: Raman spectra collected during the conversion of LDPE using H-Y as a catalyst

Time-Resolved Resonance Raman Spectroscopy of a Water Splitting Photocatalyst

We have reported new Kerr-gated Time-resolved Raman (TR^3) data for the linear polymer photocatalyst P10, and identified a new strong Raman mode of the P10 electron polaron. Interestingly experiments with P10 samples loaded with an IrO_x water oxidation catalyst also show clear evidence for long-lived electrons.The photoelectrons generated persist for >1 ns with no clear changes in the Raman spectra, indicating that electron transfer to the catalytic sites of hydrogen evolution is slow and further slow TR^3 studies could explore this potential kinetic bottleneck.

Authors: C. Li, O. Thwaites, A.M. Gardner, I.V. Sazanovich, A.J. Cowan

Contact author: A.J. Cowan (acowan@liverpool.ac.uk)

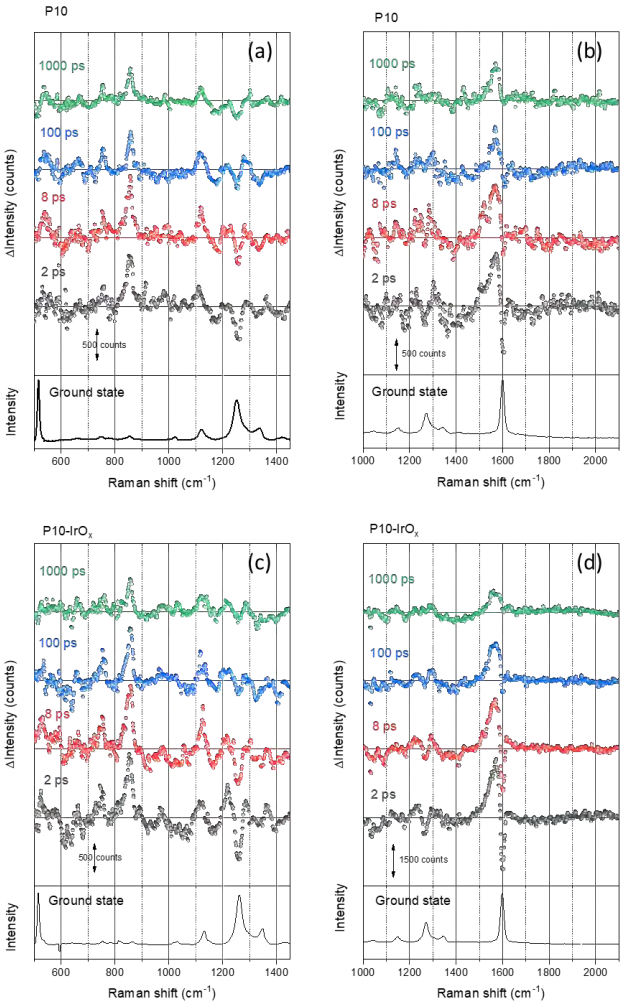

Figure 1: Kerr gated TR^3 spectra and ground state spectra (all 630 nm probe) recorded of P10 and P10-IrO_x following 400 nm excitation

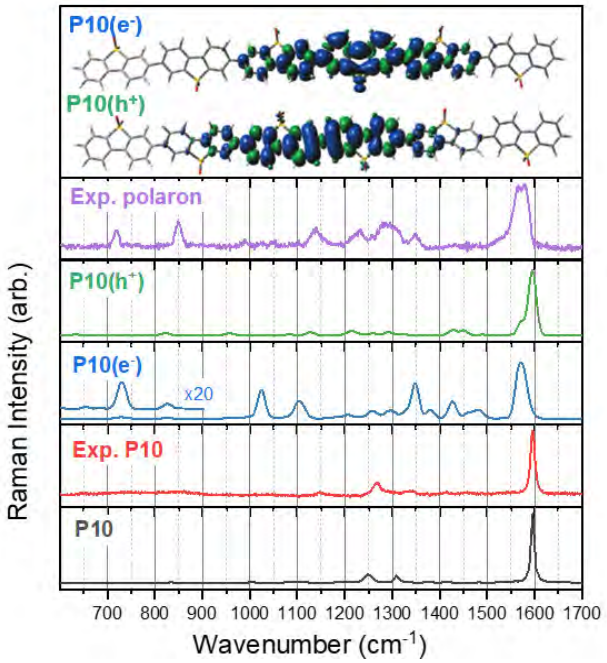

Figure 2: Density functional theory (DFT) calculated spectra and schematic of polaron localisation on a P10 hexamer (theory level ωB97XD/cc-pVDZ). Also included is a P10 polaron (electron) recorded under steady state illumination conditions

Figure 2 reproduced from J. Phys. Chem. Lett. 2021, 12, 10899−10905, under the terms of the Creative Commons CC-BY 4.0 License. doi: 10.1021/acs.jpclett.1c03073

Laser induced temperature-jump time resolved IR spectroscopy of zeolites

Combining pulsed laser heating and time-resolved infrared (TR-IR) absorption spectroscopy provides a means of initiating and studying thermally activated chemical reactions and diffusion processes in heterogeneous catalysts on timescales from nanoseconds to seconds. To this end, we investigated single pulse and burst laser heating in zeolite catalysts under realistic conditions using TR-IR spectroscopy. 1 ns, 70 µJ, 2.8 µm laser pulses from a Nd:YAG-pumped optical parametric oscillator were observed to induce temperature-jumps (T-jumps) in zeolite pellets in nanoseconds, with the sample cooling over 1 – 3 ms. By adopting a tightly focused beam geometry, T-jumps as large as 145°C from the starting temperature were achieved, demonstrated through comparison of the TR-IR spectra with temperature dependent IR absorption spectra and three dimensional heat transfer modelling using realistic experimental parameters. The simulations provide a detailed understanding of the temperature distribution within the sample and its evolution over the cooling period, which we observe to be bi-exponential. These results provide foundations for determining the magnitude of a T-jump in a catalyst/adsorbate system from its absorption spectrum and physical properties, and for applying T-jump TR-IR spectroscopy to the study of reactive chemistry in heterogeneous catalysts.

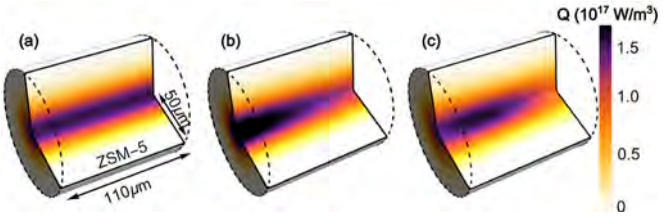

Figure 1: 3D distribution of heat supplied by the pump laser in heat transfer simulations, showing in sequence: (a) a Gaussian pump beam passing unattenuated through the sample; (b) the added effect of attenuation of the pump as it passes through the sample; (c) the added effect of the divergence of the pump beam.

Authors: A.P. Hawkins, A.E. Edmeades, C.D.M. Hutchison, M. Towrie, R.F. Howe, G.M. Greetham, P.M. Donaldson

Contact authors: A.P. Hawkins (alex.hawkins@stfc.ac.uk)

P.M. Donaldson (paul.donaldson@stfc.ac.uk)

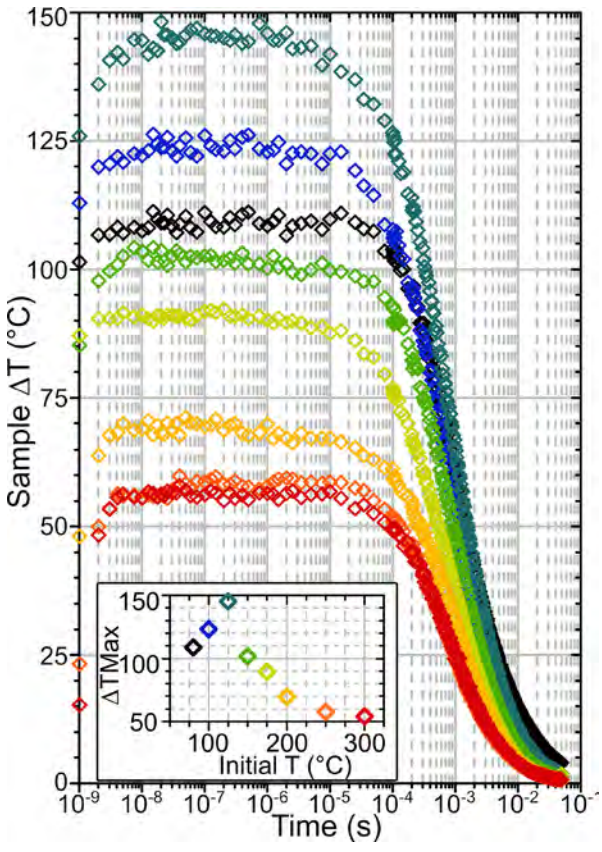

Figure 2: Sample heating vs time after ns laser heating for HOD/H_2O dosed ZSM-5, at different initial temperatures calculated based on changes in silanol mode intensity. The inset plot shows the maximum ΔT achieved against initial temperature. The colour scheme of the heating transients corresponds to that in the inset.

Ultrafast 2D-IR spectroscopy of intensely optically scattering pelleted solid catalysts

Solid, powdered samples are often prepared for infrared (IR) spectroscopy analysis in the form of compressed pellets. The intense scattering of incident light by such samples inhibits applications of more advanced IR spectroscopic techniques, such as two-dimensional (2D)-IR spectroscopy. We describe here an experimental approach that enables the measurement of high-quality 2D-IR spectra from scattering pellets of zeolites, titania, and fumed silica in the OD-stretching region of the spectrum under flowing gas and variable temperature up to ~500°C. In addition to known scatter suppression techniques, such as phase cycling and polarization control, we demonstrate how a bright probe laser beam comparable in strength with the pump beam provides effective scatter suppression. The possible nonlinear signals arising from this approach are discussed and shown to be limited in consequence. In the intense focus of 2D-IR laser beams, a free-standing solid pellet may become elevated in temperature compared with its surroundings. The effects of steady state and transient laser heating effects on practical applications are discussed.

Authors: P.M. Donaldson, R.F. Howe, A.P. Hawkins, M. Towrie, G.M. Greetham

Contact author: P.M. Donaldson (paul.donaldson@stfc.ac.uk)

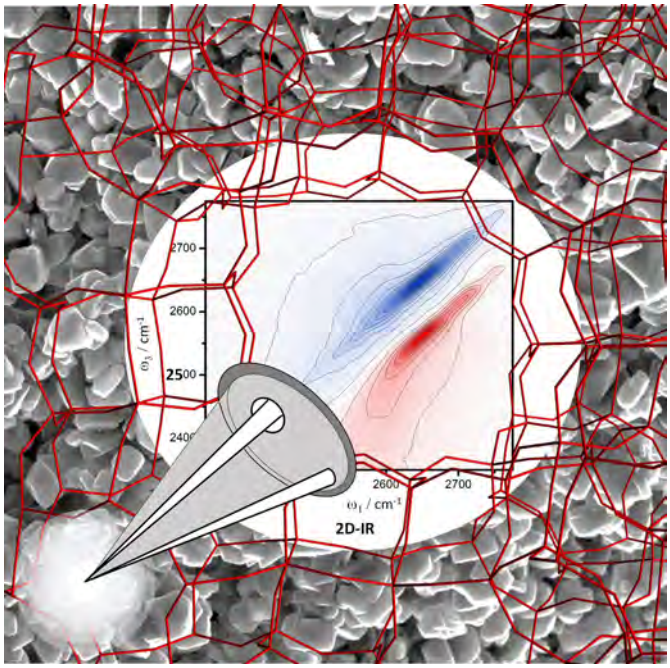

Zeolites are microcrystalline heterogeneous catalysts with nanometre scale pores, as shown in the superimposed SEM image and crystal structure. In this figure, a 2D-IR spectrum of zeolite Y is drawn in the zeolite pore. Measurement of spectra such as these was enabled by new methods developed to reject the intense optical scatter of the samples.

Spectrophotometric Concentration Analysis Without Molar Absorption Coefficients by Two-Dimensional-Infrared and Fourier Transform Infrared Spectroscopy

A spectrophotometric method for determining relative concentrations of infrared (IR)-active analytes with unknown concentration and unknown molar absorption coefficient is explored. This type of method may be useful for the characterization of complex/heterogeneous liquids or solids, the study of transient species, and for other scenarios where it might be difficult to gain concentration information by other means. Concentration ratios of two species are obtained from their IR absorption and two-dimensional (2D)-IR diagonal bleach signals using simple ratiometric calculations. A simple calculation framework for deriving concentration ratios from spectral data is developed, extended to IR-pump–probe signals, and applied to the calculation of transition dipole ratios. Corrections to account for the attenuation of the 2D-IR signal caused by population relaxation, spectral overlap, wavelength-dependent pump absorption, inhomogeneous broadening, and laser intensity variations are described. A simple formula for calculating the attenuation of the 2D-IR signal due to sample absorption is deduced and by comparison with 2D-IR signals at varying total sample absorbance found to be quantitatively accurate. 2D-IR and Fourier transform infrared spectroscopy of two carbonyl containing species acetone and N-methyl-acetamide dissolved in D_2O are used to experimentally confirm the validity of the ratiometric calculations. Finally, to address ambiguities over units and scaling of 2D-IR signals, a physical unit of 2D-IR spectral amplitude in mOD/√cm^{-1} is proposed.

Reproduced from Anal. Chem. 2022, 94, 51, 17988–17999, under the terms of a Creative Commons CC BY 4.0 License. doi: 10.1021/acs.analchem.2c04287

Author: P.M. Donaldson

Contact author: P.M. Donaldson (paul.donaldson@stfc.ac.uk)

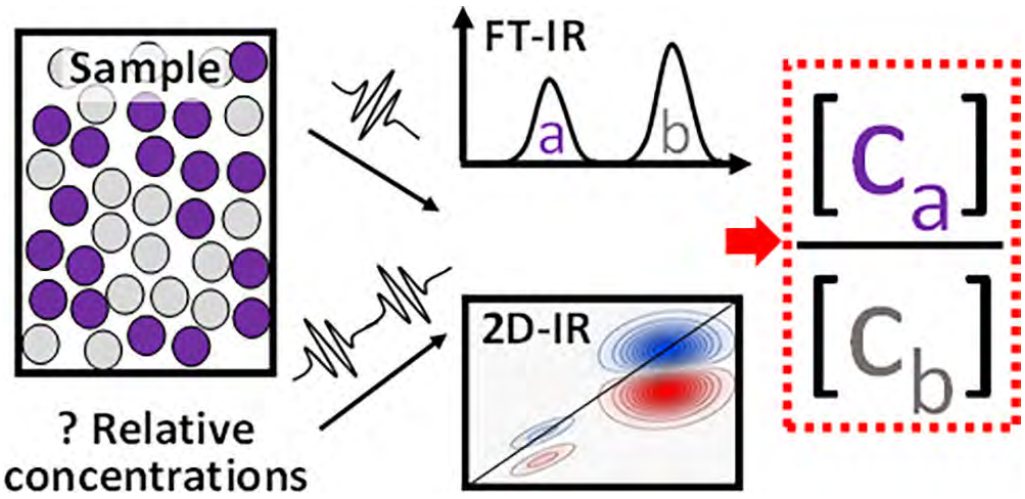

Surface enhanced Raman scattering with a Kerr-gate for fluorescence suppression

The combination of surface-enhanced and Kerr-gated Raman spectroscopy for the enhancement of Raman signal and suppression of fluorescence is reported. The technique enables the study of analytes that show weak Raman signal in highly fluorescent media under (pre)resonant conditions. This approach was exemplified by the well-defined spectra of Nile red (NR) and Nile blue (NB). Raman spectra of the fluorescent dyes were only obtained when SERS active substrates were used in combination with the Kerr-gate. To achieve enhancement of the weaker Raman scattering, Au films with different roughness or Au-core shell-isolated nanoparticles (SHINs) were used. Crucially, the use of SHINs enabled measurement of the Raman bands of fluorescent dyes upon non-SERS active, optically flat Au, Cu, and Al substrates.

Authors: G. Cabello, I.V. Sazanovich, A.R. Neale, L.J. Hardwick

Contact author: L.J. Hardwick (hardwick@liverpool.ac.uk)

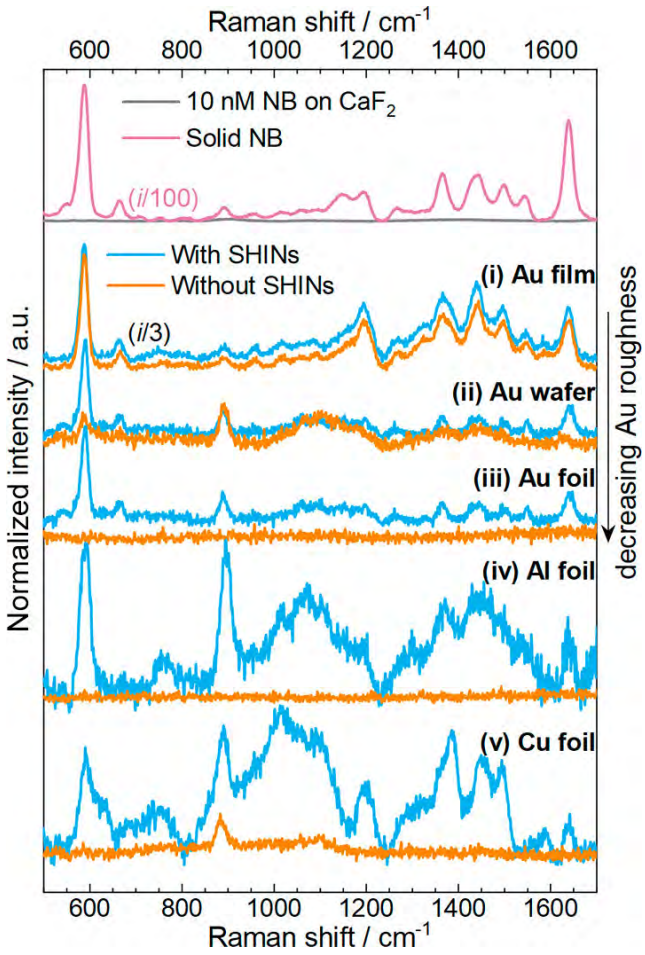

Figure 1: Kerr-gated Raman spectra for solid NB (pink), a 10 nM solution of NB in ethanol on glass (grey), and 10 nM solutions of NB in ethanol at different substrates without SHINs (orange) and with SHINs (blue): Au film, Au wafer, Au foil, Al foil, Cu foil. The intensity of spectra from Au film has been reduced three-fold. All spectra collected under 633 nm ps pulsed laser excitation.

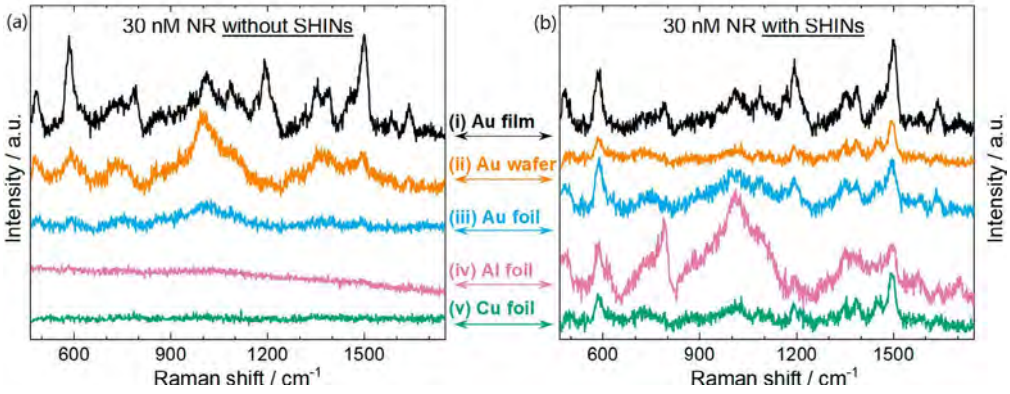

Figure 2: Kerr-gated Raman spectra, without (a) and with (b) a layer of SHINs, of a solution containing 30 nM NR in acetone on Au film (i); Au wafer (ii); Au foil (iii); Al film (iv); and Cu film (v). All spectra were collected under 633 nm ps pulsed laser excitation.

Optical Screening and Classification of Drug Binding to Proteins in Human Blood Serum

Protein–drug interactions in the human bloodstream are important factors in applications ranging from drug design, where protein binding influences efficacy and dose delivery, to biomedical diagnostics, where rapid, quantitative measurements could guide optimized treatment regimes. Current measurement approaches use multistep assays, which probe the protein-bound drug fraction indirectly and do not provide fundamental structural or dynamic information about the in vivo protein– drug interaction. We demonstrate that ultrafast 2D-IR spectroscopy can overcome these issues by providing a direct, label-free optical measurement of protein–drug binding in blood serum samples. Four commonly prescribed drugs, known to bind to human serum albumin (HSA), were added to pooled human serum at physiologically relevant concentrations. In each case, spectral changes to the amide I band of the serum sample were observed, consistent with binding to HSA, but were distinct for each of the four drugs. A machine-learning-based classification of the serum samples achieved a total cross-validation prediction accuracy of 92% when differentiating serum-only samples from those with a drug present. Identification on a per-drug basis achieved correct drug identification in 75% of cases. These unique spectroscopic signatures of the drug–protein interaction thus enable the detection and differentiation of drug containing samples and give structural insight into the binding process as well as quantitative information on protein–drug binding. Using currently available instrumentation, the 2D-IR data acquisition required just 1 min and 10 µL of serum per sample, and so these results pave the way to fast, specific, and quantitative measurements of protein–drug binding in vivo with potentially invaluable applications for the development of novel therapies and personalized medicine.

Reproduced from Anal. Chem. 2023, 95, 46, 17037–17045, published by the American Chemical Society, under the terms of a Creative Commons CC-BY 4.0 License. doi:10.1021/acs.analchem.3c03713

Authors: S.H. Rutherford, C.D.M. Hutchison, G.M. Greetham, A.W. Parker, A. Nordon, M.J. Baker, N.T. Hunt

Contact author: N.T. Hunt (neil.hunt@york.ac.uk)

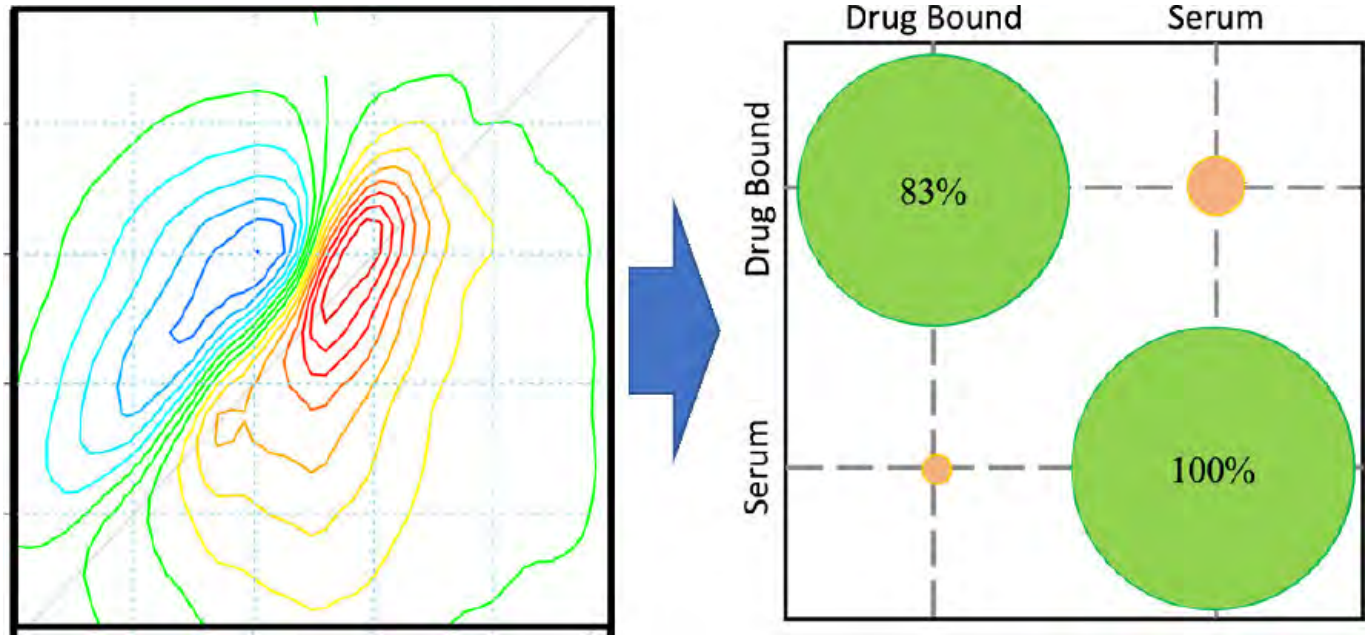

Coumarin C-H functionalization by Mn(I) carbonyls: Mechanistic insight by ultra-fast IR spectroscopic analysis

Mn(I) C–H functionalization of coumarins provides a versatile and practical method for the rapid assembly of fused polycyclic pyridinium-containing coumarins in a regioselective manner. The synthetic strategy enables application of bench-stable organomanganese reagents in both photochemical- and thermal-promoted reactions. The cyclomanganated intermediates, and global reaction system, provide an ideal testing ground for structural characterization of the active Mn(I) carbonyl-containing species, including transient species observable by ultra-fast time-resolved spectroscopic methods. The thermodynamic reductive elimination product, solely encountered from reaction between alkynes and air-stable organometallic cyclomanganated coumarins, has enabled characterization of a critical seven-membered Mn(I) intermediate, detected by time-resolved infrared spectroscopy, enabling the elucidation of the temporal profile of key steps in the reductive elimination pathway. Quantitative data are provided. Manganated polycyclic products are readily decomplexed by $AgBF_4$, opening-up an efficient route to the formation of π-extended hybrid coumarin-pyridinium compounds.

Reproduced from Chem. Eur. J. 2023, 29, e202203038, published by Wiley-VCH GmbH, under the terms of a Creative Commons Attribution License CC-BY 4.0. doi:10.1002/chem.202203038

Authors: T.J. Burden, K.P.R. Fernandez, M. Kagoro, J.B. Eastwood, T.F.N. Tanner, A.C. Whitwood, I.P. Clark, M. Towrie, J-P. Krieger, J.M. Lynam, I.J.S. Fairlamb

Contact authors: J.M. Lynam (jason.lynam@york.ac.uk)

I.J.S. Fairlamb (ian.fairlamb@york.ac.uk)

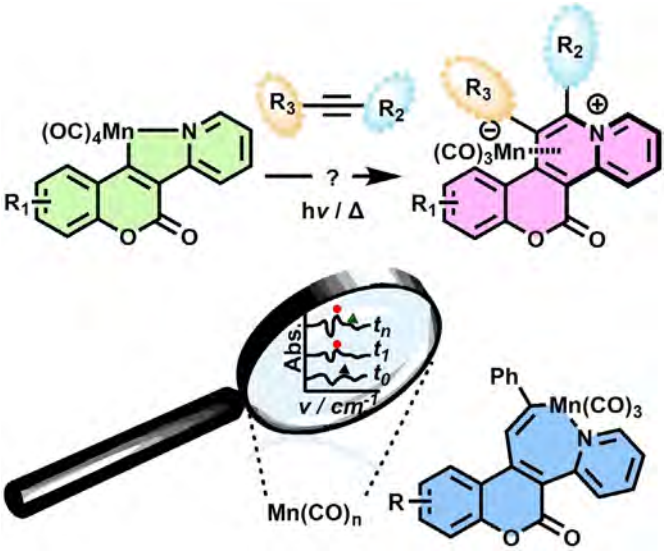

Photochemical dynamics of organic photocatalysts showing reverse intersystem crossing and thermally activated delayed fluorescence

Time-resolved infrared and fluorescence spectroscopy measurements reveal reverse intersystem crossing and delayed fluorescence emission in new designs of organic photocatalysts being tested for photoredox catalysis of atom-transfer radical polymerization. The organic photocatalysts have donor-acceptor-donor (D-A-D) structures based on a central benzophenone acceptor chromophore and pendant carbazole, phenoxazine or phenothiazine donor moieties. Comparison of the excited state relaxation timescales measured using the complementary time-resolved IR absorption and fluorescence emission techniques distinguishes organic compounds that are TADF emitters in their monomeric forms, or that only become TADF emitters upon aggregation in solution.

These contrasting behaviours account for the different efficiencies of the photocatalysts when used in photoredox catalytic cycles to initiate atom-transfer radical polymerization.

Authors: W. Whitaker, A.J. Orr-Ewing, Y. Kwon, W. Jeon, M.S. Kwon, I.V. Sazanovich

Contact author: A.J. Orr-Ewing (a.orr-ewing@bristol.ac.uk)

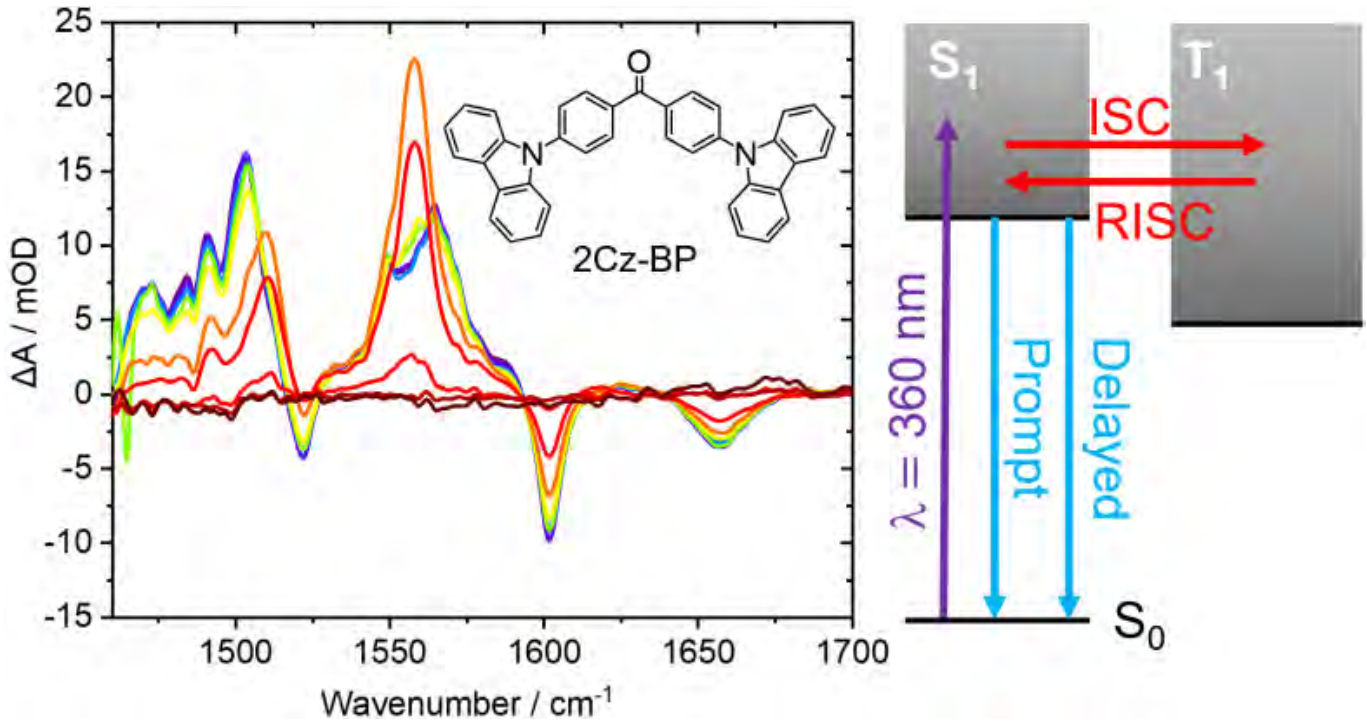

Time-resolved infra-red (TRIR) spectra (left) of a solution of the carbazole-substituted benzophenone molecule 2Cz-BP show growth and decay of triplet-state population, and relaxation of S_1 population over picosecond to microsecond timescales. These observations are consistent with forward and reverse intersystem crossing (ISC and RISC), resulting in both prompt and delayed fluorescence emission. The Jablonski diagram (right) shows these competing photochemical pathways.

Good vibrations report on the DNA quadruplex binding of an excited state amplified ruthenium polypyridyl IR probe

The nitrile containing Ru(II)polypyridyl complex $[Ru(phen)_2(11,12\text{-dCN-dppz})]^{2+}$ (**1**) is shown to act as a sensitive infrared probe of G-quadruplex (G4) structures. UV–visible absorption spectroscopy reveals enantiomer sensitive binding for the hybrid **htel(K)** and antiparallel **htel(Na)** G4s formed by the human telomer sequence $d[AG_3(TTAG_3)_3]$. Time-resolved infrared (TRIR) of **1** upon 400 nm excitation indicates dominant interactions with the guanine bases in the case of Λ-**1/htel(K)**, Δ-**1/htel(K)**, and Λ-**1/htel(Na)** binding, whereas Δ-**1/htel(Na)** binding is associated with interactions with thymine and adenine bases in the loop. The intense nitrile transient at 2232 cm^{-1} undergoes a linear shift to lower frequency as the solution hydrogen bonding environment decreases in DMSO/water mixtures. This shift is used as a sensitive reporter of the nitrile environment within the binding pocket. The lifetime of **1** in D_2O (*ca.* 100 ps) is found to increase upon DNA binding, and monitoring of the nitrile and ligand transients as well as the diagnostic DNA bleach bands shows that this increase is related to greater protection from the solvent environment.

Molecular dynamics simulations together with binding energy calculations identify the most favorable binding site for each system, which are in excellent agreement with the observed TRIR solution study. This study shows the power of combining the environmental sensitivity of an infrared (IR) probe in its excited state with the TRIR DNA "site effect" to gain important information about the binding site of photoactive agents and points to the potential of such amplified IR probes as sensitive reporters of biological environments.

Reproduced from J. Am. Chem. Soc. 2023, 145, 39, 21344-21360, published by American Chemistry Society, under the terms of a Creative Commons Attribution License CC-BY 4.0. doi: 10.1021/jacs.3c06099

Authors: M. Stitch, D. Avagliano, D. Graczyk, I.P. Clark, L. González, M. Towrie, S.J. Quinn

Contact authors: L. González (leticia.gonzalez@univie.ac.uk)

S.J. Quinn (susan.quinn@ucd.ie)

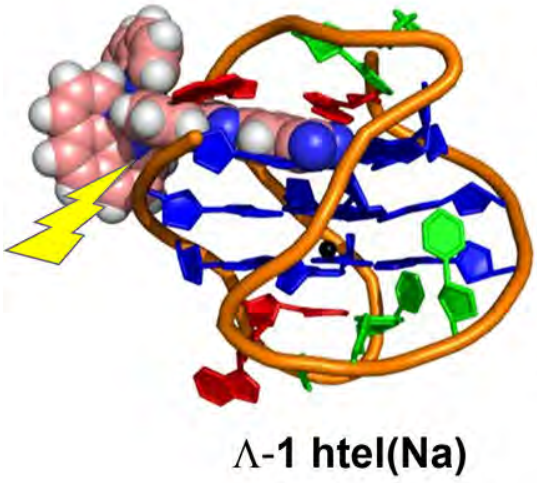

(Left) Predicted structure of the lambda enantiomer of the $[Ru(phen)_2(11,12\text{-dCN-dppz})]^{2+}$ (**1**) bound to the antiparallel G4 structure formed from the human telomere sequence $d[AG_3(TTAG_3)_3]$ in the presence of sodium ions.

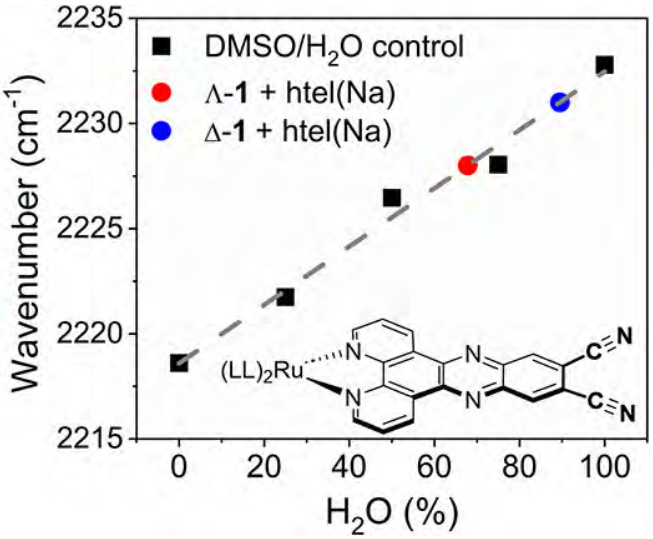

(Right) Correlation of the position of nitrile transient for G4-bound Λ-1 (red circle) and Δ-1(blue circle) to the hydrogen bonding nature of the solution environment (black squares).

G-Quadruplex Binding of an NIR Emitting Osmium Polypyridyl Probe Revealed by Solution NMR and Time-Resolved Infrared Studies

G-quadruplexes are emerging targets in cancer research and understanding how diagnostic probes bind to DNA G-quadruplexes in solution is critical to the development of new molecular tools. In this study the binding of an enantiopure NIR emitting $[Os(TAP)_2(dppz)]^{2+}$ complex to different G-quadruplex structures formed by human telomer (hTel) and cMYC sequences in solution is reported. The combination of NMR and time-resolved infrared spectroscopic techniques reveals the sensitivity of the emission response to subtle changes in the binding environment of the complex. Similar behaviour is also observed for the related complex $[Os(TAP)_2(dppp2)]^{2+}$ upon quadruplex binding.

Reproduced from Chem. Eur. J. 2023, 29, e202203250, published by Wiley-VCH GmbH, under the terms of the Creative Commons Attribution License. doi: 10.1002/chem.202203250

Authors: K. Peterková, M. Stitch, R.Z. Boota, P.A. Scattergood, P.I.P. Elliott, M. Towrie, P. Podbevšek, J. Plavec, S.J. Quinn

Contact authors: J. Plavec (janez.plavec@ki.si)

S.J. Quinn (susan.quinn@ucd.ie)

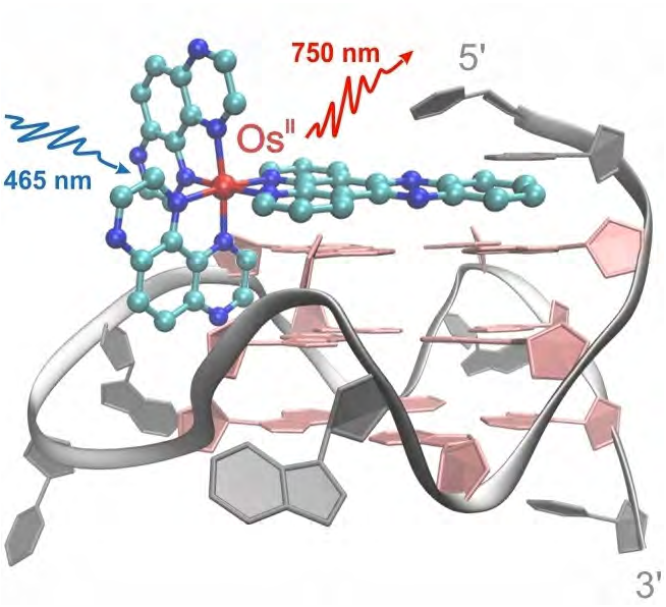

Structural modelling of the lambda enantiomer of the osmium polypyridyl light switch probe containing the extended dipyrido[3,2-a:2',3'-c]phenazine (dppz) ligand to the cMYC quadruplex structure (PDB ID: 2LBY). NMR studies reveal the role of π-π stacking of the dppz ligand at the 5'-quartet end, which is supported by time-resolved infrared measurements. Notably, the luminescent enhancement is found to be sensitive to the particular orientation at the 5'-quartet binding site.

A stronger acceptor decreases the rates of charge transfer: ultrafast dynamics and on/off switching of charge separation in organometallic donor–bridge–acceptor systems

To unravel the role of driving force and structural changes in directing the photoinduced pathways in donor–bridge–acceptor (DBA) systems, we compared the ultrafast dynamics in novel DBAs which share a phenothiazine (PTZ) electron donor and a Pt(II) trans-acetylide bridge (–C≡C–Pt–C≡C–), but bear different acceptors conjugated into the bridge (naphthalene-diimide, NDI; or naphthalene-monoimide, NAP). The excited state dynamics were elucidated by transient absorption, time-resolved infrared (TRIR, directly following electron density changes on the bridge/acceptor), and broadband fluorescence-upconversion (FLUP, directly following sub-picosecond intersystem crossing) spectroscopies, supported by TDDFT calculations. Direct conjugation of a strong acceptor into the bridge leads to switching of the lowest excited state from the intraligand ^{3}IL state to the desired charge-separated ^{3}CSS state. We observe two surprising effects of an increased strength of the acceptor in NDI vs. NAP: a *ca.* 70-fold slow-down of the ^{3}CSS formation —(971 ps)$^{-1}$vs. (14 ps)$^{-1}$, and a longer lifetime of the ^{3}CSS (5.9 vs. 1 ns); these are attributed to differences in the driving force ΔG_{et}, and to distance dependence. The 100-fold increase in the rate of intersystem crossing—to sub-500 fs—by the stronger acceptor highlights the role of delocalisation across the heavy-atom containing bridge in this process. The close proximity of several excited states allows one to control the yield of ^{3}CSS from ~100% to 0% by solvent polarity. The new DBAs offer a versatile platform for investigating the role of bridge vibrations as a tool to control excited state dynamics.

Reproduced from A.J. Auty et al. ***Chem. Sci.****, 2023,****14****, 11417-11428, under a Creative Commons Attribution 3.0 Unported License. doi:10.1039/d2sc06409j*

Authors: A.J. Auty, P.A. Scattergood, T. Keane, T. Cheng, G. Wu, H. Carson, J. Shipp, A. Sadler, T. Roseveare, I.V. Sazanovich, A.J.H.M. Meijer, D. Chekulaev, P.I.P. Elliot, M. Towrie, J.A. Weinstein

Contact authors: J.A. Weinstein (julia.weinstein@sheffield.ac.uk)

A.J.H.M. Meijer (a.meijer@sheffield.ac.uk)

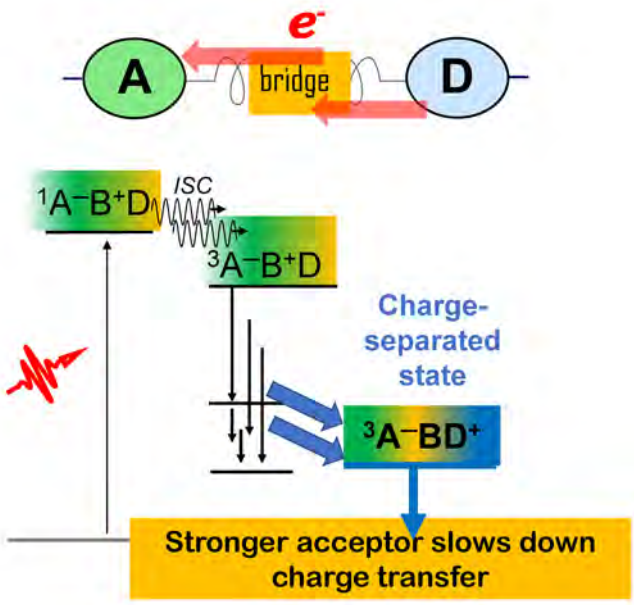

The upper part displays the schematic of a donor-bridge-acceptor system, with the acceptor being on the left, and the donor on the right, the bridge in the middle, and an arrow indicating the direction of the electron transfer. The lower part presents the schematic energy level diagram for such a system, with the photo-populated singlet A-B+D being the highest level, and the triplet state A-B+D being slightly below and getting populated promptly from the former one; the third state – the triplet and fully charge-separated A-BD+ – is positioned significantly lower than the other two. The picture illustrates that the stronger acceptor significantly slows down the rate of the full charge-separated state formation – whilst it should have been the other way around!

Operational Statistics

Gemini Operational Statistics 2022–23

Author: S. Hawkes
Central Laser Facility, STFC Rutherford Appleton Laboratory, Harwell Campus, Didcot, UK

Week beginning	
04-Apr-22	System Access
11-Apr-22	
18-Apr-22	
25-Apr-22	
02-May-22	
09-May-22	
16-May-22	
23-May-22	
30-May-22	
06-Jun-22	
13-Jun-22	
20-Jun-22	
27-Jun-22	
04-Jul-22	Sarri
11-Jul-22	
18-Jul-22	
25-Jul-22	
01-Aug-22	
08-Aug-22	
15-Aug-22	22110007
22-Aug-22	
29-Aug-22	
05-Sep-22	
12-Sep-22	
19-Sep-22	PoC Imaging 22510000
26-Sep-22	
03-Oct-22	
10-Oct-22	
17-Oct-22	
24-Oct-22	McKenna 22110009
31-Oct-22	
07-Nov-22	
14-Nov-22	
21-Nov-22	
28-Nov-22	
05-Dec-22	
12-Dec-22	
19-Dec-22	
26-Dec-22	
02-Jan-23	
09-Jan-23	
16-Jan-23	Borghesi 22110011
23-Jan-23	
30-Jan-23	
06-Feb-23	
13-Feb-23	
20-Feb-23	
27-Feb-23	
06-Mar-23	
13-Mar-23	Hooker 2221009
20-Mar-23	
27-Mar-23	

Figure 1: Gemini 2022/23 operational schedule

During the reporting year, April 22 – April 23, a total of four complete experiments were delivered in the Astra-Gemini Target Area. In total, 23 high power laser experimental weeks were delivered to the Gemini Target Area. The delivered Gemini schedule is presented in Figure 1.

The availability of the Gemini laser system (delivery to the Gemini Target Area) was 82% during normal working hours, rising to 126% with time made up from running outside of normal working hours. The reliability of the Gemini laser was 87%. An individual breakdown of the availability and reliability for the TA3 experiments conducted is presented in Figure 2.

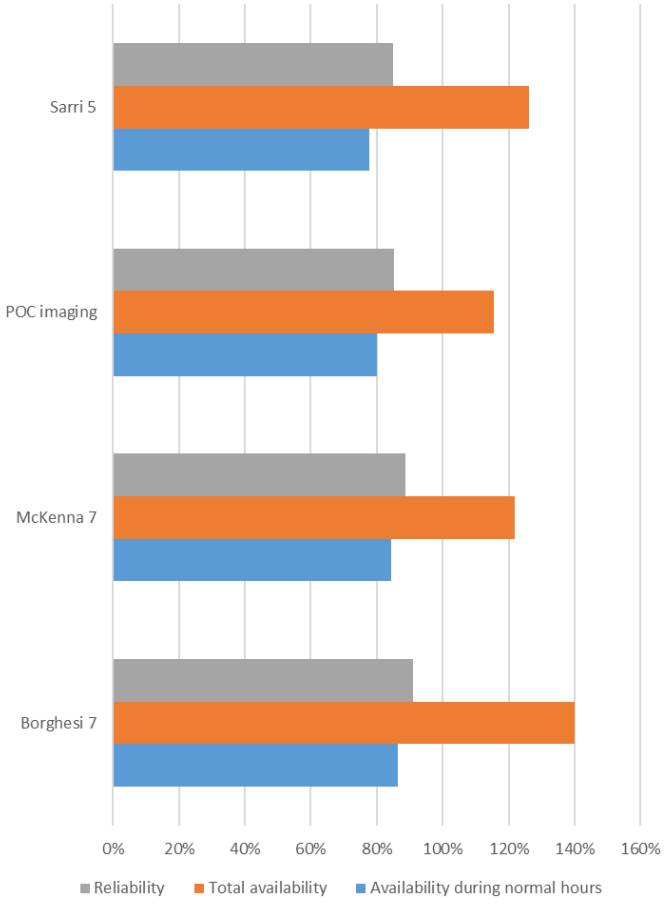

Figure 2: 2022/23 TA3 operational statistics

The high levels of total availability were made possible by the continued unique operational model employed on Gemini, which involves running the laser late into the evening. In addition, frequent weekend operational days were made available.

During the system access period, the four Quanta Ray pro 350 pump lasers for amplifier 3 were replaced by eight Lumibird QSmart 1500s. This was a major infrastructure change to the Astra laser system and took a significant portion of the year. This impacted the number of delivered weeks and number of experiments conducted, while the Sarri experiment was paused to resolve some initial install issues with the new lasers.

The upgraded pump lasers for amplifier 3 provide double the pump energy, which allows for the Astra output energy to increase up to 2.0 J, and incorporates a pump homogenization scheme. This will improve the beam homogeneity, both for the Gemini amplifier seed beam and for the TA2 main beam.

Contact Author: S. Hawkes (steve.hawkes@stfc.ac.uk)

Vulcan Operational Statistics 2022/23

Authors: S.E.J. Chapman, J. Morse, P. Oliveira
Central Laser Facility, STFC Rutherford Appleton Laboratory, Harwell Campus, Didcot, UK

Introduction

Vulcan has completed another active experimental year (April 2022 - March 2023) with 30 full experimental weeks allocated between target areas West (TAW) and Petawatt (TAP). Overall, the laser statistics show an improved operational standard with an overall reliability of 92%. Table 1 (opposite page) shows the operational schedule and statistics for this period. Information on the number of shots, energy-on-target success rate and availability hours are also provided in the table.

Numbers in parentheses indicate the total number of full energy laser shots delivered to target, followed by the number of these that failed and the percentage of successful shots. The second set of numbers are the availability of the laser to target areas during normal operating hours and including outside hours operations.

We have operated throughout the year, with short maintenance periods. Two important developments have increased both the reliability and the availability of the laser, even with reduced staff. Firstly, turn on and off was made fully automatic, with only three buttons to press when turning off, and automatic turn on at 6:00 am without any human intervention that has worked throughout the experimental campaign. Secondly, an automatic energy stabilisation system on one of the pump lasers has not only ensured that the energy has remained stable throughout the day, but has also allowed the system to be operational earlier, since the energy has been stabilised in a shorter time.

The total number of full disc amplifier shots that have been fired to target this year is 601. Table 2 shows how this figure compares with that for the previous four years. 51 shots failed to meet user requirements. The overall shot success rate to target for the year is 92%.

Table 2: Shot totals and proportion of failed shots for the past five years

	No of shots	Failed shots	Reliability
18–19	607	113	81%
19–20	653	102	84%
20–21	325	64	80%
21–22	604	73	88%
22–23	601	51	92%

Figure 1 shows the reliability of the Vulcan laser to all target areas over the past five years. The shot reliability to TAW is 93%, up 5% from the previous year. The shot reliability to TAP is 86%, down 1% from 87% in 2021-22.

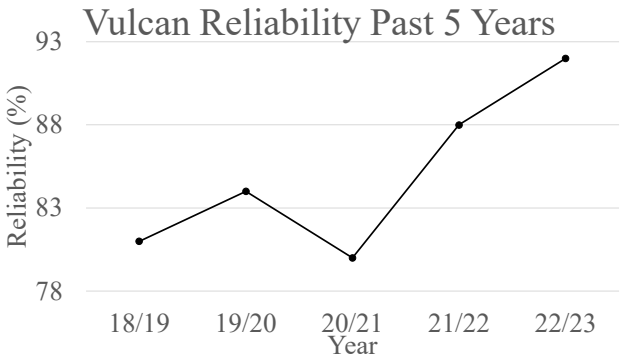

Figure 1: All areas shot reliability for each year 2018-19 to 2022-23

Uncommon shot configurations, like small energy requests or oscillator changes, have corresponded to most of the failed shots; on at least one experiment, all four oscillators changed, three of them alternately on the same beamlines.

The first experiment in TAP for about a year resulted in the lowest level of reliability. Mid-way through the second experiment, the previously mentioned automatic energy stabilisation system was implemented on the pump laser. This resulted in an increase in reliability, despite being introduced part way through the experiment.

Availability has been reduced by problems with the high voltage part of the system, in rod or disk amplifier elements.

Table 1: Experimental schedule for the period April 2022 – March 2023

Period	TAW	TAP
	2022	
9 May – 12 Jun	J Fuchs Investigation of the ion streaming instability in the laboratory and of the associated energy transfer to the background plasma (Shots 129, Failed 6, Reliability 95.3%) (Availability 94.6%, w extra hours 108.0%) (5 weeks) 20110000	
12 Sep – 15 Oct	L Gizzi Impact of Laser Bandwidth on Laser-Plasma Interaction in Shock Ignition Relevant Conditions (Shots 55, Failed 6, Reliability 89%) (Availability 94%, w extra hours 111.3%) (5 weeks) 22110010	
31 Oct – 3 Dec	DSTL Commercial Beam-time (Shots 184, Failed 9, Reliability 95.1%) (Availability 98.3%, w extra hours 117.8%) (5 weeks) 22510001	C Palmer Energetic proton beam collimation in long scale length plasmas (Shots 100, Failed 17, Reliability 83%) (Availability 96.9%, w extra hours 117.2%) (5 weeks) 22210010
	2023	
23 Jan – 25 Feb	P McKenna Measuring the role of anisotropic heating and plasma expansion on relativistic self-induced transparency (Shots 73, Failed 6, Reliability 91.8%) (Availability 95%, w extra hours 112.3%) (5 weeks) 22110008	D Carroll Investigation of EMP emissions for understanding the source mechanisms and the rules for tuning and employing them in high power lasers (Shots 60, Failed 7, Reliability 88.3%) (Availability 95.5%, w extra hours 112.8%) (5 weeks) 19210019

Throughout the year, there were 11 failures on elements on the disk amplification chain/capacitor bank, and two on the rod amplification chain. Each time there was a problem with these elements, it took between three hours and one-and-a-half days to resolve.

There is a requirement, which was originally instigated for the EPSRC FAA, that the laser system be available from 09:00 to 17:00 hours, Monday to Thursday, and from 09:00 to 16:00 hours on Fridays, during the five-week periods of experimental data collection (a total of 195 hours over the five-week experimental period). The laser has mainly met the startup target of 9:00 am, but it has been common practice to operate the laser well beyond the standard contracted finish time on several days during the week.

In addition, the introduction of early start times on some experiments continues to lead to improvements in availability.

On average, Vulcan has been available to target areas for each experiment for 95.7% of the time during contracted hours, compared with 77.3% for the previous year. The overall availability to all target areas has increased slightly to 113.2%, compared with 112.9% in 2021-22. The time that the laser is unavailable to users is primarily the time taken for beam alignment at the start of the day.

Contact Author: S.E.J. Chapman (sonya.chapman@stfc.ac.uk)

Lasers for Science Facility Operational Statistics 2022/23

Authors: B.C. Bateman, M. Szynkiewicz, S.K. Roberts, C. Sanders, D.T. Clarke
Central Laser Facility, STFC Rutherford Appleton Laboratory, Harwell Campus, Didcot, UK

Artemis facility

During this reporting period, the UK User community applied for 24 weeks of peer-reviewed access to the Artemis facility, of which 12 weeks were awarded, representing an over-subscription ratio of 2.00. A total of seven unique User groups performed eight scheduled experiments. Figure 1 shows that Condensed Matter was the most popular experiment subject conducted.

A total of 182 hours of downtime and 1390 additional hours of access were reported, corresponding to a total of 48 weeks of access time delivered to the User Community.

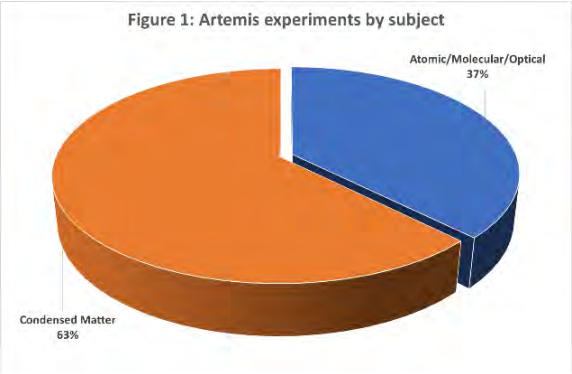

Octopus facility

During this reporting period, the UK User community applied for 158 weeks of peer-reviewed access to the Octopus facility, of which 90 weeks were awarded, representing an over-subscription ratio of 1.76. A total of 30 unique User groups performed 30 scheduled experiments. In addition, a total of 13 days proof of concept experiments and five days of commercial access were delivered. Figure 2 shows that Biology and Bio-materials was the most popular experiment subject conducted.

A total of 153 hours of downtime and 13 additional hours of access were reported.

A total of 19 formal reviewed publications were recorded through the year.

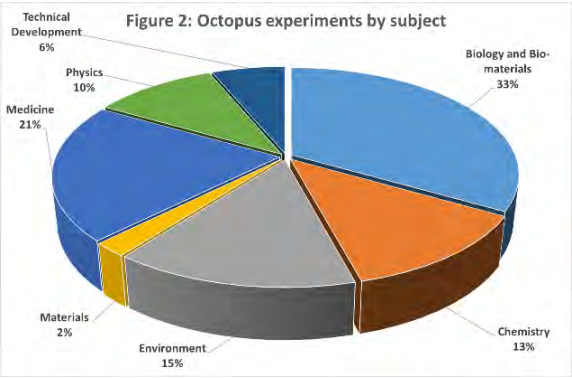

Ultra facility

During this reporting period, the UK User community applied for 75 weeks of peer-reviewed access to the Ultra facility, of which 50 weeks were awarded, representing an over-subscription ratio of 1.50. A total of 17 unique User groups performed 21 scheduled experiments. In addition, a total of 6.5 days proof of concept experiments, 11 days collaborative access and 15 days commercial access were delivered. Figure 3 shows that Chemistry was the most popular experiment subject conducted.

A total of 70 hours of downtime and 643 additional hours of access were reported. There were a total of 19 formal reviewed publications recorded through the year.

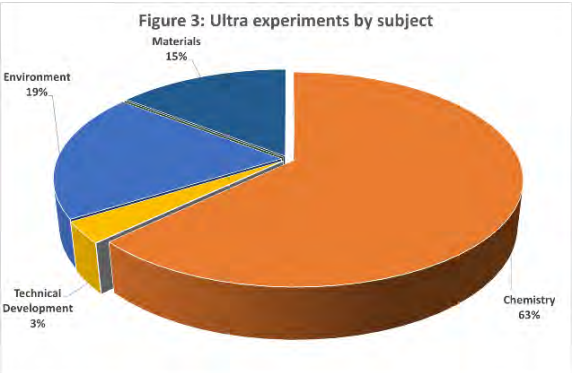

User satisfaction feedback

Surveys completed by User groups after their experimental time indicated an average satisfaction rating of 91.4% over the five specified categories.

Authors: B.C. Bateman, M. Szynkiewicz, S.K. Roberts, C. Sanders, D.T. Clarke

Contact author: D.T. Clarke (dave.clarke@stfc.ac.uk)

Figure 4: Average user satisfaction

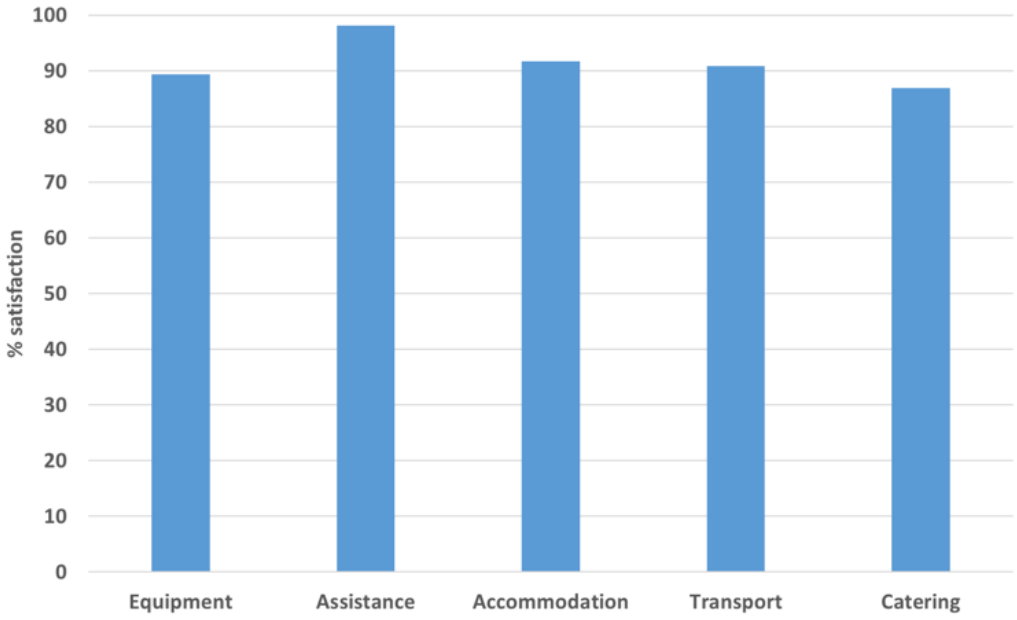

Target Fabrication Operational Statistics 2022/23

Authors: S. Astbury, D. Haddock, C. Spindloe, M. K. Tolley
Central Laser Facility, STFC Rutherford Appleton Laboratory, Harwell Campus, Didcot, UK

Introduction

This operational statistics report documents the total target delivery of the Target Fabrication Group of the Central Laser Facility over the 2022/23 operating period. The Target Fabrication Group is responsible for the supply of laser targets alongside a multitude of diagnostic elements, optical coatings and characterisation services (which are not covered in the scope of this report) for experimental campaigns across four high power laser (HPL) experimental areas at the CLF – two of which are driven by the Vulcan laser (TAP and TAW) and two by the Gemini laser (TA2 and TA3).

The Group provided targets for 10 HPL experimental campaigns at the CLF during the 2022/23 operating period, each of which typically lasted six weeks, as well as providing targets for external access experiments during the year.

A solid target comprises virtually any material (metals, polymers and ceramics), coated to nanometrically precise thicknesses in a range of geometries and characterised to ensure they fall within tight tolerances. There is generally a difference between the type of target requested for Vulcan and those for Gemini experiments. Vulcan targets are typically more complex (for example single target assemblies on posts) with a focus on precision-assembly 3D microstructures and mass-limited targets. Gemini targets are typically less complex and more mass-manufacturable to accommodate the higher repetition rate (HRR) of the laser. Typically targets include multi-layer or ultra-thin foils on arrays or tape substrates.

Supported Experiments

Over the 10 experiments that the Target Fabrication Group delivered for in the 2022/23 operating period, seven campaigns took place on Vulcan and three on Gemini. Table 1 shows the breakdown of the experiments which were supported. Not captured within the scope of this report are TA2 campaigns for which targets were usually externally provided.

Table 1: Experimental campaigns supported by the Target Fabrication Group over the 2022/23 operating period

Experiment	Area
0822 McKenna	Gemini TA3
1022 Borghesi	Gemini TA3
0323 Hooker	Gemini TA3
0422 Fuchs	Vulcan TAW
0922 Gizzi	Vulcan TAW
1122 Palmer	Vulcan TAP
0123 Carroll	Vulcan TAP
0123 McKenna	Vulcan TAW
0323 Borghesi	Vulcan TAP
0323 Armstrong	Vulcan TAW

The previous operating period (2021/22) saw a large number of simple tape-driven targets (off-the-shelf spools of material with no coating or assembly required) which were shot on TA2 and thus it was deemed necessary for future statistical reports to separate the target issue list between simple tape targets and targets which require significant fabrication effort.

Target Complexity and Classification

The variety of target types provided by the Target Fabrication Group are categorised as Class 1, 2 and 3 targets which provides a method of classifying the complexity and research/planning necessary for experimental delivery. The definitions are somewhat subjective in nature, but are typically classified as follows:

- Class 1: Targets that require fewer specialist resources to manufacture. Materials are typically procured 'off-the-shelf' and minimal specialist equipment is required for assembly. Typical targets include several-micron-thick foils or alignment wires glued to posts.
- Class 2: Targets that require the use of specialist manufacturing equipment and knowledge, which would be a very involved process for a non-Target Fabrication specialist to replicate. Examples include multi-nanometre thin-films and multilayer coatings.
- Class 3: Targets that require long-term R&D projects to establish and perfect, often referred to as "high-specification targets". Such targets include complex 3D assemblies, MEMS-components, low-density foams and multi-step tape targets.

As previously mentioned, a target can take many different forms – a single foil on a post or a large area of foil mounted on an array with many apertures (comprising many targets on one frame). It is, therefore, important to make the distinction between a component and a target. In the case above, a post or frame is considered a single component, and each shootable area on a component is considered a target.

Target Supply

For the 10 supported experiments, the Target Fabrication Group delivered a total of **1573 targets** over the 2022/23 operating period. Including tape targets, the total number of supplied targets was **5073**.

Of the 1573 targets delivered, 32.3% were manufactured for Gemini experiments and the remaining 67.7% for Vulcan experiments. Including tape targets, the percentages are 79% and 21% for Gemini and Vulcan, respectively.

Referring to the target classifications above, Figure 1 shows the breakdown of target complexity for both Vulcan and Gemini (excluding TA2) experiments over the 2022/23 operating period.

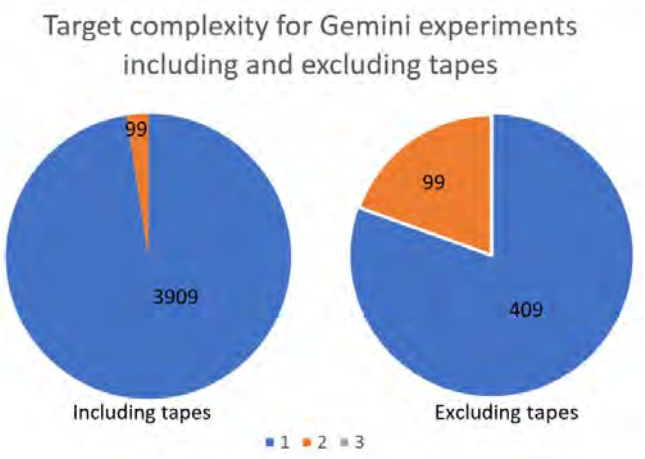

Figure 1: Target complexity breakdown for Gemini experiments over the 2022/23 operating period

As none of the targets requested for Vulcan experiments comprised tape targets, Figure 2 shows a single graph documenting the breakdown of target complexity.

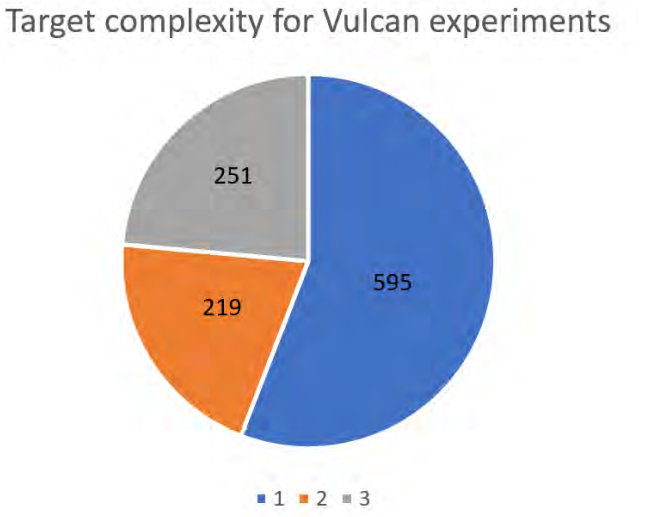

Figure 2: Target complexity breakdown for Vulcan experiments over the 2022/23 operating period

Figures 1 and 2 illustrate the difference in general target complexity requested between Gemini and Vulcan experiments.

Excluding tape, 80% of Gemini targets fall into Class 1 – primarily thick foils and alignment targets. The remaining 20% Class 2 targets are all ultra-thin foil targets.

The majority of Class 1 Vulcan targets were thick foils (44%); however, there were a considerable number of Class 3 targets (251 in total) over the period. These all comprised 3D micro-structures, which ranged from precision-machined assemblies with multiple foils per component to multi-faceted gas cells.

Target Supply Trends

The Target Fabrication Group keeps a record of all targets that have been issued to each experiment in the CLF for referencing and QA purposes, and as such is wishing to reinstate the ISO9001 quality management system, which will be especially important when shot numbers inevitably increase in the coming years.

Following the commissioning of the EPAC Facility, it is expected there will be a considerable increase in the number of tape targets required and the Target Fabrication Group is developing a tape etching and coating capability to deliver for this increase in demand. A liquid targetry system is also in development, producing rapidly replenishable and debris-free targets that will be crucial for high-repetition rate (1 Hz+) experiments.

It can be seen from Figure 3 that, if simple tape targets are excluded from the statistics, the supply of complex targets across the CLF has been relatively stable over the last decade, with an average number of 2228 targets provided per year. However, because Target Fabrication has been offering the capability of a tape-driven targetry solution to users over recent years, actual shot numbers on targets have increased substantially. This operating period saw 3500 targets shot on simple tapes – as TA2 data was not captured in this report this number is likely to be far higher. Last year, for example, saw 79000 simple tape targets shot on TA2.

Figure 3 also shows the percentage of targets requested that were not on the target list initially, and were requested by user groups in the planning phase of the experiments. Due to the complexity of target manufacture, targets are often manufactured many weeks ahead of each experiment.

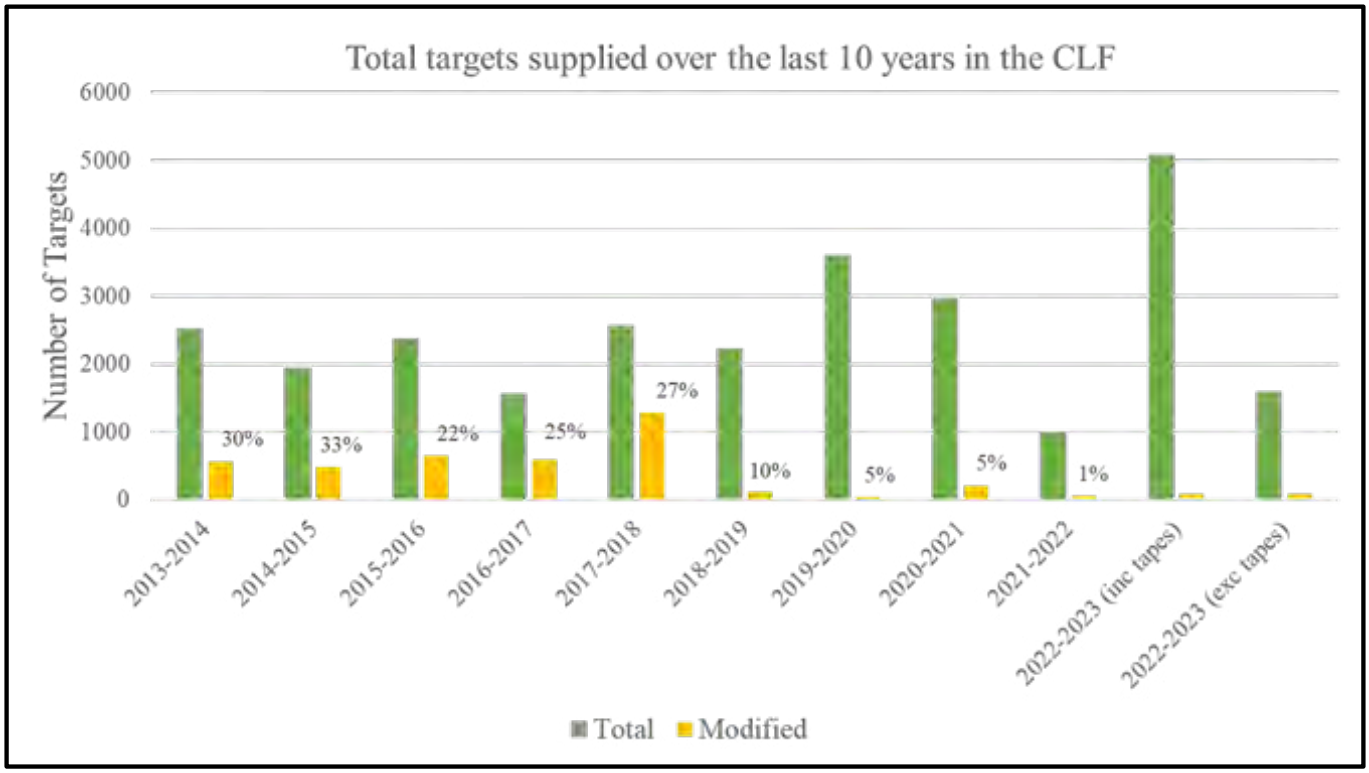

Figure 3: Target supply across the CLF over the past decade, including (green) and excluding (yellow) tape targets for the 2022/23 period

The benefit of having an embedded Target Fabrication Laboratory within the CLF is that that the Group can quickly adapt to a change in demand, and should the user groups request a last-minute change of target – within reason – it can be accommodated. Change requests are often due to an experimental objective being re-appraised during a campaign, typically because on-shot data did not agree with the data from the simulations and consequently target requests were adjusted during an experiment to better understand the physical conditions of interest. Such flexibility can often make the difference between a successful and an unsuccessful campaign and is of great benefit to users at the CLF. In total over the 2022/23 operating period, 87 of the 1573 targets (6%) supplied were modified.

Figure 4 displays the number of targets that were returned due to being out of specification. As can be seen, there has been a significant reduction over recent years in the number of returned targets, with a total of 51 targets returned over the 2022/23 period compared to 476 in the 2013/14 period, for example. The reduction suggests an improvement in general target quality, which can be attributed to better characterisation tools and more rigorous quality standards and verification practices. However, non-return of non-conforming targets without notification needs also to be considered when interpreting the target numbers.

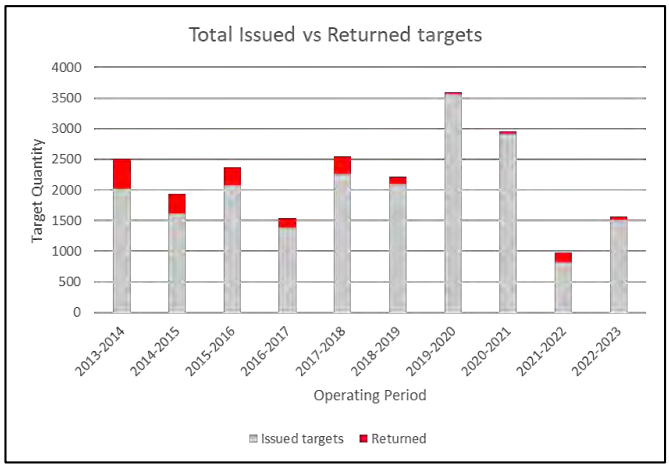

Figure 4: Returned targets vs total issued targets over the last decade

Future Targetry Supply

With the planned shutdown of the Vulcan facility in September 2023 (although the Target Fabrication Group will provide targets for CLF experiments conducted on other HPL facilities), it is anticipated that the number of higher classification targets might decrease compared to the last few years.

In anticipation of EPAC coming online in 2025, the Target Fabrication Group has developed a tape drive targetry solution for the supply of targets in vacuo and is integrating a range of technologies to be able to manufacture targets on tape substrates with custom materials, geometries and thicknesses. This is a novel capability and will allow production of thousands of targets onto a single spool of material, fed into the interaction point of the target area to a z accuracy of ±2μm. [1-3]

A liquid targetry system is also in development that can produce nanometre-range sheets of liquid (such as de-ionised water) using a high pressure liquid chromatography pump and precision-machined nozzle assemblies. The system is expected to be able to provide a targetry solution for HRR systems such as EPAC, with the intention of also modifying the technology for use as a rapidly-refreshing plasma mirror. The reader is recommended to refer to the 2022/23 annual report article by D. Crestani for further information. [4]

External Contracts

In the reporting period 2022/23, the operations of Scitech Precision Limited (SPL), Target Fabrication Group's commercial spin out, supported the user community on external facilities and continued to expand with the ability to access MEMS technology and advanced laser machining being key revenue generators. The expansion of the user community across Europe and in the US drove sales of targets to a wider array of customers. A total of 36 (up from 32 in 2021/22) institutions engaged with SPL over this period for 115 individual contracts (up from 98) to a record value of £302k, which is a significant increase in turnover from the previous years and is in part due to the licensing agreement SPL has with STFC to market and sell the

tape drive technology. In the reporting period, SPL continued to upgrade its capabilities in additive manufacturing and also further developed capabilities to deliver high repetition rate targets by integrating CLF tape systems with its Excimer laser tool.

Summary

Over the 2022/23 reporting period, the Target Fabrication group has delivered a total of 1573 laser targets over 10 HPL experiments that took place in the CLF. Excluding tape-driven targets, 67.7% of the targets were provided to the Vulcan target areas (TAP and TAW) and the remaining 32.3% were delivered to the Gemini TA3 target area. If tape-driven targets are taken into account, the respective breakdown is 21% and 79%.

The complexity of requested targets (Class 1, 2 and 3) was 55%, 21% and 24%, respectively, for Vulcan experiments and 80%, 20% and 0% for Gemini experiments.

Data has not been included for Gemini TA2 experiments, however, which accounted for by far the largest proportion of targets in the previous operating period.

It is anticipated that future target demands will move more towards complex tape driven targets and that, due to the shutdown of Vulcan in 2023, there will be a (short-term) reduction in the number of complex 3D micro-assembly targets.

References

[1] *S. Astbury, W. Robins, C. Spindloe & M. Tolley, "Progression of a tape-drive targetry solution for high rep-rate HPL experiments within the CLF", CLF Annual Report 2018-2019*

[2] *W. Robins, S. Astbury, C. Spindloe & M. Tolley, "Experimental Testing and Fielding of the CLF Precision Tape Drive in the Gemini Target Area", CLF Annual Report 2020-2021*

[3] *W. Robins, S. Astbury, C. Spindloe & M. Tolley "Advances in Tape Target Technologies towards 1Hz Operation for EPAC and other High Repetition Rate Facilities", CLF Annual Report 2021/22*

[4] *D. Crestani, S. Astbury, H. Edwards, W. Robins, C. Spindloe & M. Tolley "Liquid Targetry Development for High repetition rate experiments", CLF Annual Report 2022-2023*

Contact Author: S. Astbury (sam.astbury@stfc.ac.uk)

Publications

Journal Papers

CALTA

S Banerjee, J Spear, PJ Dalton

Laser shock peening of tungsten and its dependency on polarisation of light for induced compressive stresses

OPTICS EXPRESS, 30, 32084-32096 (2022)

S Banerjee, J Spear

Confinement and absorption layer free nanosecond laser shock peening of tungsten and its alloy

OPTICS LETTERS, 47, 4736-4739 (2022)

Gemini

G Vieux, S Cipiccia, GH Welsh, SR Yoffe, F Gärtner, MP Tooley, B Ersfeld, E Brunetti, B Eliasson, C Picken, G McKendrick, M Hur, JM Dias, T Kühl, G Lehmann, DA Jaroszynski

The role of transient plasma photonic structures in plasma-based amplifiers

COMMUNICATIONS PHYSICS, 6, 9 (2023)

B Loughran, MJV Streeter, H Ahmed, S Astbury, M Balcazar, M Borghesi, N Bourgeois, CB Curry, SJD Dann, S Dilorio, NP Dover, T Dzelzainis, OC Ettlinger, M Gauthier, L Giuffrida, GD Glenn, SH Glenzer, JS Green, RJ Gray, GS Hicks, C Hyland, V Istokskaia, M King, D Margarone, O McCusker, P McKenna, Z Najmudin, C Parisuaña, P Parsons, C Spindloe, DR Symes, AGR Thomas, F Treffert, N Xu, CAJ Palmer

Automated control and optimization of laser-driven ion acceleration

HIGH POWER LASER SCIENCE AND ENGINEERING, 11, e35 (2023)

M Streeter, C Colgan, C Cobo, C Arran, E Los, R Watt, N Bourgeois, L Calvin, J Carderelli, N Cavanagh, S Dann, R Fitzgarrald, E Gerstmayr, A Joglekar, B Kettle, P McKenna, C Murphy, Z Najmudin, P Parsons, Q Qian, P Rajeev, C Ridgers, D Symes, A Thomas, G Sarri, S Mangles

Laser Wakefield Accelerator modelling with Variational Neural Networks

HIGH POWER LASER SCIENCE AND ENGINEERING, 11, e9 (2023)

N Xu, MJV Streeter, OC Ettlinger, H Ahmed, S Astbury, M Borghesi, N Bourgeois, CB Curry, SJD Dann, NP Dover, T Dzelzainis, V Istokskaia, M Gauthier, L Giuffrida, GD Glenn, SH Glenzer, RJ Gray, JS Green, GS Hicks, C Hyland, M King, B Loughran, D Margarone, O McCusker, P McKenna, C Parisuaña, P Parsons, C Spindloe, DR Symes, F Treffert, CAJ Palmer, Z Najmudin

Versatile tape-drive target for high-repetition-rate laser-driven proton acceleration

HIGH POWER LASER SCIENCE AND ENGINEERING, 11, e23 (2023)

M Streeter, Y Ma, B Kettle, S Dann, E Gerstmayr, F Albert, N Bourgeois, S Cipiccia, J Cole, I Gallardo González, A Hussein, D Jaroszynski, K Falk, K Krushelnick, N Lemos, N Lopes, C Lumsdon, O Lundh, S Mangles, Z Najmudin, R Pattathil, R Sandberg, M Shahzad, M Smid, R Spesyvtsev, D Symes, G Vieux, A Thomas

Characterization of laser wakefield acceleration efficiency with octave spanning near-IR spectrum measurements

PHYSICAL REVIEW ACCELERATORS AND BEAMS, 25, 101302 (2022)

L Dickson, C Underwood, F Filippi, R Shalloo, JB Svensson, D Guénot, K Svendsen, I Moulanier, SD Dufrénoy, C Murphy, N Lopes, P Rajeev, Z Najmudin, G Cantono, A Persson, O Lundh, G Maynard, M Streeter, B Cros

Mechanisms to control laser-plasma coupling in laser wakefield electron acceleration

PHYSICAL REVIEW ACCELERATORS AND BEAMS, 25, 101301 (2022)

P Chaudhary, G Milluzzo, A McIlvenny, H Ahmed, A McMurray, C Maiorino, K Polin, L Romagnani, D Doria, SJ McMahon, SW Botchway, PP Rajeev, KM Prise, M Borghesi

Cellular irradiations with laser-driven carbon ions at ultra-high dose rates

PHYSICS IN MEDICINE AND BIOLOGY, 68, 25015 (2023)

Plasma Physics

R Paddock, H Martin, R Ruskov, R Scott, W Garbett, B Haines, A Zylstra, E Campbell, T Collins, R Craxton, C Thomas, V Goncharov, R Aboushelbaya, Q Feng, M von der Leyen, I Ouatu, B Spiers, R Timmis, R Wang, P Norreys

Pathways towards break even for low convergence ratio direct-drive inertial confinement fusion

JOURNAL OF PLASMA PHYSICS, 88, 905880314 (2022)

H Schmitz, R Trines, R Bingham, E Kur, P Michel

Investigations of nonlinear polarization transfer between obliquely intersecting beams

JOURNAL OF THE OPTICAL SOCIETY OF AMERICA B, 40, 922-929 (2023)

H Abu-Shawareb et al.

Lawson Criterion for Ignition Exceeded in an Inertial Fusion Experiment

PHYSICAL REVIEW LETTERS, 129, 75001 (2022)

R Scott, D Barlow, W Trickey, A Ruocco, K Glize, L Antonelli, M Khan, N Woolsey

Shock-Augmented Ignition Approach to Laser Inertial Fusion

PHYSICAL REVIEW LETTERS, 129, 195001 (2022)

K Weichman, JP Palastro, APL Robinson, R Bingham, AV Arefiev

Underdense relativistically thermal plasma produced by magnetically assisted direct laser acceleration

PHYSICAL REVIEW RESEARCH, 4, L042017 (2022)

K Weichman, APL Robinson, M Murakami, JJ Santos, S Fujioka, T Toncian, JP Palastro, AV Arefiev

Progress in relativistic laser-plasma interaction with kilotesla-level applied magnetic fields

PHYSICS OF PLASMAS, 29, 53104 (2022)

D Barlow, T Goffrey, K Bennett, RHH Scott, K Glize, W Theobald, K Anderson, AA Solodov, MJ Rosenberg, M Hohenberger, NC Woolsey, P Bradford, M Khan, TD Arber

Role of hot electrons in shock ignition constrained by experiment at the National Ignition Facility

PHYSICS OF PLASMAS, 29, 82704 (2022)

APL Robinson

Intense laser-generated ion beams in plasmas: the rapid heating regime

PLASMA PHYSICS AND CONTROLLED FUSION, 65, 55004 (2023)

APL Robinson

Intense laser-generated ion beams propagating in plasmas

PLASMA PHYSICS AND CONTROLLED FUSION, 64, 105014 (2022)

L Ceurvorst, W Theobald, MJ Rosenberg, PB Radha, C Stoeckl, R Betti, KS Anderson, JA Marozas, VN Goncharov, EM Campbell, CM Shuldberg, RW Luo, W Sweet, L Aghaian, L Carlson, B Bachmann, T Döppner, M Hohenberger, K Glize, RHH Scott, A Colaïtis, SP Regan

Development of an x-ray radiography platform to study laser-direct-drive energy coupling at the National Ignition Facility

REVIEW OF SCIENTIFIC INSTRUMENTS, 93, 105102 (2022)

Vulcan

R Singh, S White, M Charlwood, F Keenan, C Hyland, D Bailie, T Audet, G Sarri, SJ Rose, J Morton, C Baird, C Spindloe, D Riley, S Pikuz

L-Shell X-Ray Conversion Yields for Laser-Irradiated Tin and Silver Foils

LASER AND PARTICLE BEAMS, 2022, 1-10 (2022)

S Ferguson, P Martin, H Ahmed, E Aktan, M Alanazi, M Cerchez, D Doria, JS Green, B Greenwood, B Odlozilik, O Willi, M Borghesi, S Kar

Dual stage approach to laser-driven helical coil proton acceleration

NEW JOURNAL OF PHYSICS, 25, 13006 (2023)

RW Paddock, MW von der Leyen, R Aboushelbaya, PA Norreys, DJ Chapman, DE Eakins, M Oliver, RJ Clarke, M Notley, CD Baird, N Booth, C Spindloe, D Haddock, S Irving, RHH Scott, J Pasley, M Cipriani, F Consoli, B Albertazzi, M Koenig, AS Martynenko, L Wegert, P Neumayer, P Tchórz, P Rączka, P Mabey, W Garbett, RMN Goshadze, VV Karasiev, SX Hu

Measuring the principal Hugoniot of inertial-confinement-fusion-relevant TMPTA plastic foams

PHYSICAL REVIEW E, 107, 25206 (2023)

A Alejo, H Ahmed, A Krygier, R Clarke, R Freeman, J Fuchs, A Green, J Green, D Jung, A Kleinschmidt, J Morrison, Z Najmudin, H Nakamura, P Norreys, M Notley, M Oliver, M Roth, L Vassura, M Zepf, M Borghesi, S Kar

Stabilized Radiation Pressure Acceleration and Neutron Generation in Ultrathin Deuterated Foils

PHYSICAL REVIEW LETTERS, 129, 114801 (2022)

SN Ryazantsev, AS Martynenko, MV Sedov, IY Skobelev, MD Mishchenko, YS Lavrinenko, CD Baird, N Booth, P Durey, LNK Döhl, D Farley, KL Lancaster, P McKenna, CD Murphy, TA Pikuz, C Spindloe, N Woolsey, SA Pikuz

Absolute keV x-ray yield and conversion efficiency in over dense Si sub-petawatt laser plasma

PLASMA PHYSICS AND CONTROLLED FUSION, 64, 105016 (2022)

O McCusker, H Ahmed, A McIlvenny, P Martin, S Ferguson, J Green, J Jarrett, M King, S Zhai, P McKenna, S Kar, M Borghesi

Multi-species ion acceleration from sub-ps, PW interactions with ultra-thin foils

PLASMA PHYSICS AND CONTROLLED FUSION, 65, 15005 (2022)

K Makur, B Ramakrishna, S Krishnamurthy, KF Kakolee, S Kar, M Cerchez, R Prasad, K Markey, M Quinn, X Yuan, J Green, RHH Scott, P McKenna, J Osterholz, O Willi, PA Norreys, M Borghesi, M Zepf

Probing bulk electron temperature via x-ray emission in a solid density plasma

PLASMA PHYSICS AND CONTROLLED FUSION, 65, 45005 (2023)

Target Fabrication

SN Ryazantsev, AS Martynenko, MV Sedov, IY Skobelev, MD Mishchenko, YS Lavrinenko, CD Baird, N Booth, P Durey, LNK Döhl, D Farley, KL Lancaster, P McKenna, CD Murphy, TA Pikuz, C Spindloe, N Woolsey, SA Pikuz

Absolute keV x-ray yield and conversion efficiency in over dense Si sub-petawatt laser plasma

PLASMA PHYSICS AND CONTROLLED FUSION, 64, 105016 (2022)

MO Schoelmerich, T Döppner, CH Allen, L Divol, M Oliver, D Haden, M Biener, J Crippen, J Delora-Ellefson, B Ferguson, DO Gericke, A Goldman, A Haid, C Heinbockel, D Kalantar, Z Karmiol, G Kemp, J Kroll, OL Landen, N Masters, Y Ping, C Spindloe, W Theobald, TG White

Developing a platform for Fresnel diffractive radiography with 1 Î¼m spatial resolution at the National Ignition Facility

REVIEW OF SCIENTIFIC INSTRUMENTS, 94, 13104 (2023)

N Xu, MJV Streeter, OC Ettlinger, H Ahmed, S Astbury, M Borghesi, N Bourgeois, CB Curry, SJD Dann, NP Dover, T Dzelzainis, V Istokskaia, M Gauthier, L Giuffrida, GD Glenn, SH Glenzer, RJ Gray, JS Green, GS Hicks, C Hyland, M King, B Loughran, D Margarone, O McCusker, P McKenna, C Parisuaña, P Parsons, C Spindloe, DR Symes, F Treffert, CAJ Palmer, Z Najmudin

Versatile tape-drive target for high-repetition-rate laser-driven proton acceleration

HIGH POWER LASER SCIENCE AND ENGINEERING, 11, e23 (2023)

B Loughran, MJV Streeter, H Ahmed, S Astbury, M Balcazar, M Borghesi, N Bourgeois, CB Curry, SJD Dann, S Dilorio, NP Dover, T Dzelzainis, OC Ettlinger, M Gauthier, L Giuffrida, GD Glenn, SH Glenzer, JS Green, RJ Gray, GS Hicks, C Hyland, V Istokskaia, M King, D Margarone, O McCusker, P McKenna, Z Najmudin, C Parisuaña, P Parsons, C Spindloe, DR Symes, AGR Thomas, F Treffert, N Xu, CAJ Palmer

Automated control and optimization of laser-driven ion acceleration

HIGH POWER LASER SCIENCE AND ENGINEERING, 11, e35 (2023)

Ultra

M Sneha, GL Thornton, L Lewis-Borrell, ASH Ryder, SG Espley, IP Clark, AJ Cresswell, MN Grayson, AJ Orr-Ewing

Photoredox-HAT Catalysis for Primary Amine α-C–H Alkylation: Mechanistic Insight with Transient Absorption Spectroscopy

ACS CATALYSIS, 13, 8004-8013 (2023)

J Tolentino Collado, JN Iuliano, K Pirisi, S Jewlikar, K Adamczyk, GM Greetham, M Towrie, JRH Tame, SR Meech, PJ Tonge, A Lukacs

Unravelling the Photoactivation Mechanism of a Light-Activated Adenylyl Cyclase Using Ultrafast Spectroscopy Coupled with Unnatural Amino Acid Mutagenesis

ACS CHEMICAL BIOLOGY, 17, 2643-2654 (2022)

AR Neale, DC Milan, F Braga, IV Sazanovich, LJ Hardwick

Lithium Insertion into Graphitic Carbon Observed via Operando Kerr-Gated Raman Spectroscopy Enables High State of Charge Diagnostics

ACS ENERGY LETTERS, 7, 2611-2618 (2022)

SH Rutherford, GM Greetham, M Towrie, AW Parker, S Kharratian, TF Krauss, A Nordon, MJ Baker, NT Hunt

Detection of paracetamol binding to albumin in blood serum using 2D-IR spectroscopy

ANALYST, 147, 3464-3469 (2022)

P Sharma, M Sharma, M Dearg, M Wilding, TJ Slater, CRA Catlow

Cd/Pt Precursor Solution for Solar H2 Production and in-situ Photochemical Synthesis of Pt Single-atom Decorated CdS Nanoparticles

ANGEWANDTE CHEMIE INTERNATIONAL EDITION, 135, e202301239 (2023)

K Sowoidnich, M Towrie, P Matousek

Shifted Excitation Raman Difference Spectroscopy Combined with Wide Area Illumination and Sample Rotation for Wood Species Classification

APPLIED SPECTROSCOPY, 77, 666-681 (2023)

LA Hammarback, JB Eastwood, TJ Burden, CJ Pearce, IP Clark, M Towrie, A Robinson, IJS Fairlamb, JM Lynam

A comprehensive understanding of carbon-carbon bond formation by alkyne migratory insertion into manganacycles

CHEMICAL SCIENCE, 13, 9902-9913 (2022)

TJ Burden, KPR Fernandez, M Kagoro, J Eastwood, TFN Tanner, AC Whitwood, IP Clark, M Towrie, J Krieger, JM Lynam, IJS Fairlamb

Coumarin C-H Functionalization by Mn Carbonyls: Mechanistic Insight by Ultra-Fast IR Spectroscopic Analysis

CHEMISTRY: A EUROPEAN JOURNAL, 29, e202203038 (2023)

K Peterková, M Stitch, RZ Boota, P Scattergood, P Elliott, M Towrie, P Podbevsek, J Plavec, SJ Quinn

G-Quadruplex Binding of an NIR Emitting Osmium Polypyridyl Probe Revealed by Solution NMR and Time-Resolved Infrared Studies

CHEMISTRY: A EUROPEAN JOURNAL, 29, e202203250 (2022)

NP Gallop, J Ye, GM Greetham, TLC Jansen, L Dai, SJ Zelewski, R Arul, JJ Baumberg, RLZ Hoye, AA Bakulin

The effect of caesium alloying on the ultrafast structural dynamics of hybrid organic-inorganic halide perovskites

JOURNAL OF MATERIALS CHEMISTRY A: MATERIALS FOR ENERGY AND SUSTAINABILITY, 10, 22408-22418 (2022)

CP Howe, GM Greetham, B Procacci, AW Parker, NT Hunt

Sequence-Dependent Melting and Refolding Dynamics of RNA UNCG Tetraloops Using Temperature-Jump/Drop Infrared Spectroscopy

JOURNAL OF PHYSICAL CHEMISTRY B, 127, 1586-1597 (2023)

NBC Pfukwa, M Rautenbach, NT Hunt, OO Olaoye, V Kumar, AW Parker, L Minnes, PH Neethling

Temperature-Induced Effects on the Structure of Gramicidin S

JOURNAL OF PHYSICAL CHEMISTRY B, 127, 3774-3786 (2023)

CP Howe, GM Greetham, B Procacci, AW Parker, NT Hunt

Measuring RNA UNCG Tetraloop Refolding Dynamics Using Temperature-Jump/Drop Infrared Spectroscopy

JOURNAL OF PHYSICAL CHEMISTRY LETTERS, 13, 9171-9176 (2022)

M Speirs, SJO Hardman, AI Iorgu, LO Johannissen, DJ Heyes, NS Scrutton, IV Sazanovich, S Hay

Photoinduced Electron Transfer from a 1,4,5,6-Tetrahydro Nicotinamide Adenine Dinucleotide Analogue to Oxidized Flavin in an Ene-Reductase Flavoenzyme

JOURNAL OF PHYSICAL CHEMISTRY LETTERS, 14, 3236-3242 (2023)

CJ Kulka-Peschke, A Schulz, C Lorent, Y Rippers, S Wahlefeld, J Preissler, C Schulz, C Wiemann, CCM Bernitzky, C Karafoulidi-Retsou, SLD Wrathall, B Procacci, H Matsuura, GM Greetham, C Teutloff, L Lauterbach, Y Higuchi, M Ishii, NT Hunt, O Lenz, I Zebger, M Horch

Reversible Glutamate Coordination to High-Valent Nickel Protects the Active Site of a [NiFe] Hydrogenase from Oxygen

JOURNAL OF THE AMERICAN CHEMICAL SOCIETY, 144, 17022-17032 (2022)

JB Eastwood, LA Hammarback, TJ Burden, IP Clark, M Towrie, A Robinson, IJS Fairlamb, JM Lynam

Understanding Precatalyst Activation and Speciation in Manganese-Catalyzed C-H Bond Functionalization Reactions

ORGANOMETALLICS, 42, 1766-1773 (2023)

J Dobkowski, IV Sazanovich, A Gorski, J Waluk

Energy Relaxation of Porphycene in Atomic and Molecular Cryogenic Matrices

PHOTOCHEM, 2, 299-307 (2022)

A Šrut, S Mai, IV Sazanovich, J Heyda, A Vlček, L González, S Záliš

Nonadiabatic excited-state dynamics of ReCl in two different solvents

PHYSICAL CHEMISTRY CHEMICAL PHYSICS, 24, 25864-25877 (2022)

PM Keane, C Zehe, FE Poynton, SA Bright, S Estayalo-Adrián, SJ Devereux, PM Donaldson, IV Sazanovich, M Towrie, SW Botchway, CJ Cardin, DC Williams, T Gunnlaugsson, C Long, JM Kelly, SJ Quinn

Time-resolved infra-red studies of photo-excited porphyrins in the presence of nucleic acids and in HeLa tumour cells: insights into binding site and electron transfer dynamics

PHYSICAL CHEMISTRY CHEMICAL PHYSICS, 24, 27524-27531 (2022)

SLD Wrathall, B Procacci, M Horch, E Saxton, C Furlan, J Walton, Y Rippers, JN Blaza, GM Greetham, M Towrie, AW Parker, J Lynam, A Parkin, NT Hunt

Ultrafast 2D-IR spectroscopy of [NiFe] hydrogenase from E. coli reveals the role of the protein scaffold in controlling the active site environment

PHYSICAL CHEMISTRY CHEMICAL PHYSICS, 24, 24767-24783 (2022)

LJ Dodd, C Lima, D Costa-Milan, AR Neale, B Saunders, B Zhang, A Sarua, R Goodacre, LJ Hardwick, M Kuball, T Hasell

Raman analysis of inverse vulcanised polymers

POLYMER CHEMISTRY, 14, 1369-1386 (2023)

SH Rutherford, GM Greetham, AW Parker, A Nordon, MJ Baker, NT Hunt

Measuring proteins in H2O using 2D-IR spectroscopy: pre-processing steps and applications toward a protein library

THE JOURNAL OF CHEMICAL PHYSICS, 157, 205102 (2022)

Octopus

CR Barker, FK Lewns, G Poologasundarampillai, AD Ward

In Situ Sol-Gel Synthesis of Unique Silica Structures Using Airborne Assembly: Implications for In-Air Reactive Manufacturing

ACS APPLIED NANO MATERIALS, 5, 11699-11706 (2022)

C Qiu, Y Odarchenko, Q Meng, S Xu, I Lezcano-Gonzalez, P Olalde-Velasco, F Maccherozzi, L Zanetti-Domingues, M Martin-Fernandez, AM Beale

Resolving the Effect of Oxygen Vacancies on Co Nanostructures Using Soft XAS/X-PEEM

ACS CATALYSIS, 12, 9125-9134 (2022)

M Forouhan, WF Lim, LC Zanetti Domingues, CJ Tynan, TC Roberts, B Malik, R Manzano, AA Speciale, R Ellerington, A Garcia-Guerra, P Fratta, G Sorarú, L Greensmith, M Pennuto, MJA Wood, C Rinaldi

AR cooperates with SMAD4 to maintain skeletal muscle homeostasis

ACTA NEUROPATHOLOGICA, 143, 713-731 (2022)

Á dos Santos, N Fili, Y Hari-Gupta, RE Gough, L Wang, M Martin-Fernandez, J Aaron, E Wait, T Chew, CP Toseland

Binding partners regulate unfolding of myosin VI to activate the molecular motor

BIOCHEMICAL JOURNAL, 479, 1409-1428 (2022)

BM Davis, SR Needham, S Iyer, SK Roberts, LCZ Domingues, M Martin-Fernandez, DJ Rolfe

Towards cloud-enabled fully automated end-to-end single molecule imaging

BIOPHYSICAL JOURNAL, 122, 278a (2023)

TA Eastwood, K Baker, BR Streather, N Allen, L Wang, SW Botchway, IR Brown, JR Hiscock, C Lennon, DP Mulvihill

High-yield vesicle-packaged recombinant protein production from E. coli

CELL REPORTS METHODS, 3, 100396 (2023)

HK Saeed, PJ Jarman, S Sreedharan, R Mowll, AJ Auty, AAP Chauvet, CGW Smythe, JB de la Serna, JA Thomas

From Chemotherapy to Phototherapy - Changing the Therapeutic Action of a Metallo-Intercalating Ru-II-Re-I Luminescent System by Switching its Sub-Cellular Location

CHEMISTRY: A EUROPEAN JOURNAL, 29, e202300617 (2023)

T Spatola Rossi, C Pain, SW Botchway, V Kriechbaumer

FRET-FLIM to Determine Protein Interactions and Membrane Topology of Enzyme Complexes

CURRENT PROTOCOLS, 2, e598 (2022)

RH Shepherd, MD King, AR Rennie, AD Ward, MM Frey, N Brough, J Eveson, S Del Vento, A Milsom, C Pfrang, MWA Skoda, RJL Welbourn

Measurement of gas-phase OH radical oxidation and film thickness of organic films at the air-water interface using material extracted from urban, remote and wood smoke aerosol

ENVIRONMENTAL SCIENCE: ATMOSPHERES, 2, 574-590 (2022)

SR Gardeta, EM García-Cuesta, G D'Agostino, B Soler Palacios, A Quijada-Freire, P Lucas, J Bernardino de la Serna, C Gonzalez-Riano, C Barbas, JM Rodríguez-Frade, M Mellado

Sphingomyelin Depletion Inhibits CXCR4 Dynamics and CXCL12-Mediated Directed Cell Migration in Human T Cells

FRONTIERS IN IMMUNOLOGY, 13, 925559 (2022)

AV Nunn, GW Guy, SW Botchway, JD Bell

SARS-CoV-2 and EBV; the cost of a second mitochondrial "whammy"?

IMMUNITY & AGEING, 18, 40 (2021)

ML Martin-Fernandez

A perspective of fluorescence microscopy for cellular structural biology with EGFR as witness

JOURNAL OF MICROSCOPY, 291, 73-91 (2022)

N Goonawardane, L Upstone, M Harris, IM Jones, MT Heise

Identification of Host Factors Differentially Induced by Clinically Diverse Strains of Tick-Borne Encephalitis Virus

JOURNAL OF VIROLOGY, 96, e00818-22 (2022)

DT Hinds, SA Belhout, PE Colavita, AD Ward, SJ Quinn

Microsphere-Supported Gold Nanoparticles for SERS detection of Malachite Green

MATERIALS ADVANCES, 4, 1481-1489 (2023)

Á dos Santos, RE Gough, L Wang, CP Toseland

Measuring Nuclear Organization of Proteins with STORM Imaging and Cluster Analysis

METHODS IN MOLECULAR BIOLOGY, 2476, 293-309 (2022)

Y Zhu, CW Koo, CK Cassidy, MC Spink, T Ni, LC Zanetti-Domingues, B Bateman, ML Martin-Fernandez, J Shen, Y Sheng, Y Song, Z Yang, AC Rosenzweig, P Zhang

Structure and activity of particulate methane monooxygenase arrays in methanotrophs

NATURE COMMUNICATIONS, 13, 5221 (2022)

E Clancy, S Ramadurai, SR Needham, K Baker, TA Eastwood, JA Weinstein, DP Mulvihill, SW Botchway

Fluorescence and phosphorescence lifetime imaging reveals a significant cell nuclear viscosity and refractive index changes upon DNA damage

SCIENTIFIC REPORTS, 13, 422 (2023)

MGR Guastamacchia, R Xue, K Madi, WTE Pitkeathly, PD Lee, SED Webb, SH Cartmell, PA Dalgarno

Instantaneous 4D micro-particle image velocimetry via multifocal microscopy

SCIENTIFIC REPORTS, 12, 18458 (2022)

V Jackson, J Hermann, CJ Tynan, DJ Rolfe, RA Corey, AL Duncan, M Noriega, A Chu, AC Kalli, EY Jones, MS Sansom, ML Martin-Fernandez, E Seiradake, M Chavent

The guidance and adhesion protein FLRT2 dimerizes in cis via dual small-X3-small transmembrane motifs

STRUCTURE, 30, 1354-136500000 (2022)

M Fray, D Clarke, M Martin-Fernandez, L Cuff, A Piotrowska, R Amos, R Thomas

Life science and healthcare

CRYOGENICS, CHAPTER 8, 1-35 (2022)

Individual Contributions and Collaborative Science

MO Schoelmerich, T Döppner, CH Allen, L Divol, M Oliver, D Haden, M Biener, J Crippen, J Delora-Ellefson, B Ferguson, DO Gericke, A Goldman, A Haid, C Heinbockel, D Kalantar, Z Karmiol, G Kemp, J Kroll, OL Landen, N Masters, Y Ping, C Spindloe, W Theobald, TG White

Developing a platform for Fresnel diffractive radiography with 1 μm spatial resolution at the National Ignition Facility

REVIEW OF SCIENTIFIC INSTRUMENTS, 94, 13104 (2023)

A Masood, T Iqbal, S Afsheen, KN Riaz, G Nabi, MI Khan, N Al-Zaqri, I Warad, H Ahmed

Theoretical and experimental analysis of La-doped CuO for their application an efficient photocatalyst

BIOMASS CONVERSION AND BIOREFINERY (2023)

M Yousaf, T Iqbal, S Afsheen, KN Riaz, N Al-Zaqri, I Warad, H Ahmed, M Asghar, M Shafiq

Effect of TiN-Based Nanostructured Coatings on the Biocompatibility of NiTi Non-ferrous Metallic Alloy by Cathodic Cage Plasma Processing

JOURNAL OF INORGANIC AND ORGANOMETALLIC POLYMERS AND MATERIALS, 33, 1164-1176 (2023)

DR Rusby, GE Cochran, A Aghedo, F Albert, CD Armstrong, A Haid, AJ Kemp, SM Kerr, PM King, N Lemos, MJ Manuel, T Ma, AG MacPhee, I Pagano, A Pak, GG Scott, CW Siders, RA Simpson, M Sinclair, SC Wilks, GJ Williams, AJ Mackinnon

Enhanced electron acceleration by high-intensity lasers in extended preplasma in cone targets

PHYSICS OF PLASMAS, 30, 23103 (2023)

I Alonso et al.

Cold atoms in space: community workshop summary and proposed road-map

EPJ QUANTUM TECHNOLOGY, 9, 30 (2022)

C Arrowsmith, A Dyson, J Gudmundsson, R Bingham, G Gregori

Inductively-coupled plasma discharge for use in high-energy-density science experiments

JOURNAL OF INSTRUMENTATION, 18, P04008 (2023)

K Beyer, G Marocco, C Danson, R Bingham, G Gregori

Parametric co-linear axion photon instability

PHYSICS LETTERS B, 839, 137759 (2023)

JJ Lee, RT Ruskov, H Martin, S Hughes, MW von der Layen, RW Paddock, R Timmis, I Ouatu, QS Feng, S Howard, E Atonga, R Aboushelbaya, TD Arber, R Bingham, PA Norreys

Toward more robust ignition of inertial fusion targets

PHYSICS OF PLASMAS, 30, 22702 (2023)

TE Yap, B Davis, P Bloom, MF Cordeiro, E Normando

Glaucoma rose plots: redesigning circumpapillary progression analysis

INVESTIGATIVE OPHTHALMOLOGY & VISUAL SCIENCE, 63, 4262 (2022)

TE Yap, BM Davis, PA Bloom, MF Cordeiro, EM Normando

Glaucoma Rose Plot Analysis Detecting Early Structural Progression Using Angular Histograms

OPHTHALMOLOGY GLAUCOMA, 5, 562-571 (2022)

PM Donaldson

Spectrophotometric Concentration Analysis Without Molar Absorption Coefficients by Two-Dimensional-Infrared and Fourier Transform Infrared Spectroscopy

ANALYTICAL CHEMISTRY, 94, 17988-17999 (2022)

S Maiti, S Mitra, CA Johnson, KC Gronborg, S Garrett-Roe, PM Donaldson

pH Jumps in a Protic Ionic Liquid Proceed by Vehicular Proton Transport

JOURNAL OF PHYSICAL CHEMISTRY LETTERS, 13, 8104-8110 (2022)

PM Donaldson, RF Howe, AP Hawkins, M Towrie, GM Greetham

Ultrafast 2D-IR spectroscopy of intensely optically scattering pelleted solid catalysts

THE JOURNAL OF CHEMICAL PHYSICS, 158, 114201 (2023)

A Zachariou, AP Hawkins, P Collier, RF Howe, SF Parker, D Lennon

Neutron scattering studies of the methanol-to-hydrocarbons reaction

CATALYSIS SCIENCE & TECHNOLOGY, 13, 1976-1990 (2023)

S Mosca, A Milani, C Castiglioni, V Hernández Jolín, C Meseguer, JT López Navarrete, C Zhao, K Sugiyasu, MC Ruiz Delgado

Raman Fingerprints of π--Electron Delocalization in Polythiophene-Based Insulated Molecular Wires

MACROMOLECULES, 55, 3458-3468 (2022)

M von der Leyen, J Holloway, Y Ma, P Campbell, R Aboushelbaya, Q Qian, A Antoine, M Balcazar, J Cardarelli, Q Feng, R Fitzgarrald, B Hou, G Kalinchenko, J Latham, A Maksimchuk, A McKelvey, J Nees, I Ouatu, R Paddock, B Spiers, A Thomas, R Timmis, K Krushelnick, P Norreys

Observation of Monoenergetic Electrons from Two-Pulse Ionization Injection in Quasilinear Laser Wakefields

PHYSICAL REVIEW LETTERS, 130, 105002 (2023)

M Oliver, CH Allen, L Divol, Z Karmiol, OL Landen, Y Ping, R Wallace, M Schölmerich, W Theobald, T Döppner, TG White

Diffraction enhanced imaging utilizing a laser produced x-ray source

REVIEW OF SCIENTIFIC INSTRUMENTS, 93, 93502 (2022)

S Mosca, K Sowoidnich, M Mehta, WH Skinner, B Gardner, F Palombo, N Stone, P Matousek

10-kHz Shifted-Excitation Raman Difference Spectroscopy with Charge-Shifting Charge-Coupled Device Read-Out for Effective Mitigation of Dynamic Interfering Backgrounds

APPLIED SPECTROSCOPY, 77, 569-582 (2023)

C Castiglioni, A Botteon, C Conti, M Tommasini, P Matousek

Non-Destructive Analysis of Concentration Profiles in Turbid Media using micro-spatially offset Raman spectroscopy: A physical model

JOURNAL OF RAMAN SPECTROSCOPY, 53, 1592-1603 (2022)

N Yin, AW Parker, P Matousek, HL Birch

Chemical Markers of Human Tendon Health Identified Using Raman Spectroscopy: Potential for In Vivo Assessment

INTERNATIONAL JOURNAL OF MOLECULAR SCIENCES, 23, 14854 (2022)

A Sahoo, PP Rajeev, S Krishnan

All-optical investigations of intense femtosecond pulse ionization in transparent dielectrics with applications

JOURNAL OF OPTICS, 24, 64004 (2022)

D Curcio, K Volckaert, D Kutnyakhov, SY Agustsson, K Bühlmann, F Pressacco, M Heber, S Dziarzhytski, Y Acremann, J Demsar, W Wurth, CE Sanders, P Hofmann

Tracking the surface atomic motion in a coherent phonon oscillation

PHYSICAL REVIEW B, 106, L201409 (2022)

A Chikina, G Bhattacharyya, D Curcio, CE Sanders, M Bianchi, N Lanatà, M Watson, C Cacho, M Bremholm, P Hofmann+D41

One-dimensional electronic states in a natural misfit structure

PHYSICAL REVIEW MATERIALS, 6, L092001 (2022)

S Ren, Y Shi, QY van den Berg, MF Kasim, H Chung, EV Fernandez-Tello, P Velarde, JS Wark, SM Vinko

Non-thermal evolution of dense plasmas driven by intense x-ray fields

COMMUNICATIONS PHYSICS, 6, 99 (2023)

S Azadi, ND Drummond, SM Vinko

Correlation energy of the paramagnetic electron gas at the thermodynamic limit

PHYSICAL REVIEW B, 107, L121105 (2023)

H Poole, D Cao, R Epstein, I Golovkin, T Walton, SX Hu, M Kasim, SM Vinko, JR Rygg, VN Goncharov, G Gregori, SP Regan

A case study of using x-ray Thomson scattering to diagnose the in-flight plasma conditions of DT cryogenic implosions

PHYSICS OF PLASMAS, 29, 72703 (2022)

J Krása, V Nassisi, T Burian, V Hajkova, J Chalupsky, S Jelinek, K Frantálová, M Krupka, Z Kuglerová, SK Singh, V Vozda, L Vysin, J Wild, M Smid, P Perez-Martin, X Pan, M Kühlman, J Pintor, J Cikhardt, M Dreimann, D Eckermann, F Rosenthal, SM Vinko, A Forte, T Gawne, T Campbell, S Ren, Y Shi, T Hutchinson, O Humphries, T Preston, M Makita, M Nakatsutsumi, A Koehler, M Harmand, S Toleikis, K Falk, L Juha, S Bajt, S Guizard

Ion emission from plasmas produced by femtosecond pulses of short-wavelength free-electron laser radiation focused on massive targets: an overview and comparison with long-wavelength laser ablation

PROCEEDINGS OF SPIE, 12578, 125780J (2023)

CR Barker, ML Poole, M Wilkinson, J Morison, A Wilson, G Little, EJ Stuckey, RJ Welbourn, AD Ward, MD King

Ultraviolet refractive index values of organic aerosol extracted from deciduous forestry, urban and marine environments

ENVIRONMENTAL SCIENCE: ATMOSPHERES, 3, 1008-1024 (2023)

Theses

Gemini

von dey Leyen, M.

Study of novel electron injection mechanisms for laser-wakefield accelerators

University of Oxford (2021)

Colgan, C.

Laser-Plasma Interactions as Tools for Studying Processes in Quantum Electrodynamics

Imperial College London (2022)

Backhouse, M.

Measurement and optimisation of beam quality from laser wakefield accelerators

Imperial College London (2023)

Odlozilik, B.

Biological effects of laser-accelerated proton bursts

Queen's University Belfast (2022)

Vulcan

Spiers, B.

Laser-accelerated ions and their applications

University of Oxford (2022)

Greenwood, B.

Studies of laser-driven ions and kilo-amp pulses in novel regimes

Queen's University Belfast (2022)

Davidson, Z.

Multi-Channel Optical Probing of High Power Laser Plasma Interactions

University of Strathclyde (2023)

Plasma Physics

Khan, M.

Advanced Direct Drive Shock Ignition Studies

University of York (2022)

Ultra

Saeed, K.

Mechanistic studies of solar fuel generation at electrode surfaces

University of Liverpool (2022)

Thornton, G.

Transient Absorption Spectroscopy Studies of Photochemical Reactions Initiated by Electron Transfer

University of Bristol (2022)

Stitch, M.

Advanced Spectroscopic Studies of Structurally Diverse DNA Systems Towards New Therapeutics and Diagnostics

University College Dublin (2023)

Gallop, N.

On the electronic and vibronic behaviour of organic and perovskite photovoltaics

Imperial College London (2021)

Howe, C.

Sequence Dependent RNA UNCG and DNA TNCG Tetraloop Hairpin Melting and Refolding Dynamics Using Temperature-Jump Infrared Spectroscopy

University of York (2023)

Cerpentier, F.

The use of spectroscopic, electrochemical and spectroelectrochemical techniques in the development of organic and inorganic photocatalysts for the production of solar fuels

Dublin City University (2023)

Wu, G.

The Ultrafast Excited States Dynamics of Pt(II) Organometallic Compounds

University of Sheffield (2023)

Appleby, M.

Ultrafast Dynamics of Cu(I) complexes for Light-Driven Antibacterial Water Purification

University of Sheffield (2023)

Shipp, J.

Transition metal complexes as chromophores and catalysts for artificial photosynthesis

University of Sheffield (2022)

Peralta-Arriaga, S.

Biomimetic materials for hydrogen production

University of Sheffield (2023)

Nicolaidou, E.

Conformational effects on the photophysics of thiophene-based materials

University of Cyprus (2022)

Placket, E.

Studies into the effects of hydrogen-bonding on excited state dynamics

University of Southampton (2023)

Octopus

Davies, G.

Sustainable Catalytic Science and Engineering through Hydrothermal Synthesis

University of Sheffield (2022)

Barber, E.

Non-Photochemical Laser-Induced Nucleation (NPLIN): an Experimental Investigation via Real-Time Imaging and Product Analysis

University of Edinburgh (2022)

Barker, C.

Investigation of the Optical Properties of Atmospheric Aerosol Using Ultraviolet Light and Dual-Optical Trapping

Royal Holloway University of London (2022)

Hanifi, M.

Development of an RNA-targeting CRISPR system for the treatment of type 1 myotonic dystrophy (DM1)

University of Oxford (2023)

Panel Membership and CLF Structure

Laser for Science Facility Access Panel 2022/23

Reviewers

Professor P. Kukura (Panel Chair)
Department of Chemistry
University of Oxford

Dr S. Ameer-Beg
School of Cancer and Pharmaceutical Sciences
King's College London

Professor A. Beale
Department of Chemistry
University College London

Dr J. Bernadino de la Serna
Faculty of Medicine
Imperial College London

Professor J. Bredenbeck
Johann Wolfgang Goethe-Universität
Institut für Biophysik

Professor S. Charalambous-Hayes
Department of Chemistry
University of Cyprus

Dr A. Cowan
Department of Chemistry
University of Liverpool

Dr E. Gibson
School of Natural and Environmental Sciences
University of Newcastle

Professor M. King
Department of Earth Sciences
Royal Holloway, University of London

Dr. V. Kriechbaumer
Department of Biological and Medical Sciences
Oxford Brookes University

Dr S. Leveque-Fort
Institut des Sciences Moléculaires d'Orsay
Université Paris-Sud

Professor J. Lynam
Department of Chemistry
University of York

Professor G. McConnell
Centre for Biophotonics
University of Strathclyde

Professor J. Moger
University of Exeter

Professor Tom Oliver
School of Chemistry
University of Bristol

Professor Ray Owens
Nuffield Department of Medicine
University of Oxford
and Rosalind Franklin Institute

Professor Lothar Schermelleh
Department of Biochemistry
University of Oxford

Research Council Representatives

C. Miles
BBSRC

A. Chapman
EPSRC

A. Staines
MRC

L. Bettington
NERC

E. Lech
STFC

A. Wilcox
STFC

Science and Technology Facilities Council Representatives

Dr D. T. Clarke (Head of Laser for Science Facility)
Central Laser Facility
Science and Technology Facilities Council

Prof J.L Collier (Director)
Central Laser Facility
Science and Technology Facilities Council

Dr G.M. Greetham (ULTRA Group Leader
Central Laser Facility
Science and Technology Facilities Council

Dr M. Martin-Fernandez (OCTOPUS Group Leader)
Central Laser Facility
Science and Technology Facilities Council

Dr E. Gozzard
ISIS and CLF User Office
Science & Technology Facilities Council

Dr S.R. Needham (Panel Secretary)
Central Laser Facility
Science and Technology Facilities Council

Artemis Facility Access Panel 2022/23

Reviewers

Professor H. Fielding (Panel Chair)
University College London, UK

Professor M. Aeschlimann
University of Kaiserslautern, Germany

Dr A. Taleb
Synchrotron SOLEIL, Essonne, France

Professor L. Perfetti
Ecole Polytechnique, 91120 Palaiseau, France

Professor P. King
University of St Andrews, UK

Dr J. Stähler
Fritz Haber Institute, Berlin, Germany

Professor J. Tisch
Imperial College, London

Professor V. Stavros
University of Warwick, UK

Dr C. Cacho
Diamond Light Source, Harwell, Didcot, UK

Science and Technology Facilities Council Representatives

Professor J.L. Collier (Director)
Central Laser Facility
Science & Technology Facilities Council

Ms C. Hernandez-Gomez (Head, High Power Laser Programme)
Central Laser Facility
Science & Technology Facilities Council

Dr E. Springate (Artemis Group Leader)
Central Laser Facility
Science & Technology Facilities Council

Dr R.T. Chapman (Artemis, AMO and Imaging)
Central Laser Facility
Science & Technology Facilities Council

Dr D.T Clarke (Head of Laser for Science Facility)
Central Laser Facility
Science & Technology Facilities Council

Professor M. Towrie (Molecular and Structural Dynamics)
Central Laser Facility
Science & Technology Facilities Council

Vulcan, Astra TA2 & Gemini Facility Access Panel 2022/23

Reviewers

Professor N. Woolsey (Panel Chair)
York Plasma Institute
University of York

Professor B. Dromey
Department of Pure and Applied Physics
Queen's University of Belfast

Professor G. Gregori
Clarendon Laboratory
University of Oxford

Dr S. Mangles
Blackett Laboratory
Imperial College London

Dr J. Pasley
York Plasma Institute
University of York

Professor B. Hidding
Department of Physics
University of Strathclyde

Professor T. Arber
Department of Physics
University of Warwick

Dr R. Kingham
Blackett Laboratory
Imperial College London

Dr A. Klisnick
Institut des Sciences Moléculaires d'Orsay
Université Paris-Saclay

Dr B. Cros
Laboratory of Gas Physics and Plasmas
Université Paris-Sud

Research Council Representatives

Mr C. Danson
AWE

Mr S. Pitt
AWE

Science and Technology Facilities Council Representatives

Professor J.L. Collier (Director)
Central Laser Facility
Science & Technology Facilities Council

Ms C. Hernandez-Gomez (Head, High Power Laser Programme)
Central Laser Facility
Science & Technology Facilities Council

Dr I.O. Musgrave (Vulcan Group Leader)
Central Laser Facility
Science & Technology Facilities Council

Mr R.J. Clarke (Experimental Science Group Leader)
Central Laser Facility
Science & Technology Facilities Council

Panel Membership and CLF Structure

Central Laser Facility Structure

Director
Professor John Collier
john.collier@stfc.ac.uk

Lasers for Science Division
Dr Dave Clarke
dave.clarke@stfc.ac.uk

CALTA Division
Dr Tom Butcher
thomas.butcher@stfc.ac.uk

High Power Lasers Division
Ms Cristina Hernandez-Gomez
cristina.hernandez-gomez@stfc.ac.uk

Engineering and Technology Division
Mr Steve Blake
steve.blake@stfc.ac.uk

Ultra
Dr Greg Greetham
greg.greetham@stfc.ac.uk

Octopus
Prof Marisa Martin-Fernandez
marisa.martin-fernandez@stfc.ac.uk

Artemis
Dr Emma Springate
emma.springate@stfc.ac.uk

Gemini
Dr Rajeev Pattathil
rajeev.pattathil@stfc.ac.uk

Experimental Science
Mr Rob Clarke
rob.clarke@stfc.ac.uk

Target Fabrication
Mr Martin Tolley
martin.tolley@stfc.ac.uk

Vulcan
Vacancy

Plasma Physics
Dr Alex Robinson
alex.robinson@stfc.ac.uk

Mechanical
Mr Steve Hook
steven.hook@stfc.ac.uk

Electrical
Mr Kenny Rodgers
kenny.rodgers@stfc.ac.uk

Author Index

Page number	Author Name	Institutions/Organisations
26, 40, 56	C.D. Armstrong	Experimental Science Group, Central Laser Facility, STFC Rutherford Appleton Laboratory, Harwell Campus, Didcot, UK
29	C. Arran	York Plasma Institute, School of Physics, Engineering and Technology, University of York, UK
24, 27, 51, 53, 54, 85	S. Astbury	Target Fabrication Group, Central Laser Facility, STFC Rutherford Appleton Laboratory, Harwell Campus, Didcot, UK
40	Z. Athawes-Phelps	Central Laser Facility, STFC Rutherford Appleton Laboratory, Harwell Campus, Didcot, UK
66, 80	A.J. Auty	Department of Chemistry, University of Sheffield, UK
78	D. Avagliano	Institute of Theoretical Chemistry, Faculty of Chemistry, University of Vienna, Austria; Department of Chemistry, Chemical Physics Theory Group, University of Toronto, Canada
48	T.B. Avni	Central Laser facility, Research Complex at Harwell, STFC Rutherford Appleton Laboratory, Harwell Campus, Didcot, UK
56	C. Baird	Experimental Science Group, Central Laser Facility, STFC Rutherford Appleton Laboratory, Harwell Campus, Didcot, UK
64	K. Baker	School of Biosciences, University of Kent, Canterbury, UK
75	M.J. Baker	School of Medicine and Dentistry, University of Central Lancashire, Preston, UK
24	M. Balcazar	Gérard Mourou Center for Ultrafast Optical Science, University of Michigan, MI, USA

Author Index

Author Index

Page number	Author Name	Institutions/Organisations
30	E. Brunetti	Scottish Universities Physics Alliance and University of Strathclyde, Glasgow, UK
59	B. Büchner	Institute for Solid State Research, Leibniz IFW Dresden, Germany; Institute of Solid State and Materials Physics and Würzburg-Dresden Cluster of Excellence CT.QMAT, Technische Universität Dresden, Germany
43	S. Buck	Central Laser Facility, STFC Rutherford Appleton Laboratory, Harwell Campus, Didcot, UK
76	T.J. Burden	Department of Chemistry, University of York, UK
51	L. Bushnell	RAL Space, STFC Rutherford Appleton Laboratory, Harwell Campus, Didcot, UK
33	T.J. Butcher	Central Laser Facility, STFC Rutherford Appleton Laboratory, Harwell Campus, Didcot, UK
74	G. Cabello	Stephenson Institute for Renewable Energy, Department of Chemistry, University of Liverpool, UK
25, 26, 29	L. Calvin	School of Mathematics and Physics, Queen's University Belfast, UK
69	E. Campbell	School of Chemistry, Cardiff University, UK
29	J. Carderelli	Gérard Mourou Center for Ultrafast Optical Science, University of Michigan, USA
57	E. Carpene	IFN-CNR, Dipartimento di Fisica, Politecnico di Milano, Italy

Page number	Author Name	Institutions/Organisations
31, 56	D.C. Carroll	Experimental Science Group, Central Laser Facility, STFC Rutherford Appleton Laboratory, Harwell Campus, Didcot, UK
80	H. Carson	Department of Chemistry, The University of Sheffield, UK
61	S.H. Cartmell	Department of Materials, School of Natural Sciences, Faculty of Science and Engineering, University of Manchester, UK; The Henry Royce Institute, University of Manchester, UK
68	C.K. Cassidy	Department of Biochemistry, University of Oxford, UK
25, 26, 29	N. Cavanagh	School of Mathematics and Physics, Queen's University Belfast, UK
32, 56	O. Cavanagh	Centre for Light-Matter Interactions, School of Mathematics and Physics, Queen's University Belfast, UK
57	G. Cerullo	Dipartimento di Fisica, Politecnico di Milano, Italy
57, 58, 59	R. T. Chapman	Central Laser Facility, Research Complex at Harwell, STFC Rutherford Appleton Laboratory, Harwell Campus, Didcot, UK
90	S.E.J. Chapman	Central Laser Facility, STFC Rutherford Appleton Laboratory, Harwell Campus, Didcot, UK
22	J. Chappell	John Adams Institute for Accelerator Science and Department of Physics, University of Oxford, UK
47, 57	G. Chatterjee	Central Laser Facility, Research Complex at Harwell, STFC Rutherford Appleton Laboratory, Harwell Campus, Didcot, UK

Author Index

Page number	Author Name	Institutions/Organisations
25, 32	P. Chaudhary	Patrick G. Johnston Centre for Cancer Research, Queen's University Belfast, UK; Centre for Light-Matter Interactions, School of Mathematics and Physics, Queen's University Belfast, UK
66	A.A.P. Chauvet	Department of Chemistry, University of Sheffield, UK
60	M. Chavent	Institut de Pharmacologie et Biologie Structurale, IPBS, Universite´ de Toulouse, France
80	D. Chekulaev	Department of Chemistry, The University of Sheffield, UK
31	S.N. Chen	Horia Hulubei National Institute for R&D in Physics and Nuclear Engineering (IFIN-HH), Bucharest-Magurele, Romania
80	T. Cheng	Department of Chemistry, The University of Sheffield, UK
67	T-L. Chew	Advanced Imaging Center, HHMI Janelia Research Campus, Ashburn, USA
60	A. Chu	Department of Biochemistry, University of Oxford, UK
31	A. Ciardi	Sorbonne Université, Observatoire de Paris, Université PSL, CNRS, LERMA, Paris, France
28, 30	S. Cipiccia	Diamond Light Source, Harwell Science and Innovation Campus, Didcot, UK; Scottish Universities Physics Alliance and University of Strathclyde, Glasgow, UK
76, 78	I.P. Clark	Central Laser Facility, Research Complex at Harwell, STFC Rutherford Appleton Laboratory, Harwell Campus, Didcot, UK

Author Index

Page number	Author Name	Institutions/Organisations
71, 72, 73	P.M. Donaldson	Central Laser Facility, Research Complex at Harwell, STFC Rutherford Appleton Laboratory, Harwell Campus, Didcot, UK
21	D. Doria	Centre for Light–Matter Interactions, School of Mathematics and Physics, Queen's University Belfast, UK; Extreme Light Infrastructure (ELI-NP) and Horia Hulubei National Institute for R & D in Physics and Nuclear Engineering (IFIN-HH), Romania
67	Á. dos Santos	Department of Oncology and Metabolism, University of Sheffield, UK
24	N.P. Dover	The John Adams Institute for Accelerator Science, Imperial College London, UK
27	N.P. Dover	John Adams Institute for Accelerator Science, Blackett Laboratory, Imperial College London, UK
60	A.L. Duncan	Department of Biochemistry, University of Oxford, UK
24, 27, 37, 40	T. Dzelzainis	Central Laser Facility, STFC Rutherford Appleton Laboratory, Harwell Campus, Didcot, UK
76	J.B. Eastwood	Department of Chemistry, University of York, UK
64	T.A. Eastwood	School of Biosciences, University of Kent, Canterbury, UK
71	A.E. Edmeades	Central Laser Facility, Research Complex at Harwell, STFC Rutherford Appleton Laboratory, Harwell Campus, Didcot, UK
51	H. Edwards	Central Laser Facility, STFC Rutherford Appleton Laboratory, Harwell Campus, Didcot, UK

Author Index

Author Index

Page number	Author Name	Institutions/Organisations
24, 27	M. Gauthier	SLAC National Accelerator Laboratory, Menlo Park, CA, USA
28, 29	E. Gerstmayr	The John Adams Institute for Accelerator Science, Imperial College London, UK
24, 27	L. Giuffrida	ELI Beamlines Centre, Institute of Physics, Czech Academy of Sciences, Czech Republic
24, 27	G.D. Glenn	SLAC National Accelerator Laboratory, Menlo Park, CA, USA; Department of Applied Physics, Stanford University, CA, USA
24, 27	S.H. Glenzer	SLAC National Accelerator Laboratory, Menlo Park, CA, USA
78	L. González	Institute of Theoretical Chemistry, Faculty of Chemistry, University of Vienna, Austria; Vienna Research Platform on Accelerating Photoreaction Discovery, University of Vienna, Austria
67	R.E. Gough	Department of Oncology and Metabolism, University of Sheffield, UK
78	D. Graczyk	School of Chemistry, University College Dublin, Ireland
24, 27	R.J. Gray	Department of Physics, SUPA, University of Strathclyde, UK
24, 27, 56	J.S. Green	Experimental Science Group, Central Laser Facility, STFC Rutherford Appleton Laboratory, Harwell Campus, Didcot, UK
47, 48, 49, 71, 72, 75	G.M. Greetham	Central Laser facility, Research Complex at Harwell, STFC Rutherford Appleton Laboratory, Harwell Campus, Didcot, UK
23	X.J. Gu	Scientific Computing Department, STFC Daresbury Laboratory, Warrington, UK

Page number	Author Name	Institutions/Organisations
61	M.G.R. Guastamacchia	EPSRC Centre for Doctoral Training in Applied Photonics, Heriot-Watt University, Edinburgh, UK; Central Laser Facility, Research Complex at Harwell, STFC Rutherford Appleton Laboratory, Harwell Campus, Didcot, UK; Institute of Biological Chemistry, Biophysics and Bioengineering, Heriot-Watt University, Edinburgh, UK
40	A. Gunn	The John Adams Institute for Accelerator Science, Imperial College London, UK
85	D. Haddock	Target Fabrication Group, Central Laser Facility, STFC Rutherford Appleton Laboratory, Harwell Campus, Didcot, UK
56	T.H. Hall	Experimental Science Group, Central Laser Facility, STFC Rutherford Appleton Laboratory, Harwell Campus, Didcot, UK
74	L.J. Hardwick	Stephenson Institute for Renewable Energy, Department of Chemistry, University of Liverpool, UK
67	Y. Hari-Gupta	School of Biosciences, University of Kent, Canterbury, UK
81	S. Hawkes	Central Laser Facility, STFC Rutherford Appleton Laboratory, Harwell Campus, Didcot, UK
71, 72	A.P. Hawkins	Central Laser Facility, Research Complex at Harwell, STFC Rutherford Appleton Laboratory, Harwell Campus, Didcot, UK
48, 49	I.A. Heisler	Instituto de Física Universidade Federal do Rio Grande do Sul – UFRGS, Porto Alegre, Brazil
44	Y. Hemani	Advanced Analytical Technologies, Swiss Federal Laboratories for Materials Science and University of Zurich, Switzerland

Author Index

Page number	Author Name	Institutions/Organisations
46	J.R. Henderson	Accelerator Science and Technology Centre (ASTeC), STFC Daresbury Laboratory, Warrington, UK
60	J. Hermann	Department of Biochemistry, University of Oxford, UK
35	C. Hernandez-Gomez	Central Laser Facility, STFC Rutherford Appleton Laboratory, Harwell Campus, Didcot, UK
24	G.S. Hicks	The John Adams Institute for Accelerator Science, Blackett Laboratory, Imperial College London, UK
65	D.T. Hinds	School of Chemistry, University College Dublin, Ireland
64	J.R. Hiscock	School of Chemistry and Forensics, University of Kent, Canterbury, UK
59	P. Hofmann	Department of Physics and Astronomy, Interdisciplinary Nanoscience Center, Aarhus University, Denmark
22	S.M. Hooker	John Adams Institute for Accelerator Science and Department of Physics, University of Oxford, UK
58	D.A. Horke	Institute for Molecules and Materials, Radboud University, The Netherlands
71, 72	R.F. Howe	Department of Chemistry, University of Aberdeen, UK
58	D.J. Hughes	School of Chemistry, University of Southampton, UK
75	N.T. Hunt	Department of Chemistry and York Biomedical Research Institute, University of York, UK

Page number	Author Name	Institutions/Organisations
69	S. Kondrat	Loughborough University, UK
68	C.W. Koo	Departments of Molecular Biosciences and of Chemistry, Northwestern University, IL, USA
63	V. Kreichbaumer	Endomembrane Structure and Function Research Group, Biological and Medical Sciences, Oxford Brookes University, UK
76	J-P. Krieger	Syngenta Crop Protection AG, Münchwilen, Switzerland
58	P. Krüger	Institute for Molecules and Materials, Radboud University, The Netherlands
39	N. Krumpa	Central Laser Facility, STFC Rutherford Appleton Laboratory, Harwell Campus, Didcot, UK
28	K. Krushelnick	Center for Ultrafast Optical Science, University of Michigan, USA
30	T. Kühl	GSI Helmholtzzentrum für Schwerionenforschung, Darmstadt, Germany
59	A. Kuibarov	Institute for Solid State Research, Leibniz IFW Dresden, Germany
77	M.S. Kwon	Seoul National University, Seoul, South Korea
77	Y. Kwon	Seoul National University, Seoul, South Korea
61	P.D. Lee	Department of Materials, School of Natural Sciences, Faculty of Science and Engineering, University of Manchester, UK; The Henry Royce Institute, University of Manchester, UK

Author Index

Page number	Author Name	Institutions/Organisations
30	G. Lehmann	Institut für Theoretische Physik I, Heinrich-Heine-Universität Düsseldorf, Germany
31	R. Lelièvre	LULI - CNRS; École Polytechnique, CEA; Université Paris-Saclay; UPMC Université Paris 06; Sorbonne Université, France
28	N. Lemos	Lawrence Livermore National Laboratory (LLNL), California, USA
64	C. Lennon	Fujifilm-Diosynth Biotechnologies UK Ltd, Billingham, UK
70	C. Li	Stephenson Institute for Renewable Energy and Department of Chemistry, University of Liverpool, UK
62	G. Little	Environment and Climate Change Canada, Nova Scotia, Canada
28	N.C. Lopes	The John Adams Institute for Accelerator Science, Imperial College London, UK; GoLP/Instituto de Plasmas e Fusão Nuclear, Instituto Superior Técnico, Universidade de Lisboa, Portugal
29	E.E. Los	The John Adams Institute for Accelerator Science, Imperial College London, UK
24, 27	B. Loughran	School of Mathematics and Physics, Queen's University Belfast, UK
28	C. Lumsdon	ork Plasma Institute, Department of Physics, University of York, UK
28	O. Lundh	Department of Physics, Lund University, Sweden
76	J.M. Lynam	Department of Chemistry, University of York, UK

Page number	Author Name	Institutions/Organisations
40	R. Lyon	Central Laser Facility, STFC Rutherford Appleton Laboratory, Harwell Campus, Didcot, UK
28	Y. Ma	Center for Ultrafast Optical Science, University of Michigan, USA; The Cockcroft Institute, Daresbury, UK; Physics Department, Lancaster University, UK
61	K. Madi	Department of Materials, School of Natural Sciences, Faculty of Science and Engineering, University of Manchester
21	C. Maiorino	Centre for Light–Matter Interactions, School of Mathematics and Physics, Queen's University Belfast, UK; Laboratori Nazionali del Sud, Istituto Nazionale di Fisica Nucleare, Sicily, Italy; Extreme Light Infrastructure (ELI-NP) and Horia Hulubei National Institute for R & D in Physics and Nuclear Engineering (IFIN-HH), Romania; University College Cork, College of Medicine and Health, Discipline of Diagnostic Radiography and Radiation Therapy, Ireland
59	P. Majchrzak	Department of Physics and Astronomy, Interdisciplinary Nanoscience Center, Aarhus University, Denmark
28, 29	S.P.D. Mangles	The John Adams Institute for Accelerator Science, Imperial College London, UK
24, 27	D. Margarone	School of Mathematics and Physics, Queen's University Belfast, UK; ELI Beamlines Centre, Institute of Physics, Czech Academy of Sciences, Czech Republic
41	V.A. Marshall	Central Laser Facility, STFC Rutherford Appleton Laboratory, Harwell Campus, Didcot, UK
31, 32, 56	P. Martin	Centre for Plasma Physics, School of Mathematics and Physics, Queen's University Belfast, UK; Centre for Light-Matter Interactions, School of Mathematics and Physics, Queen's University Belfast, UK

Author Index

Page number	Author Name	Institutions/Organisations
21, 25	S.J. McMahon	The Patrick G. Johnston Centre for Cancer Research, Queen's University Belfast, UK
21	A. McMurray	Centre for Light–Matter Interactions, School of Mathematics and Physics, Queen's University Belfast, UK
49	A.E.D. Meades	Central Laser Facility, Research Complex at Harwell, STFC Rutherford Appleton Laboratory, Harwell Campus, Didcot, UK
48, 49	S.R. Meech	School of Chemistry, University of East Anglia, Norwich, UK
80	A.J.H.M. Meijer	Department of Chemistry, The University of Sheffield, UK
21	G. Milluzzo	Centre for Light–Matter Interactions, School of Mathematics and Physics, Queen's University Belfast, UK; Laboratori Nazionali del Sud, Istituto Nazionale di Fisica Nucleare, Sicily, Italy
58	R.S. Minns	School of Chemistry, University of Southampton, UK
69	P. Moreau	Plastic Energy, Loughborough, UK
62	J. Morison	Forest Research, Alice Holt Lodge, Farnham, UK
40	B. Morkot	Central Laser Facility, STFC Rutherford Appleton Laboratory, Harwell Campus, Didcot, UK
32	J. Morrow	Centre for Light-Matter Interactions, School of Mathematics and Physics, Queen's University Belfast, UK
46, 90	J. Morse	Central Laser Facility, STFC Rutherford Appleton Laboratory, Harwell Campus, Didcot, UK

Page number	Author Name	Institutions/Organisations
77	A.J. Orr-Ewing	University of Bristol, Bristol, UK
40	T. Pacey	The Cockcroft Institute, Accelerator Science and Technology Centre, STFC Sci-Tech Daresbury, Warrington, UK
63	C. Pain	Endomembrane Structure and Function Research Group, Biological and Medical Sciences, Oxford Brookes University, UK
24, 27, 51, 56	C.A.J. Palmer	School of Mathematics and Physics, Queen's University Belfast, UK
39	Z. Pan	Technology Department, STFC Rutherford Appleton Laboratory, Harwell Campus, Didcot, UK
24, 27	C. Parisuaña	SLAC National Accelerator Laboratory, Menlo Park, CA, USA; Department of Mechanical Engineering, Stanford University, CA, USA
75	A.W. Parker	STFC Central Laser Facility, Research Complex at Harwell, Rutherford Appleton Laboratory, Harwell Campus, Didcot, UK
58	M.A. Parkes	Department of Chemistry, University College London, UK
24, 27, 29, 42, 51	P. Parsons	School of Mathematics and Physics, Queen's University Belfast, UK; Central Laser Facility, STFC Rutherford Appleton Laboratory, Harwell Campus, Didcot, UK
35	R. Pattathil	Central Laser Facility, STFC Rutherford Appleton Laboratory, Harwell Campus, Didcot, UK
47	Y. Pertot	Fastlite, Antibes, France

Author Index

Page number	Author Name	Institutions/Organisations
69, 70, 74, 77, 80	I. V. Sazanovich	Central Laser Facility, Research Complex at Harwell, STFC Rutherford appleton Laboratory, Harwell Campus, Didcot, UK
79, 80	P.A. Scattergood	Department of Chemical Sciences, School of Applied Sciences, University of Huddersfield, UK
60	E. Seiradake	Department of Biochemistry, University of Oxford, UK
40	C. Selig	Central Laser Facility, STFC Rutherford Appleton Laboratory, Harwell Campus, Didcot, UK
28	M. Shahzad	SUPA, Department of Physics, University of Strathclyde, Glasgow, UK; The Cockcroft Institute, Daresbury, UK
68	J. Shen	Division of Structural Biology, Wellcome Trust Centre for Human Genetics, University of Oxford, UK
68	Y. Sheng	Diamond Light Source, Harwell Science and Innovation Campus, Didcot, UK
46	B. Shi	Optoelectronic Research Centre, University of Southampton, UK
80	J. Shipp	Department of Chemistry, The University of Sheffield, UK
31	A. Sladkov	Light Stream Labs LLC, Palo Alto, CA, USA
46	R. Slavik	Optoelectronic Research Centre, University of Southampton, UK
28	M. Smid	Helmholtz-Zentrum Dresden-Rossendorf, Germany

Author Index

Page number	Author Name	Institutions/Organisations
78, 79	M. Stitch	School of Chemistry, University College Dublin, Ireland
64	B.R. Streather	School of Biosciences, University of Kent, Canterbury, UK
24, 25, 26, 27, 28, 29	M.J.V. Streeter	The Cockcroft Institute, Daresbury, UK; Physics Department, Lancaster University, UK; The John Adams Institute for Accelerator Science, Imperial College London, UK; School of Mathematics and Physics, Queen's University Belfast, UK
62	E.J. Stuckey	ISIS Pulsed Neutron and Muon Source, STFC Rutherford Appleton Laboratory, Harwell Campus, Didcot, UK
40	R. Sugumar	Indian Institute of Technology Hyderabad, Telengana, India
26	W. Sun	National Physical Laboratory, Teddington, UK
23, 24, 26, 27, 28, 29, 37, 38, 40	D.R. Symes	Central Laser Facility, STFC Rutherford Appleton Laboratory, Didcot, UK
40	I. Symonds	Central Laser Facility, STFC Rutherford Appleton Laboratory, Harwell Campus, Didcot, UK
83	M. Szynkiewicz	Central Laser Facility, STFC Rutherford Appleton Laboratory, Harwell Campus, Didcot, UK
76	T.F.N. Tanner	Department of Chemistry, University of York, UK
47	N. Thiré	Fastlite, Antibes, France

Author Index

Page number	Author Name	Institutions/Organisations
47, 71, 72, 76, 78, 79, 80	M. Towrie	Central Laser Facility, Research Complex at Harwell, STFC Rutherford Appleton Laboratory, Harwell Campus, Didcot, UK
24, 27	F. Treffert	SLAC National Accelerator Laboratory, Menlo Park, CA, USA; Institut für Kernphysik, Technische Universität Darmstadt, Germany
60	C.J. Tynan	Central Laser Facility, Research Complex at Harwell, STFC Rutherford Appleton Laboratory, Harwell Campus, Didcot, UK
28, 30	G. Vieux	SUPA, Department of Physics, University of Strathclyde, Glasgow, UK; The Cockcroft Institute, Daresbury, UK
67	E. Wait	Advanced Imaging Center, HHMI Janelia Research Campus, Ashburn, USA
22	R. Walczak	John Adams Institute for Accelerator Science and Department of Physics, University of Oxford, UK
69	S. Wallbridge	Loughborough University, UK
64, 67	L. Wang	Central Laser Facility, Research Complex at Harwell, STFC Rutherford Appleton Laboratory, Harwell Campus, Didcot, UK
22	W. Wang	John Adams Institute for Accelerator Science and Department of Physics, University of Oxford, UK
62, 65	A.D. Ward	Central Laser Facility, Research Complex at Harwell, STFC Rutherford Appleton Laboratory, Harwell Campus, Didcot, UK
26	J.M. Warnett	WMG, University of Warwick, Coventry, UK

Author Index

Page number	Author Name	Institutions/Organisations
35	A.M. Wojtusiak	Central Laser Facility, STFC Rutherford Appleton Laboratory, Harwell Campus, Didcot, UK
57	D. Wolverson	Centre for Nanoscience and Nanotechnology, Department of Physics, University of Bath, UK
43	M. Woodward	Central Laser Facility, STFC Rutherford Appleton Laboratory, Harwell Campus, Didcot, UK
80	G. Wu	Department of Chemistry, The University of Sheffield, UK
47, 57, 59	A.S. Wyatt	Central Laser Facility, Research Complex at Harwell, STFC Rutherford Appleton Laboratory, Harwell Campus, Didcot, UK
50	D. Wyatt	Target Fabrication Group, Central Laser Facility, STFC Rutherford Appleton Laboratory, Harwell Campus, Didcot, UK
24, 27	N. Xu	The John Adams Institute for Accelerator Science, Blackett Laboratory, Imperial College London, UK
61	R. Xue	Department of Materials, School of Natural Sciences, Faculty of Science and Engineering, University of Manchester, UK; The Henry Royce Institute, University of Manchester, UK
68	Z. Yang	Diamond Light Source, Harwell Science and Innovation Campus, Didcot, UK
31	W. Yao	LULI - CNRS; École Polytechnique, CEA; Université Paris-Saclay; UPMC Université Paris 06; Sorbonne Université, France
30	S.R. Yoffe	Scottish Universities Physics Alliance and University of Strathclyde, Glasgow, UK

Author Index

Page number	Author Name	Institutions/Organisations
68	L.C. Zanetti-Domingues	Central Laser Facility, Research Complex at Harwell, STFC Rutherford Appleton Laboratory, Harwell Campus, Didcot, UK
68	P. Zhang	Division of Structural Biology, Wellcome Trust Centre for Human Genetics, University of Oxford, UK; Diamond Light Source, Harwell Science and Innovation Campus, Didcot, UK
47, 57, 59	Y. Zhang	Central Laser Facility, Research Complex at Harwell, STFC Rutherford Appleton Laboratory, Harwell Campus, Didcot, UK
68	Y. Zhu	Division of Structural Biology, Wellcome Trust Centre for Human Genetics, University of Oxford, UK

Science and
Technology
Facilities Council

Central Laser Facility